La Spezia, Italy

April – September 2010

Master Thesis Report

Terrain Based Navigation using a Particle Filter for Long range glider missions

- Feasibility study and simulations -

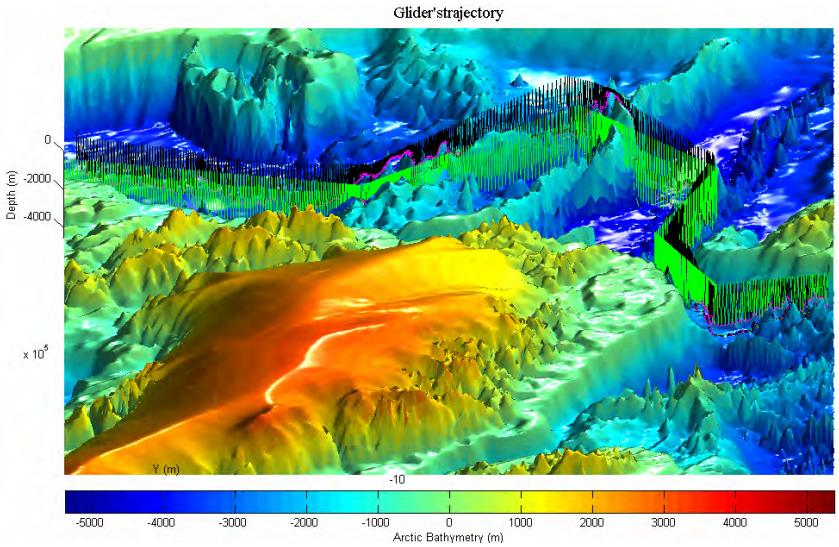

Julien Lagadec
ENSIETA – Ecole Nationale Supérieure D'Ingénieurs

Project supervisor: Michel Rixen

Abstract

The navigation of a totally autonomous AUV is a major challenge. Most AUVs are based on low drift inertial navigation systems designed to sustain submerged operations for long periods of time. To improve the navigation estimation, we can rely either on long or on ultra short baseline acoustic positioning. But those processes require for one, the set up of a series of transponders, and for the other the assistance of a mother ship. Due to operational costs, it is desirable to reduce the amount of external equipment required for an AUV to operate independently.

Moreover, for a glider mission, many others aspects such as energy savings, complete autonomy, payload constraints, have to be taken into account for the navigation estimation process.

In this context, the use of underwater terrain navigation provides an enabling capability for low-cost navigation on underwater vehicles. The idea towards using terrain information for the purpose of navigation is to incorporate information provided by a priori maps into the estimation process. Thus, the ability to use natural features will allow a submersible body to be deployed in a large range of environments without the need to introduce artificial beacons or rely on acoustic tracking technology.

The aim of this simulation is to implement on a glider an underwater terrain navigation algorithm using particle filtering.

The main objective of particle filtering is to track a variable of interest as it evolves over time, typically with a non-Gaussian and potentially multi modal probability density function (pdf). The basis of the method is to construct a sample-based representation of the entire pdf, distributing weights to particles according to the likelihood between the depth measured at their position and the own glider's depth measurement.

The final objective of this feasibility study is to simulate a glider's deployment under the Arctic using this method for its navigation estimation; and to find an answer to the fundamental question: "Can we use a terrain navigation approach for a long range under ice mission in the Arctic Ocean?"

Acknowledgements

I would like to express my sincere thanks and appreciation to Michel Rixen (the supervisor of the present study), Daniele Cecchi and Raffaele Grasso for their attention and support during the whole period of this project. Their comments and suggestions have always been constructive and helped me during the development of this study.

Working at the Nato Undersea Research Center has been a pleasant and rewarding experience and allowed me, on the one hand, to encounter many highly skilled experts and students coming from all over the world. On the other hand, this experience allowed me to face the challenging and exciting scientific problem of the underwater positioning.

Contents

List of figures

Introduction

Oceans are the key element that drives our climate. In association with the atmosphere they constitute a real thermal machine. Men have always tried to understand and explore those huge basins of water as Sir Wyville Thompson on board of the Challenger expedition (1872-1876). Nowadays we try to continue this work of understanding through data collection all over the world in order to establish, validate and feed our global and local oceanographic models.

Data collection

Oceans are the backbone of our ecosystem. Progress in understanding our climate depends in part on the gathering of scientific data from the oceans. Because of the distributed nature of ocean dynamics, data is needed over a wide temporal and spatial range.

Traditional methods for gathering data include the use of surface ships, towed sleds, manned-submersible, fixed moorings, drifters, and bottom-mounted instrumentation. However, ships are expensive to operate and are limited in number and availability. Fixed moorings give data about only one location, while drifters cannot choose their path through the ocean. Each of these systems has its place in oceanographic research, but deployment, operation, and recovery can be expensive. In this context, autonomous platforms such as gliders overcome many of these difficulties and seem to be a perfect compromise.

Gliders

The first application of underwater glider, and the inspiration for their design, has been oceanographic data collection. Use of gliders in a distributed fleet is part of the original vision for their use in oceanography.

Gliders are unique in the AUV world, in that varying vehicle buoyancy creates the forward propulsion. Wings and control surfaces convert the vertical velocity into forward velocity so that the vehicle glides downward when denser than water and glides upward when buoyant. Gliders require no propeller and operate in a vertical saw tooth trajectory which ensures a high resolution in data sampling.

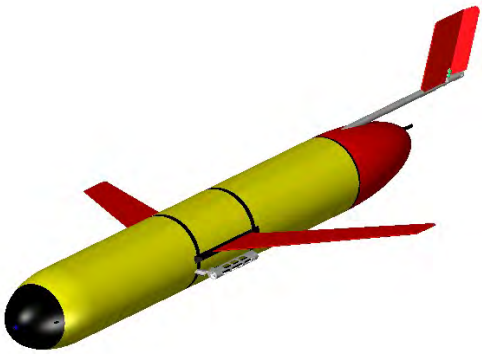

Figure 0-1: Slocum Glider

The Slocum Battery Glider dead reckons to waypoints, inflecting at set depths and altitudes based on a mission text file. As set by the mission, the Glider periodically surfaces to communicate data and instructions and to obtain a GPS fix for location. Any difference in dead reckoning and position is attributed to current and that knowledge is used on the subsequent segment. (source: Slocum glider user's manual)

However, given that gliders operate at a relatively low speed (about 0.3 m/s) they are constrained by currents, and so their underwater position estimation is neither very accurate nor precise. The definition of both accuracy and precision is illustrated in the figure 0-2.

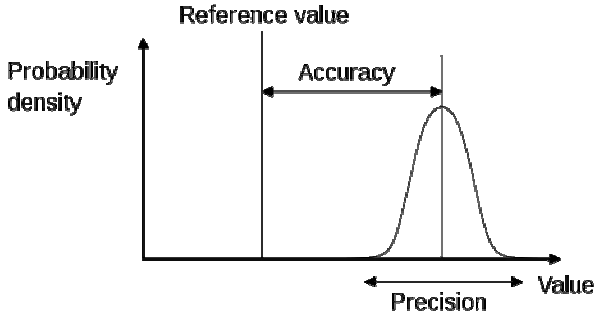

Figure 0-2: precision and accuracy definition

Underwater positioning

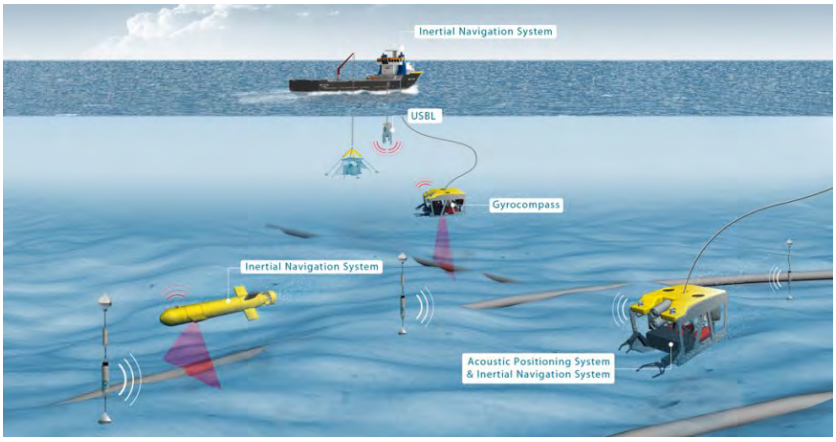

Figure 0-3: Underwater positioning solutions (*source www.ixsea.com*)

Effective localization and navigation is critical to AUV mission accomplishment. Modern sea navigation systems are often based on satellite information from the global positioning system (GPS) in order to keep high permanent position accuracy. However, the radio-frequency signals used in GPS cannot effectively penetrate seawater, so AUVs can only use GPS directly to constrain position error when they are at or very close to the surface.

As a consequence, most underwater vehicle navigation is based on some form of dead reckoning with varying techniques to bound the error growth using external information. Dead reckoning is the process of using knowledge of a vehicle's motion since its last known position to estimate the vehicle location at any given time.

But, this underwater position estimation process is burdened by drifting and position uncertainty growth. Even navigation systems based on sophisticated sensors, such as Inertial Navigation Systems (INS), require periodic reinitialization with external information to bound their continually growing error.

Terrain navigation

Terrain navigation seems to be a promising technique for the challenges encountered in underwater navigation. In fact, it offers the unique ability of being totally independent, and this in a possibly low cost way.

Terrain navigation has been used for vehicles traveling over land. A classical application is the cruise missile, which updates its position periodically using stored maps between the launch and target sites.

The key idea of terrain navigation lies in the comparison between measurements and a stored map as illustrated on figure 0-4. To make it simple, we could outline that terrain navigation works in the same way than our orientation sense. We know where we are by making comparison between what we are seeing and what is stored in our memory.

Thanks to progress done in bathymetric data acquisition, the seafloor is now increasingly understood and contains interesting bathymetric features (seamounts, canyons, knolls, ridges, trenches, banks, rises, slopes, shoals…), which may have enough variability to support bathymetric navigation.

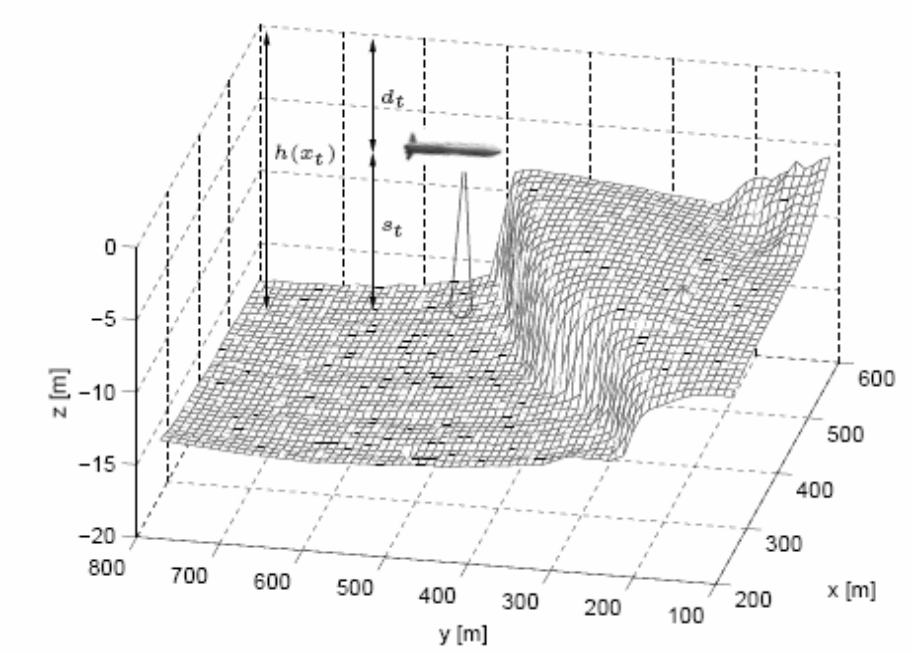

Figure 0-4: Terrain navigation using sonar depth measurements (source: particle filter for underwater terrain navigation – R. Karlsson, F. Gustafson [18])

Objective of this project

The objective of this project is to see if an improvement in the glider's underwater positioning using the terrain navigation principle is possible. So the idea is to combine the dead reckoning process already existing with the bathymetric data in order to improve the positioning accuracy (see figure 0-5). This improvement must take into consideration that we are operating gliders and thus, that the energy budget is limited.

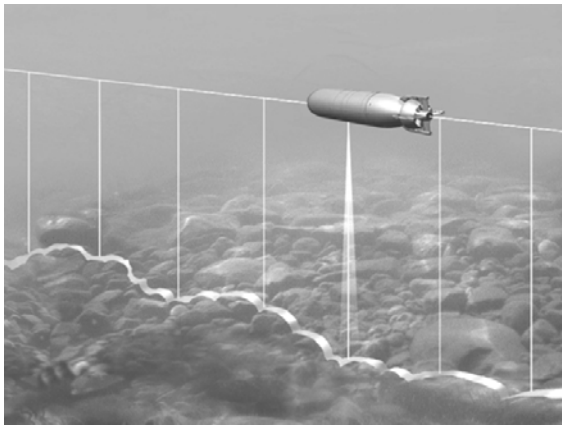

Figure 0-5: Terrain navigation principle. The AUV is measuring the depth by one sonar beam at each sampling event. Likely positions are positions in the map with the same depth. (Source: *Terrain Navigation for Underwater Vehicles Using the Correlator Method* - Ingemar Nygren)

The project consists in the development of a simulation tool based on terrain navigation using particle filter. Given this simulation we are willing to test the feasibility of the Terrain Based Navigation Particle Filter (TBN-PF) on a long range glider's mission, and especially under-ice missions in Arctic and covert military operations. This simulation will also be a tool to answer fundamental questions but also to test the expected accuracy on underwater positioning given:

- The pinging policy
- Specifications of navigation instruments
- The desired trajectory
- The current data on the area
- The *a priori* bathymetric map

1 Underwater navigation

In this section we would like to give an overview of existing underwater navigation technologies before tackling the terrain navigation. The figure 1-1 represents the AUV HUGIN, which is able to use many different systems of underwater navigation (DVL aided Inertial, acoustic, terrain navigation).

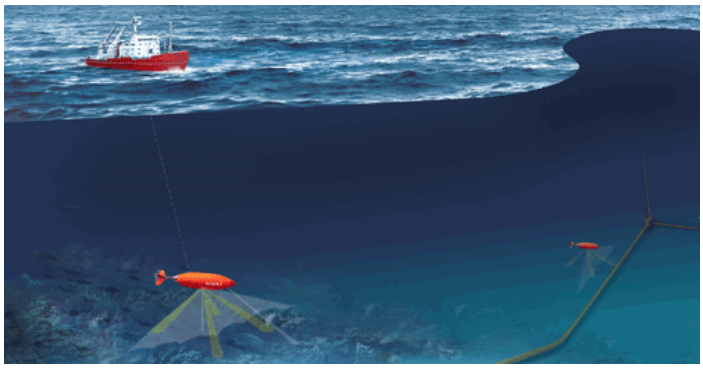

Figure 1-1: Kongsberg Hugin AUV

Accurate underwater navigation remains a substantial challenge to all underwater platforms. Both Autonomous operation in deep water and covert military operations require the AUV to remain submerged for long periods of time. Many navigation technologies are available for AUVs. Some require accurate knowledge of the vehicle state (internal navigation), and others are dependent on underwater communication (external navigation). Thus we can sort all those technologies into two distinct categories:

- Internal: dead reckoning, inertial navigation
- External: radio, acoustic and geophysical navigation

1.1 *Internal navigation*

1.1.1 Inertial Navigation System

Most of underwater vehicles rely on inertial measurement sensors to estimate their position.

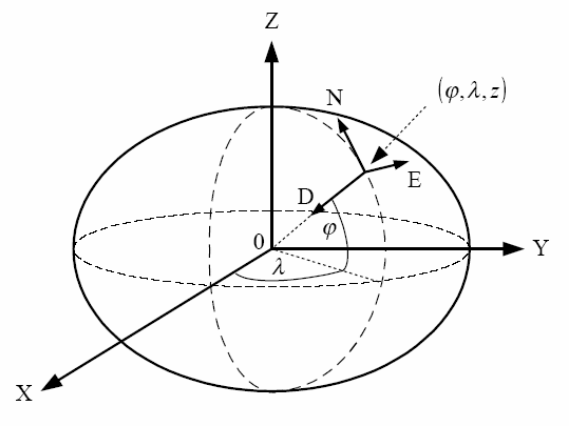

Figure 1-2 The relationship between the global geographical frame of reference XYZ and the local horizontal frame of reference NED
Source: P. Kaniewsky, "***Integrated Positing System for AUV***"

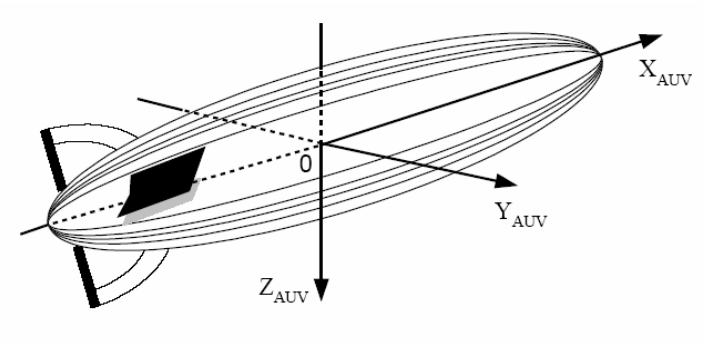

Figure 1-3 the body frame of reference
Source: P. Kaniewsky, "***Integrated Positing System for AUV***"

An INS calculates position (φ,λ,z), velocity $V_{NED}=[V_N\ V_E\ V_D]^T$ and attitude using high frequency data from an Inertial Measurement Unit (IMU). Figures 1-2 and 1-3 provide the coordinates framework. An IMU consists of three accelerometers and three gyros measuring angular rate. An INS is an integrated system of many navigation devices:

IMU:	Inertial measurement unit	DVL:	Doppler velocity log
EC:	Electronic compass	DS:	Depth sensor

These sensors are usually integrated thanks to a Kalman filter, which performs this integration in a mathematically optimal way. Here, the Kalman filter is based on an error-state model and provides a much higher total navigation performance than the one obtained from the individual sensors alone.

The structure of the positioning system is composed of two parts, a group of navigation devices and an algorithm of joint data processing as shown on figure 1-4.

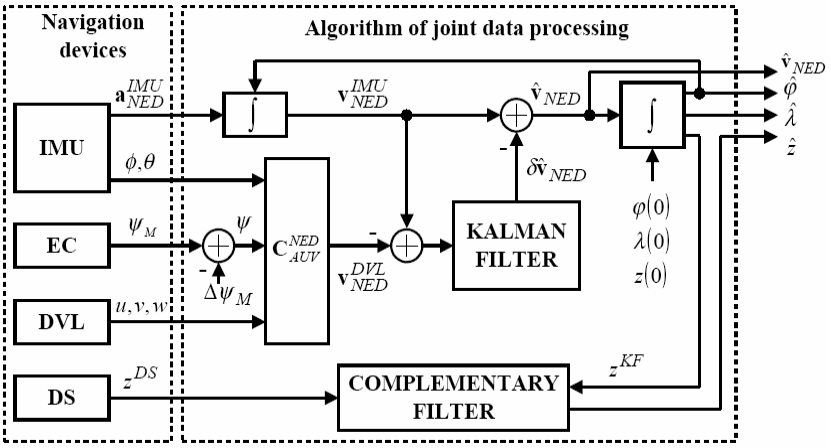

Figure 1-4 Structure of the positioning process for an AUV – source: *INTEGRATED POSITIONING SYSTEM FOR AUV* (Piotr KANIEWSKI, Military University of Technology, Warsaw, POLAND)

- The IMU provides for three components of acceleration $a_{NED}^{IMU} = [a_N \; a_E \; a_D]^T$ in the local horizontal frame, and two inclination angles (roll ϕ and pitch θ).

- The electronic compass (EC) complements these angles with the magnetic heading of the vehicle ψ_M. This magnetic heading has to be corrected, by subtracting from it a local magnetic variance $\Delta\psi_M$, and this way the true heading is calculated.

- The Doppler velocity log (DVL) provides ideally three components of velocity relative to the seafloor (u, v, w) in the body frame.

- The depth sensor (DS) is a water pressure meter and provides for the depth z^{DS} of AUV relative to the sea level.

Thus, this positioning system provides for position (φ, λ, z) and velocity $V_{NED} = [V_N \; V_E \; V_D]^T$ of the underwater vehicle. With all those measurement devices, the position estimation process is almost autonomous or self sufficient. Unfortunately, given the double integration process, INS is also burdened by an error drift. The chapter 6 of this report tackles an implementation of an INS uncertainty algorithm. However we can find in literature typical ranges for performances of this system (table 1.1-1):

Navigation system	- Long term accuracy - DVL range	AUV speed	Error drift
IMU stand alone			1 nautical mile/hour
INS with a 300 kHz DVL	0.4% of speed 200m	2 m/s	28.8 m/h
INS with a 1200 kHz DVL	0.2% of speed 30 m	2 m/s	14.4 m/h

Table 1.1-1 AUVs position error drift found in literature – source: *Making AUVs truly Autonomous* – P. E. Hagen, Kongsberg Maritime/Norwegian Defense Research Establishment (FFI) [19]

1.1.2 Dead Reckoning Navigation

Dead reckoning is the most fundamental and intuitive of all navigation systems and requires the least amount of observation. It simply updates the position thanks to a measured velocity vector. However this low cost method is burdened by a soaring position error.

In the case of a glider, where place and energy budget are key limiting factors, it seems difficult to run a full INS positioning system. That's why a kind of low cost position estimation process has been chosen in most existing coastal gliders. Thus, measurement devices that can be found onboard a glider are:

- Attitude sensor measuring pitch and roll
- Electronic compass providing the magnetic heading
- Depth sensor

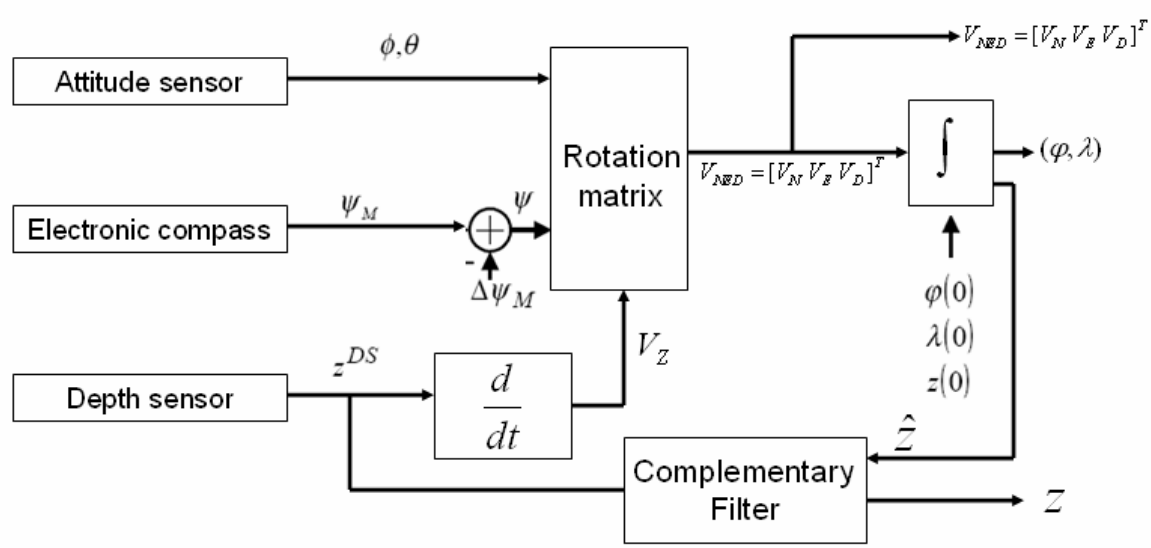

Figure 1-5 Structure of the positioning process for a glider

The main objective of this paper is to develop and test a simulation tool to combine this low cost positioning process (figure 1-5) with a terrain navigation algorithm and to examine the range of expected accuracy.

1.2 *External Navigation*

1.2.1 Radio Navigation

Unfortunately, due to the attenuation in sea water of Global Positioning System (GPS) radio waves. AUVs can not rely on radio navigation. In this context GPS can only be used when the AUV is surfacing in order to obtain a GPS fix and so to reinitialize the internal navigation process.

1.2.2 Acoustic Navigation

1.2.2.1 Short Baseline Navigation

A hydroacoustic positioning system consists of both a transmitter (transducer) and a receiver (transponder). A signal (pulse) is sent from the mother ship's transducer, and is aimed towards the AUV transponder (figure 1-6). This pulse activates the transponder, which responds immediately to the vessel transducer.

Figure 1-6 Acoustic Navigation SBL- source: www.geo-marine-tech.com

The transducer, with corresponding electronics, calculates an accurate position of the transponder relative to the vessel. The calculation of positioning is based on range, and on vertical and horizontal angle measurements, from a single multi element transducer. The system provides three-dimensional transponder positions relative to the vessel. In deep water, deploying and following the AUV with a survey vessel is the preferred method for obtaining maximum position accuracy. Product specifications state that the position accuracy of single measurements from the standalone HiPAP (High Precision Acoustic Positioning - Kongsberg) is in the order of 0.2% of the range (line of sight from the surface ship to the AUV).

1.2.2.2 Long Baseline Navigation

Long Baseline navigation systems use an array of acoustic beacons. The calculation of position is based on range measurements only. The AUV interrogates the LBL network, and uses the reply from each transponder to calculate the range from the AUV to the transponders, and so its position thanks to a least square algorithm process (figure 1-7).

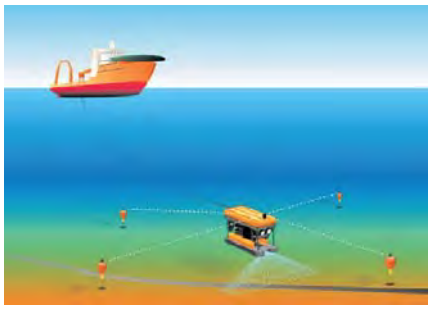

Figure 1-7 Long Baseline beacons' array – source: Kongsberg maritime

However, the location of these beacons must be determined in a very precise and accurate way. Thus, the cost in time, equipment and effort is very expensive, especially when the beacon network is significant and set in a fairly deep area far from shore. Moreover, the vehicle is constrained to stay within the acoustic range of the array.

1.2.3 Geophysical Navigation

Given the cost of the previous underwater navigation systems, there has been an increasing interest in geophysical navigation systems based on the knowledge of:

a) The earth's gravitational field

b) The earth's magnetic field

c) Bathymetry

Those systems require a priori maps. To make it simple, both gravitational field and magnetic field anomalies can be viewed as beacons, and the AUV thanks to field intensity measurements estimates its position in this array.

a) The Earth's gravitational field fluctuates due to local variations in topography and geology. It is theoretically possible to use either gravity variations or anomalies for navigation.

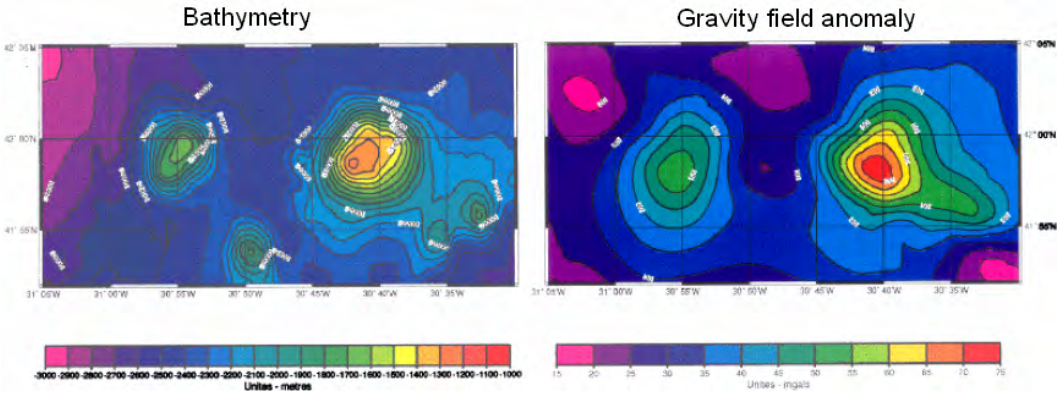

Figure 1-8: Earth's gravity field anomaly – correlation between bathymetry/Gravity field anomaly (source: Ensieta Geophysics lecture – Lalancette, Shom)

b) The International Geomagnetic Reference Field (IGRF) is a global model of the geomagnetic field. It allows spot values of the geomagnetic field vector to be calculated anywhere from the Earth's core out into space. The IGRF websites provides codes that allow computing the global magnetic field intensity. The figure 1-8 is the representation of this global magnetic field.

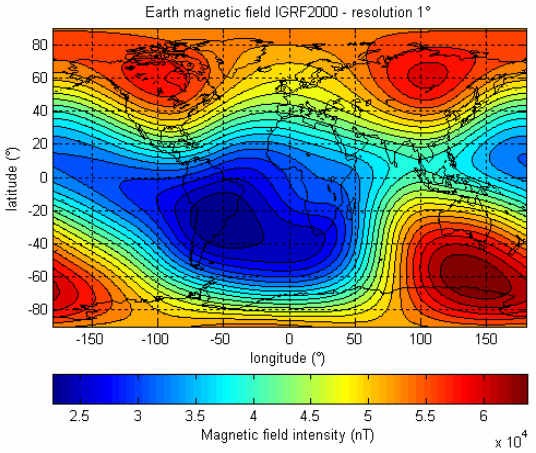

Figure 1-9 Earth's magnetic field intensity (nT) – IGRF

c) Bathymetry is the third geophysical parameter, the terrain based navigation principles for underwater vehicles are discussed in papers [2], [5], [7], [9], [17]. The idea is to exploit known natural features of the seafloor in order to estimate the AUV position. The terrain-based navigation is the focus of this paper and will be developed in the following chapter.

2 Terrain Based Navigation

2.1 *Principle*

The terrain navigation has been developed in 1958 to bound the error drift of cruise missile inertial navigation system. Thanks to comparisons between measurements and pre-assigned trajectory, the terrain contour matching algorithm (TERCOM) of the missile was able to bring itself back on the right track and to reset its inertial navigation system.

In theory, Terrain navigation is very simple and consists in the correlation between a pre-obtained digital terrain model of the seafloor and bathymetric measurements from onboard sensors. As a result the AUV position within this Digital Terrain Model (DTM) may be estimated.

It seems in fact natural to exploit known natural features to estimates the position. Oceans seafloor represents a strong source of information with a unique significant variability. The figure 2-1 represents the bathymetric chart of the Arctic Ocean.

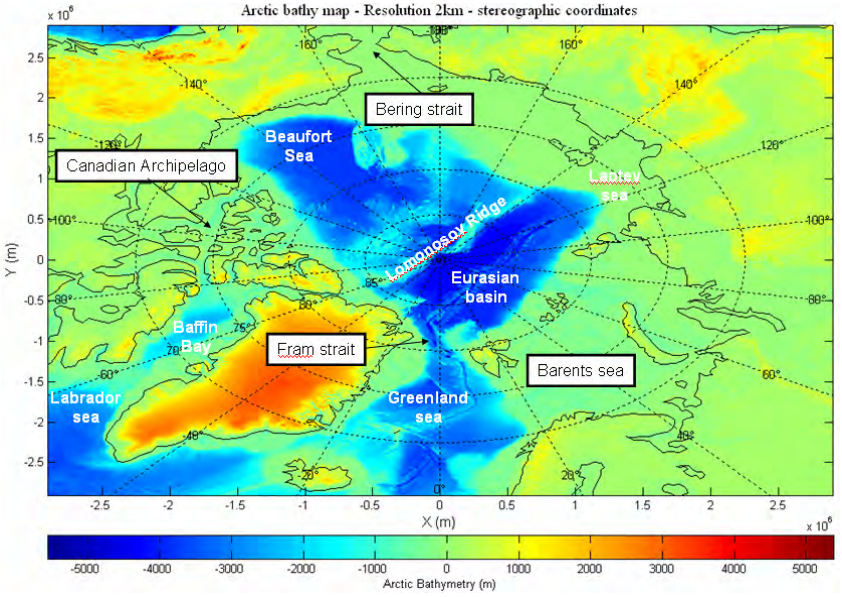

Figure 2-1: IBCAO International bathymetric chart of Arctic Ocean Resolution 2 km

We can clearly outline that even if it presents abyssal plains, the Arctic seafloor also presents a high variability. Thus nowadays, thanks to former explorations' legacy and given continuous improvements in multibeam echo sounders, oceans' seafloor is increasingly understood, making the terrain navigation a promising alternative for underwater positioning.

2.2 *Bayesian Reasoning*

We have to keep in mind that what we want to estimate is the position of the glider. As for any other position estimation process, we can not be sure of the exact position. However we can define a probability density function (*pdf*) that represents a possible area of where the glider could be. The Bayesian approach provides a general framework for the estimation of the state of the glider, This Bayesian approach is discussed in [1] and [4] and provides the framework for the estimation of the state of our glider. The idea is to incorporate information provided by a priori maps into the estimation process. By using Bayesian methods, it is possible to incorporate bathymetric observations into the navigation loop in order to establish the probability distribution of the glider's position.

Bayes' theorem adjusts probabilities of a hypothesis H given new evidence E in the following way:

$$p(H \mid E) = \frac{p(E \mid H)\, p(H)}{p(E)} \qquad \textbf{(1)}$$

- H represents a specific hypothesis
- $p(H)$ is called the prior probability of H that was inferred before new observation
- E is the observation or evidence
- $p(E \mid H)$ is called the conditional probability of seeing the evidence E if the hypothesis H happens to be true. It is also called a likelihood function when it is considered as a function of H for fixed E.
- $p(E)$ is called the marginal probability of E: the a priori probability of witnessing the new evidence E under all possible hypotheses.
- $p(H \mid E)$ is called the posterior probability of H given E.

Thus the Bayesian method can be applied for terrain navigation. In our context we want to adjust the probability of our glider's position given a bathymetric observation.

$$p(x_k \mid x_0, \alpha_j, z_j)_{j=1:k} = \frac{p(z_k \mid x_k)\, p(x_k \mid x_0, \alpha_j, z_j)_{j=1:k-1}}{p(z_k \mid x_0, \alpha_j, z_j)_{j=1:k-1}} \qquad \textbf{(2)}$$

$p(x_k \mid x_0, \alpha_j, z_j)_{j=1:k}$ is the posterior probability of the glider's state

$p(z_k \mid x_k)$ is the conditional probability, it can be seen as a likelihood function

$p(x_k \mid x_0, \alpha_j, z_j)_{j=1:k-1}$ is the prior probability that was inferred thanks to the dead reckoning process

$p(z_k \mid x_0, \alpha_j, z_j)_{j=1:k-1}$ is the marginal probability of the bathymetric observation

Here, we are acting recursively given the last GPS fix position known, by first predicting the prior probability of x_k from the previous posterior probability of the position x_{k-1} and the action taken α_k, and then updating using the latest bathymetric observation z_k in order to obtain the posterior distribution of the position x_k. The figure 2-2 illustrates this principle.

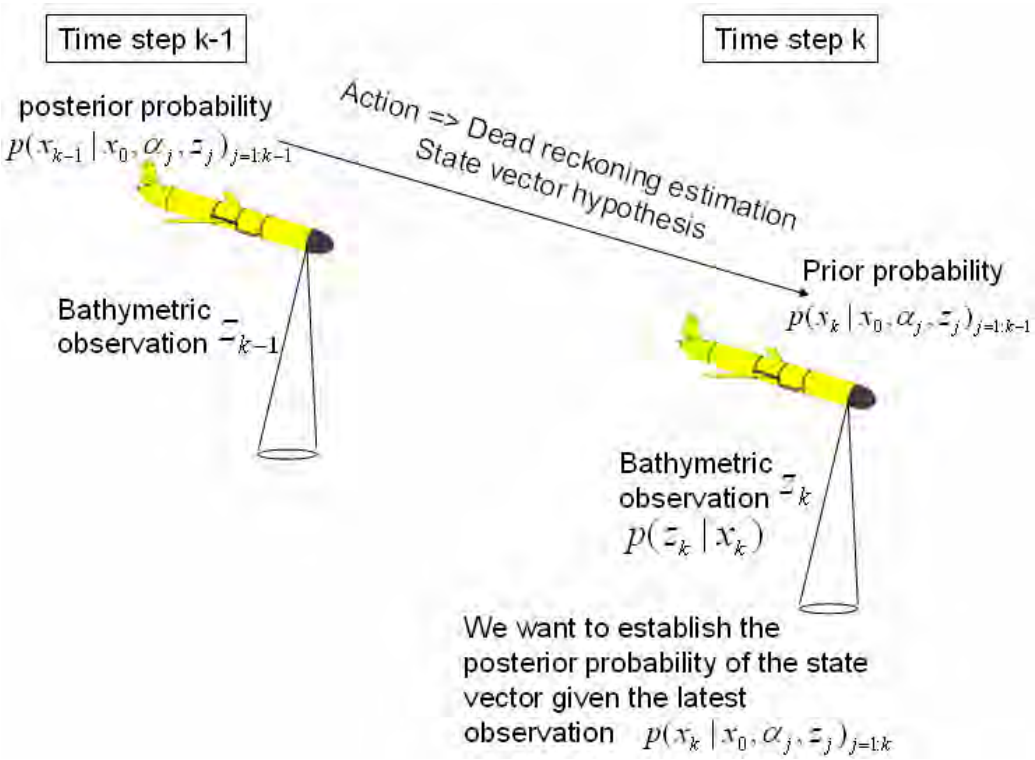

Figure 2-2 Bayesian reasoning

2.3 *Kalman filter*

As outlined in the previous section, the terrain navigation consists in the assimilation of an observation, here the depth of the glider, into the navigation process. In this context the Kalman filter could be an efficient computational means to estimate the state of the glider. The Kalman filter minimizes the mean of the squared error [13].

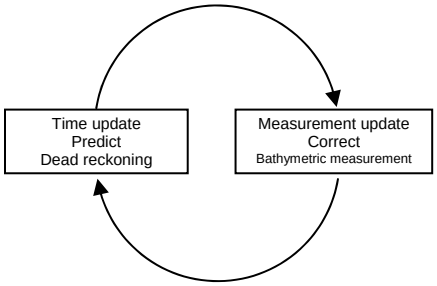

Figure 2-3: The Kalman filter estimates the glider position using a feedback control

Measurement update equation:

$$\hat{x}_k = \hat{x}_k^- + K(z_k - H\hat{x}_k^-) \qquad \textbf{(3)}$$

With: $\hat{x}_k$ a posteriori state estimate

$\hat{x}_k^-$ dead reckoning estimate

z_k actual bathymetric measurement

K gain or blending factor

$H\hat{x}_k^-$ predicted measurement

The matrix K is chosen in order to minimize the error covariance

$$P_k = E[e_k e_k^T] = E[(x_k - \hat{x}_k)(x_k - \hat{x}_k)^T] \qquad \textbf{(4)}$$

One form of the matrix K that minimizes this error covariance is:

$$K_k = \frac{P_k^- H^T}{HP_k^- H^T + R} \qquad \textbf{(5)}$$

- If the measurement error covariance R is close to zero, the gain K gives more weight to the residual $(z_k - H\hat{x}_k^-)$, thus the bathymetric measurement z_k is increasingly trusted.

- If the a priori estimate error covariance P_k^- approaches zero, the dead reckoning state estimate has now a more significant weight.Thus, the Kalman filter computes an estimate of the state of a discrete-time controlled process that is governed by a linear stochastic difference equation.

$$\hat{x}_k^- = A\hat{x}_{k-1} + Bu_{k-1} + w_{k-1} \qquad \textbf{(6)}$$

$\hat{x}_k^-$ dead reckoning estimate of the state at step k — B : control input matrix — u_{k-1} : control input

$\hat{x}_{k-1}$: posterior probability of the state at step $k-1$ — A : transition matrix — w_{k-1} : process noise

However, given that glider's physical parameters evolve along the trajectory, its evolution can not be described by a simple linear relation, the transition matrix A can not be constant. We have to consider a non linear evolution (f : non linear function):

$$\hat{x}_k^- = f(\hat{x}_{k-1}, u_{k-1}, w_{k-1}) \qquad \textbf{(7)}$$

In this context, we have to use a Kalman filter that linearizes the estimation around the current estimate using the partial derivates of the process and measurement functions. This technique is called Extended Kalman Filter (EKF). However in this paper we focus on another means, the particle filter, which has a strong ability to describe non linear model and non-Gaussian noises.

2.4 *Particle filter*

2.4.1 Principle

The core of the particle filter is the estimation of the probability density function. The particle filter enables a promising solution to the combined task of navigation and tracking [18]. The particle filter models an unknown probability distribution by a large number of samples. Given sufficient particles, the distribution will provide an accurate model of the underlying process it is attempting to describe. In other words, the interest of the particle filter lies in the fact that the cloud of particles gives an estimation of the position using a discrete representation of a probability density function. The figure 2-4 represents the evolution of the probability density function using the terrain navigation particle filter. It represents the number of particle per cell of a grid. The grid is based on horizontal differences (Δx and Δy) between the particle position and the real position. Then given the weight distribution (according to a likelihood function) and thanks to the re-sampling process, the cloud of particles evolves until convergence to the real position.

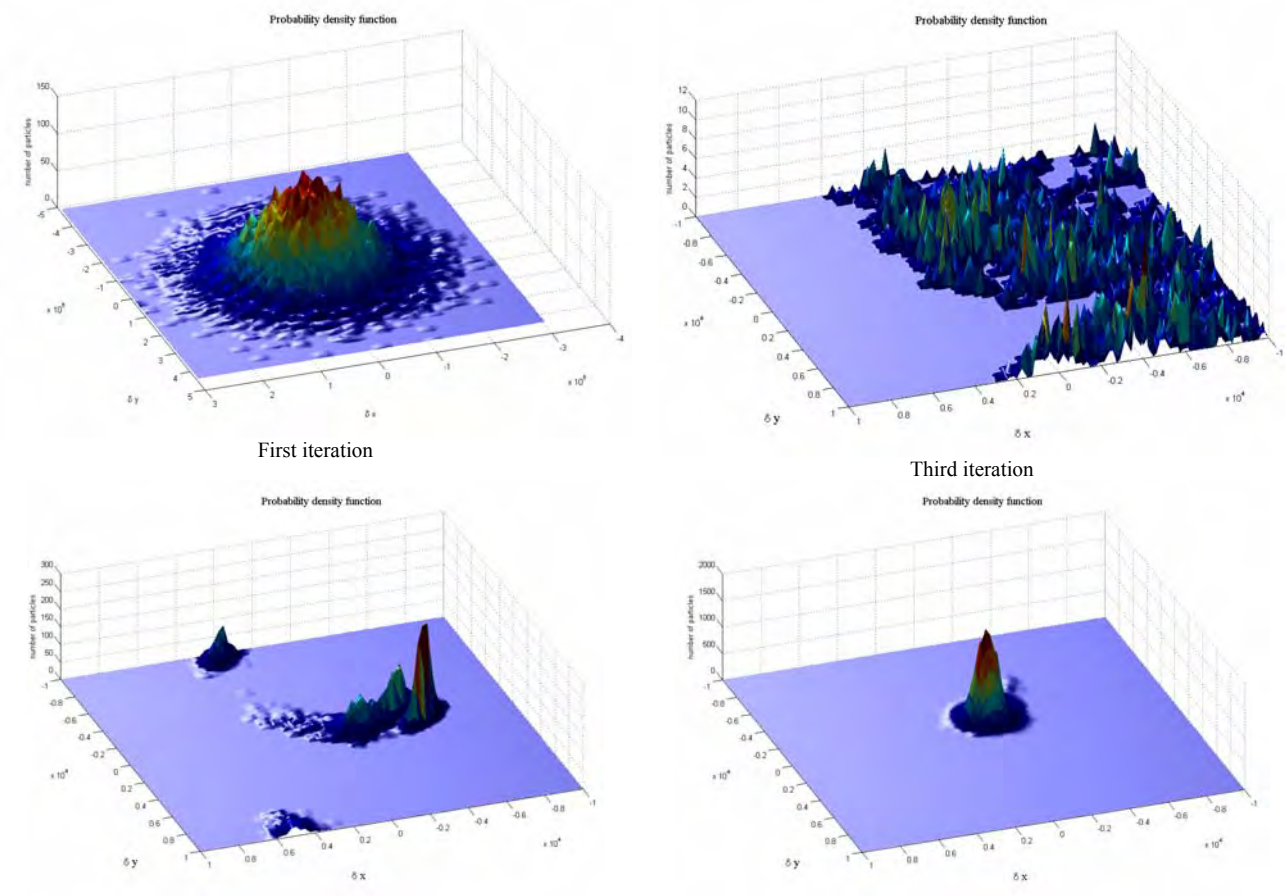

First iteration

Third iteration

Sixth iteration

Fifteenth iteration

Figure 2-4: Probability density function (pdf) evolution (grid 20x20 Km)

The particle filter is also able to efficiently track multi modal and non Gaussian probability densities. The figure 2-5 illustrates this ability on a "*sinus cardinal*" bathymetry

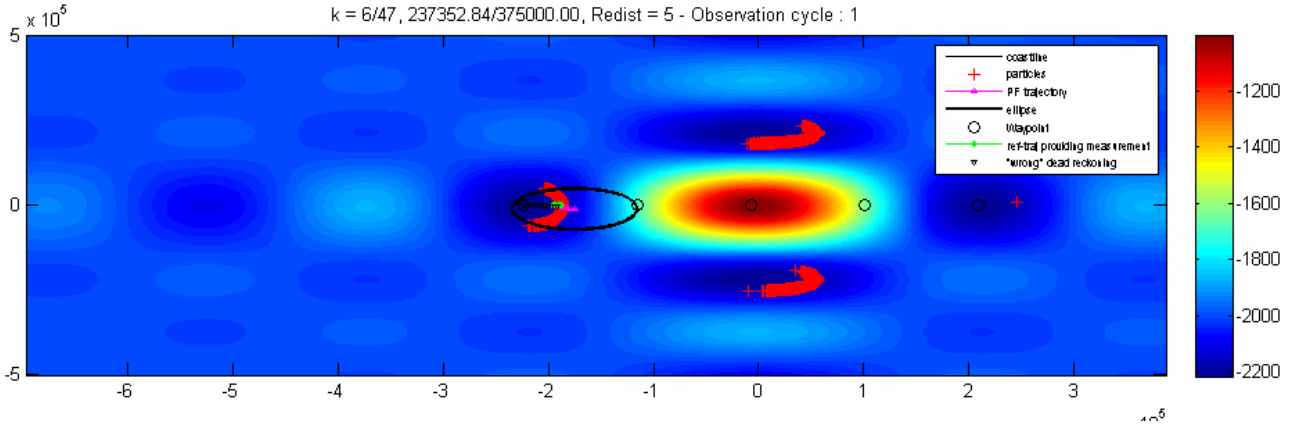

Figure 2-5: multi-modal pdf – particles are represented by red crosses

The particle filter uses an ensemble of particles representing the random variable of interest. Each one of those particles is associated with a weight that represents the confidence on that particle given the bathymetric observation. Then, an estimate of the variable of interest is obtained by the weighted sum of all the particles.

The particle filter operates in a recursive way and is made of two phases: prediction and update.

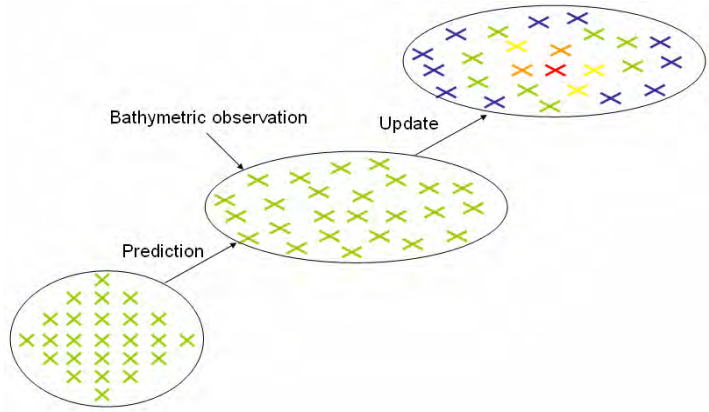

Figure 2-6: Particle filter principle

The prediction stage consists in the propagation of the particle cloud according to the dead reckoning process of the glider. It also includes noises from navigation sensors (electronic compass, attitude sensor, depth sensor).

The update phase uses the information obtained from the single beam echo sounder to update the particle weights (confidence color code on the figure 2-6). At times the particles with infinitesimally small weights are eliminated thanks to the re-sampling process.

2.4.2 Prediction stage

As underlined before, the prediction phase is the step when both particles and the current state of the glider are projected forward in time using a kinematics model. The prior probability $p(x_k \mid x_0, \alpha_j, z_j)_{j=1:k-1}$ used in equation (2) has to be established. In order to perform this operation, we need first to establish a glider kinematics model. The figure 2-7 replaces the prediction step in the Bayesian context.

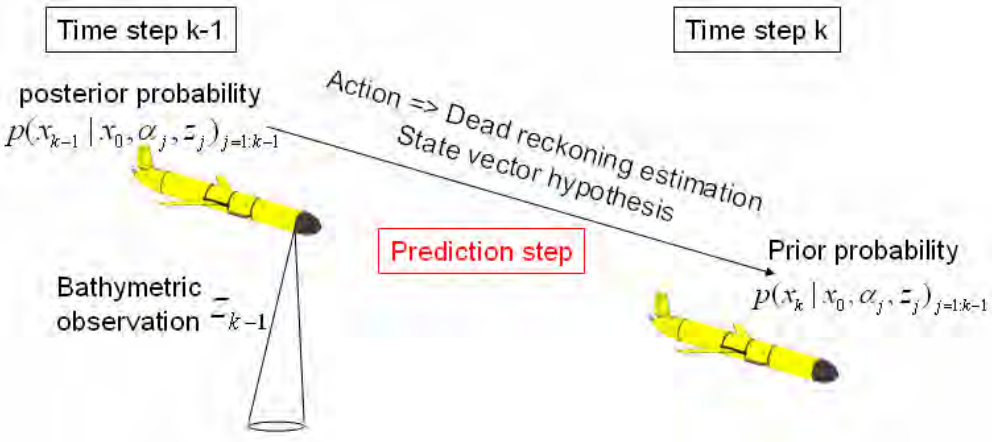

Figure 2-7: prediction step in the Bayesian framework

2.4.3 Update stage

We want here to establish the likelihood function $p(z_k \mid x_k)$ used in equation (2).

The update phase occurs when a new bathymetric measurement is available. It consists in updating the weight of each particle given the likelihood between the real bathymetric measurement and the particle's one. The figure 2-8 replaces the update step in the Bayesian context.

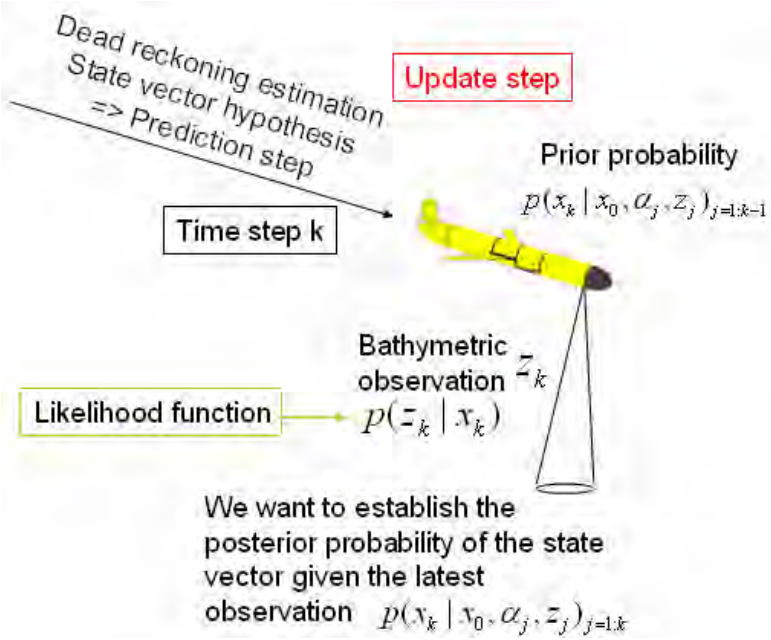

Figure 2-8: update stage in the Bayesian reasoning framework

2.4.4 Particle re-sampling

One of the problems that appear with the use of particle filters is the depletion of the population after a few iterations. Due to the prediction step, most of particles have drifted far enough for their weight to contribute to the pdf. The key point with re-sampling is to prevent high concentration of probability mass at a few particles.

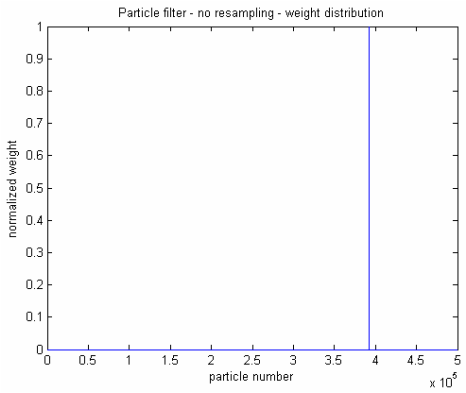

Figure 2-9: weight distribution without re-sampling

Without this step, some weights will converge to 1 and we have a degeneracy of the particle filtering. In papers [1] and [3], some re-sampling methods are outlined. The figure 2-9 highlights what happens if we do not apply re-sampling. The idea of the re-sampling algorithm is to retrieve indices of "significant" particles. When the effective sample size drops below a fixed threshold, the particle population is resampled. In every case, the input is an array of the weights of particles (normalized to sum up to one) and the output is an array of indices that indicates which particles are going to propagate forward. The premise of the algorithm is that particles with high weights are going to be duplicated while the particles with small weights are going to be eliminated.

2.4.5 State estimation thanks to the particle cloud

In order to describe the particles' cloud and also to find an estimation of the possible current position of the glider we have to compute the two first statistic moments:

- Mean

We saw that the likelihood function gives a weight to each particle according to the likelihood between the depth measured and the depth seen per each particle. In this context the estimated depth by the particle filter is a simple weighted sum. Equation (8) is the example on the depth. The mean will give an idea of the accuracy of the filter.

$$z_{PF} = \frac{\sum_{i=1}^{N} w_i z_i}{\sum_{i=1}^{N} z_i} \qquad \begin{array}{l} z_{PF} \text{ : estimated depth} \\ w_i \text{ : weight attributed to particle i} \\ z_i \text{ : depth at particle "i" 's location} \end{array} \qquad \textbf{(8)}$$

- Variance

The variance of a random variable or distribution is the expectation, or mean, of the squared deviation of that variable from its expected value or mean. Thus the variance is a measure of the amount of variation within the values of that variable, taking into account all possible values and their probabilities or weightings. In other words, it describes how far values (position or depth seen per each particle for example) lie from the mean.

$$\mathrm{var}(Z) = \begin{pmatrix} z_1 - z_{PF} & z_2 - z_{PF} & \dots & z_N - z_{PF} \end{pmatrix} \begin{pmatrix} w_1 & & & 0 \\ & w_2 & & \\ & & \ddots & \\ 0 & & & w_N \end{pmatrix} \begin{pmatrix} z_1 - z_{PF} \\ z_2 - z_{PF} \\ \vdots \\ z_N - z_{PF} \end{pmatrix} \quad \textbf{(9)}$$

Thanks to those two statistics moments we are able to describe the particles' cloud distribution and so to establish the uncertainty on the estimated position. The figure 2-10 illustrates the evolution of uncertainty ellipse on particle filter estimated position. We can also easily imagine to give an uncertainty ellipsoid on estimated position.

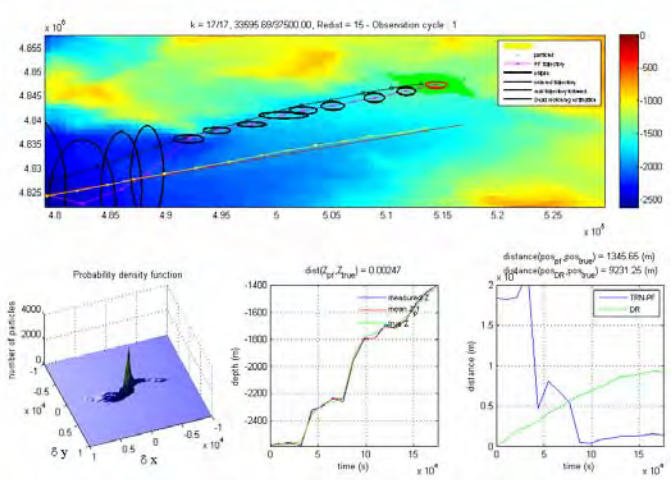

Figure 2-10: Particle filter – 2D uncertainty ellipse on positioning

The figure 2-11 illustrates the evolution of the uncertainty ellipsoid we have with the use of the TBN-PF algorithm. We can clearly see an improvement in the confidence we have on the estimated position with the increasing number of observation. We can notice that thanks to the accuracy of the pressure sensor, the vertical uncertainty beside can be significantly reduced.

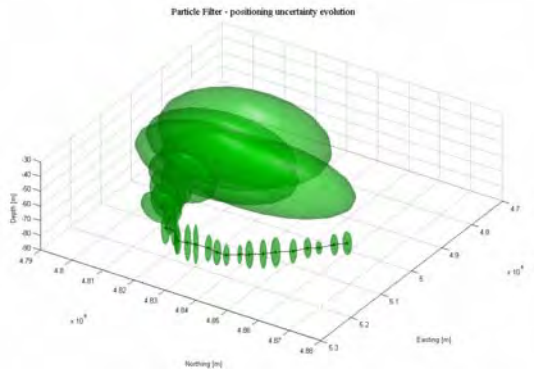

Figure 2-11: TBN-PF uncertainty ellipsoid of estimated position

3 Terrain Based Navigation Particle Filter algorithm (TBN-PF)

3.1 *Particle Filter implementation*

3.1.1 Prediction step

This section defines the simple kinematics model used to propagate forward in time the state of both glider and particles.

3.1.1.1 Glider's dynamic

In situ, navigation sensors provide all the data needed. Those sensors are for example:

- Single beam echo sounder
- Pressure sensor
- Speed sensor
- Magnetic compass, …

But here, in the context of a simulation we have to provide data to the filter, thus we have to create a trajectory of reference. This trajectory of reference will contain information such as (for each time integration step):

- Pitch angle
- Position
- Heading
- Time

Thanks to this data we are able to generate "virtual noisy" measurements that the glider is going to sample. Virtual measurements such as:

- Glider's instantaneous speed (used for the dead reckoning process)
- Bathymetry

In order to create this upstream desired trajectory, the user defines:

1- Waypoints location: waypoints must be loaded in latitude/longitude decimal

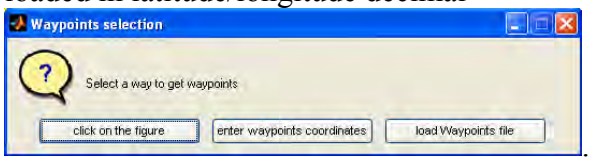

2- If he wants the glider to surface at each waypoint

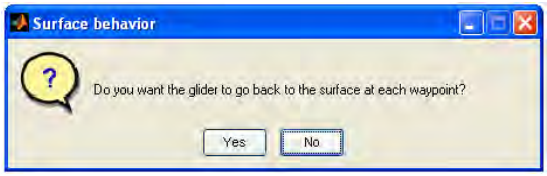

3- The pitch angle of diving and climbing

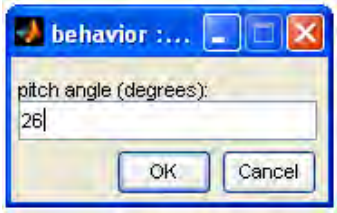

4- The diving and climbing target depths

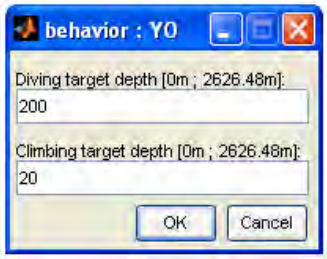

5- The pinging policy

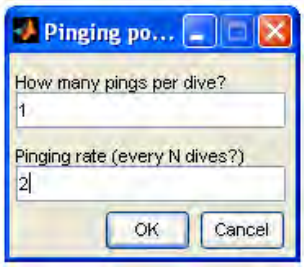

All those simulation parameters will allow to define the desired trajectory.

Red dots on the figure 3-1 represent here bathymetric observations.

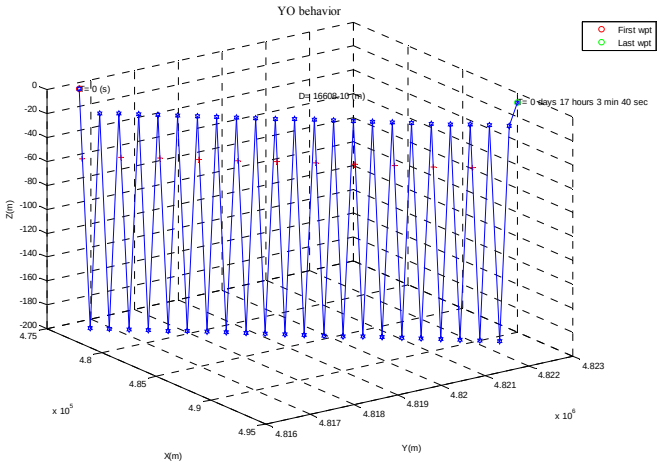

Figure 3-1: generation of the reference trajectory

3.1.1.2 Glider's navigation estimation model

Being able to generate virtual measurements, we can now define the dead reckoning process. Central for all navigation and tracking applications is the motion model to which various kinds of filters can be applied. Models which are linear in the state dynamics and non-linear in the measurements are considered:

$$X_{k+1} = f_k(X_k, u_k, w_k)$$
$$z_k = h_k(X_k) + v_k \qquad \textbf{(10)}$$

X_k : state vector — w_k : process noise — v_k : measurement error

u_k : measured input — z_k : observation — f_k : linear function

The application considered in this work is the estimation of the vehicle horizontal position subjected to a current field. A simple model that is suitable in this case is a two dimensional horizontal plane kinematics model fed by a two dimensional current field averaged along the depth. The model parameters include also the vehicle heading θ, the pitch φ and the vertical velocity V_z [15]. In our case, if we consider a simple dynamic model based either on a constant speed during each integration time step or a speed measurement:

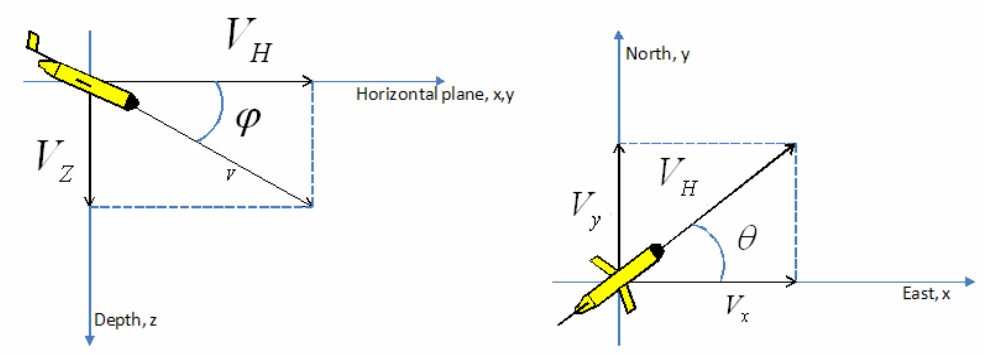

Figure 3-2: Glider evolution

The glider evolves in the vertical plane along a *yo-yo* segment (descending or ascending) and in absence of currents navigates with a pitch angle φ and a constant vertical velocity V_z which is a nominal parameter of the glider's specification (see figure 3-2). The discrete state space equation estimates the (x_k, y_k) position of the glider at the k^{th} time instant, knowing the position (x_{k-1}, y_{k-1}), the horizontal plane velocity module $V_{H,k-1}$, the glider heading angle θ_{k-1} at the $(k-1)^{th}$ time instant and the current components $(u(x_{k-1}, y_{k-1}), v(x_{k-1}, y_{k-1}))$ at the previous location is given by the following equations:

$$x_k = x_{k-1} + \Delta T(\dot{x}_{k-1} + U_{x,k-1} + u(x_{k-1}, y_{k-1}) + w_{k-1}) \quad \textbf{(11)}$$

$$y_k = y_{k-1} + \Delta T(\dot{y}_{k-1} + U_{y,k-1} + v(x_{k-1}, y_{k-1}) + w_{k-1}) \quad \textbf{(12)}$$

where U_{k-1} refers to the command law (set to 0 in the glider's case), w_{k-1} stands for the noise on speed measurement and ΔT is the integration time step.

We can also define speed. We consider here that without measurements we keep the same speed as the previous step.

$\dot{x}_k = \dot{x}_{k-1}$ *or* $\dot{x}_k = measured_{speed} + w_{k-1}$

$\dot{y}_k = \dot{y}_{k-1}$ *or* $\dot{y}_k = measured_{speed} + w_{k-1}$

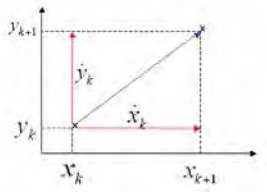

$\dot{x}_{k-1} = V_{H,k-1}\cos(\theta_{k-1})$

$\dot{y}_{k-1} = V_{H,k-1}\sin(\theta_{k-1})$

3.1.1.3 Algorithm implementation

The state vector to be estimated using particle filter is $X = (x \quad \dot{x} \quad y \quad \dot{y})^T$ and contains both positions and velocities in the horizontal plane.

The state dynamics can be modeled as:

$$X_{k+1} = F_k X_k + G_k^u U + N(0,Q) \quad \text{with} \quad \begin{matrix} Q = \text{cov}(G_k w_k) = \text{E}(G_k w_k (G_k w_k)^T) \\ G_k = (\Delta T \quad 1 \quad \Delta T \quad 1)^T \end{matrix} \qquad \textbf{(13)}$$

writing this model equation in matrix form, we obtain:

$$\begin{pmatrix} x \\ \dot{x} \\ y \\ \dot{y} \end{pmatrix}_{k+1} = \begin{pmatrix} 1 & \Delta T & 0 & 0 \\ 0 & 1 & 0 & 0 \\ 0 & 0 & 1 & \Delta T \\ 0 & 0 & 0 & 1 \end{pmatrix} \begin{pmatrix} x \\ \dot{x}+u \\ y \\ \dot{y}+v \end{pmatrix}_k + \begin{pmatrix} 0 \\ \Delta V_x \\ 0 \\ \Delta V_y \end{pmatrix} + chol(w_k^2 . \begin{pmatrix} \Delta T^2 & \Delta T & 0 & 0 \\ \Delta T & 1 & 0 & 0 \\ 0 & 0 & \Delta T^2 & \Delta T \\ 0 & 0 & \Delta T & 1 \end{pmatrix})$$

chol refers to Cholesky factorization, w_k stands for a the noise on the speed measurement, here represented by a normal distribution $\mathcal{N}(0,1)$, (u,v) are the components of the current field at the "right" location, and $(\Delta V_x, \Delta V_y)$ stands for the command law to apply to reach a point.

Process noise implementation: $N(0,Q)$

We used here the normal distribution centered on zero. The graph of the associated probability density function is bell-shaped, with a peak at the mean.

$$f(x) = \frac{1}{\sqrt{2\pi\sigma^2}} e^{-\frac{(x-\bar{x})^2}{2\sigma^2}}$$

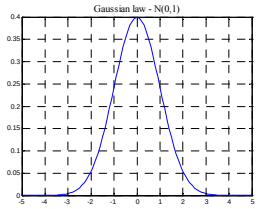

Where $\bar{x}$ and σ^2 are the mean and the variance of the distribution.

The figure 3-3 illustrates the iterative dynamic model implementation (equation 11 and 12) and the current influence on glider's trajectory.

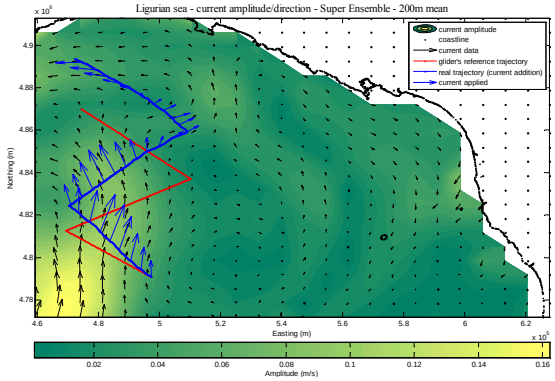

Figure 3-3: taking current into account– desired trajectory (red) – real trajectory followed (blue)

The assumption we are making here is that the glider is not able to assimilate the current in its dead reckoning process (approximately, there are no current's shear which come to modify both pitch and heading of the glider). In other words we can consider the current as a "conveyor" on which the glider is moving.

Thus while the glider believes to follow the reference trajectory (green trajectory), in facts it is constrained by currents and follows the black trajectory of the figure 3-4.

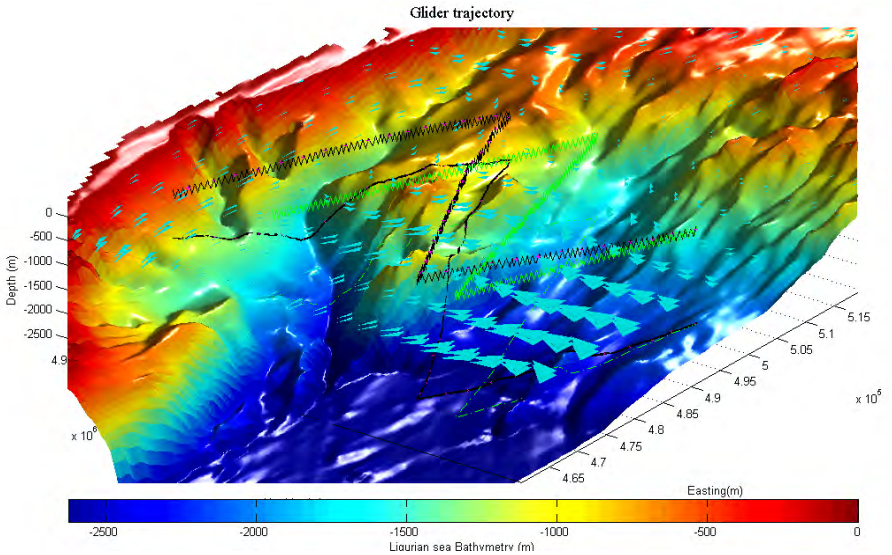

Figure 3-4: 3D view of the glider's trajectory - Desired trajectory (green) – Real trajectory followed (black)

Unfortunately due to a limited energy budget, we can not get a bathymetric measurement at each time step. Thus, given that the prediction phase occurs between two observations, it can enclose many time steps. The figure 3-5 spells out the particle filter principle on the trajectory.

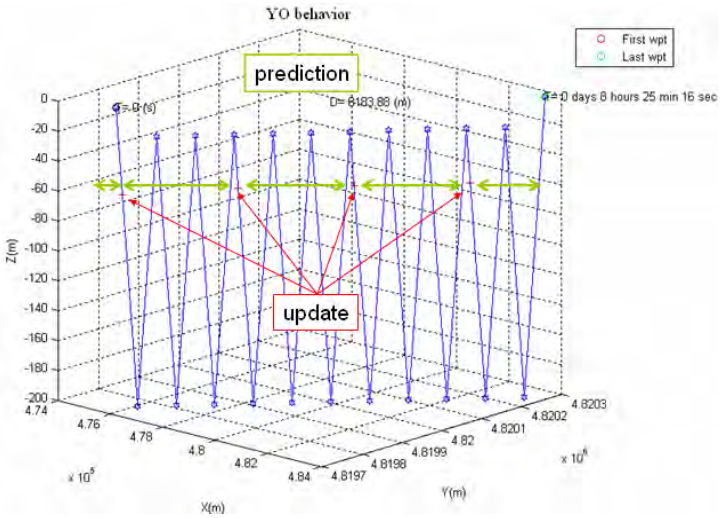

Figure 3-5: Prediction / Update sequence on a glider trajectory – pinging policy of one ping every 3 dive.

3.1.2 Update step

The update step is responsible for the "feedback", in other words this step manages to incorporate a new measurement into the a priori estimation in order to improve the position estimation. As underlined in section 2.4.3 it consists in updating the weight of each particle given the likelihood between the real bathymetric measurement and the particle's one.

3.1.2.1 Likelihood function

The key element of the update phase is the determination of the likelihood function. This mathematical function must represent the conditional probability $p(z_k \mid x_k)$ used in the Bayesian framework equation (2). More the depth seen by a particle is close to the real bathymetric observation and more the weight will be significant.

$$p(z_k \mid x_k) = \frac{1}{\sqrt{2\pi}.\sigma_{bathy}}.e^{\frac{-(Z-Zi)^2}{2.\sigma_{bathy}^2}} \qquad \textbf{(14)}$$

z_i : depth seen by the particle i given its position
Z : bathymetric observation
σ_{bathy} : uncertainty on depth measurement

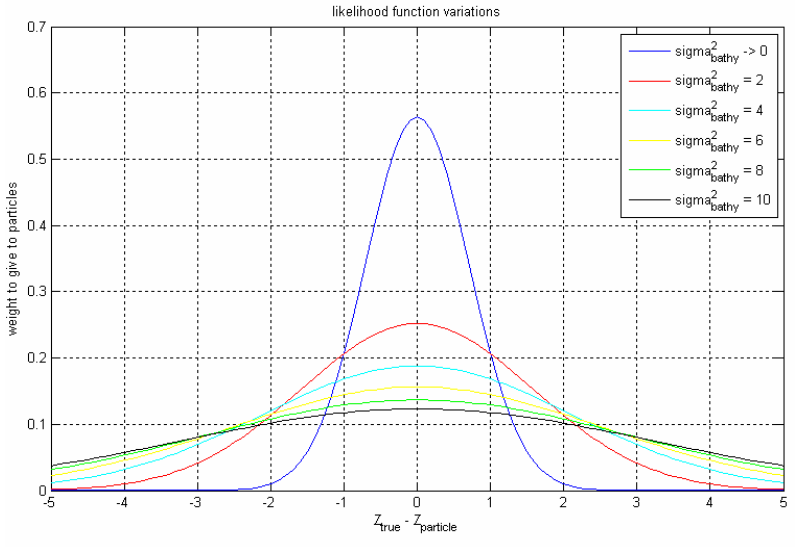

Figure 3-6: likelihood function shape – function of uncertainty

This likelihood function manages the weight distribution of particles given the confidence σ_{bathy} we have in the bathymetric measurement Z. This function leads the convergence of the filter attributing an appropriate weight to each particle. The figure 3-6 highlights that more we

are confident in our measurement more the shape of the function will be sharp. Figures 3-7 and 3-8 also illustrate this idea on a hill.

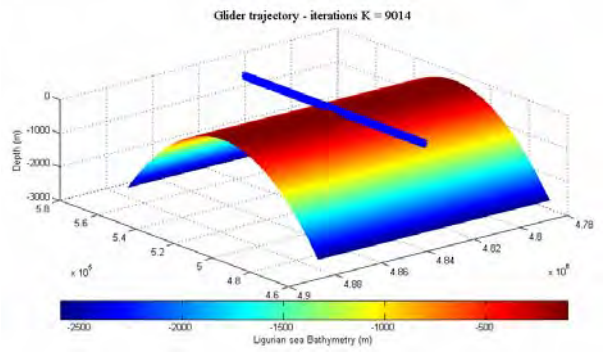

Figure 3-7 Bathymetry as a hill from 3000m to 500m deep

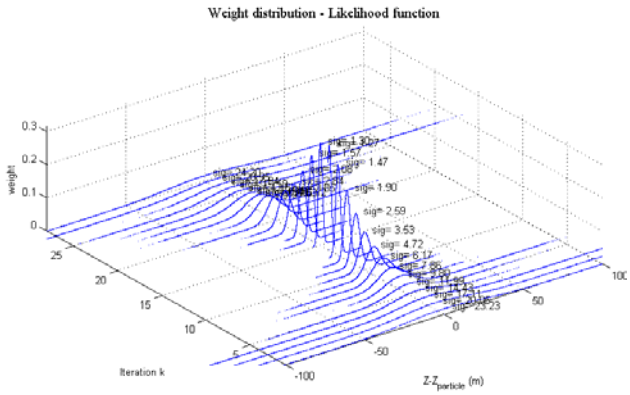

Figure 3-8: thinning of the likelihood function thanks to the confidence's improvement

Thus, the uncertainty on depth measurement σ_{bathy} is crucial because it controls the shape of the likelihood function, and so the convergence process of the filter.

3.1.2.2 Depth measurement uncertainty σ_{bathy}

Measurement's noises act "two" times along the algorithm, on the one hand for the depth measurement itself and on the other hand during the weight attribution to particles where we have to give a confidence to the current measurement.

The acoustic wave path plays a significant role in the accuracy of depth's determination since the acoustic wave is subject to ray bending, transmission losses, ambient noise along its course. In this section, we would like to correlate this measurement uncertainty with the depth.

The figure 3-9 illustrates the "tolerated" variance on depth measurements sampled during a bathymetric survey. Those tolerated variances are obtained thanks to the S44 International Hydrographic Organization (IHO) publication source:

http://www.iho-ohi.net/iho_pubs/IHO_Download.ht.

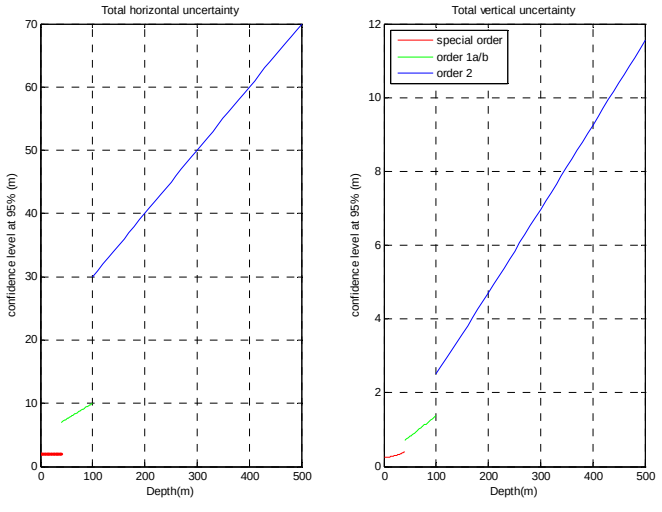

Figure 3-9: IHO S44 tolerated uncertainties – legend applied for both figures

As far as our application is concerned we don't need to reach such accuracy, anyway this publication provides us an idea of the expected accuracy on depth measurement we can have using a sounder.

Bathymetric measurement uncertainty with a single beam echo sounder

As for any kind of measure, we can't be sure at 100% that the depth we are sampling is the "real" depth. Each measurement has its uncertainty depending on the sounder itself, the depth, ambient noise, sound velocity profile… The figure 3-10 illustrates what we understand by the term "uncertainty".

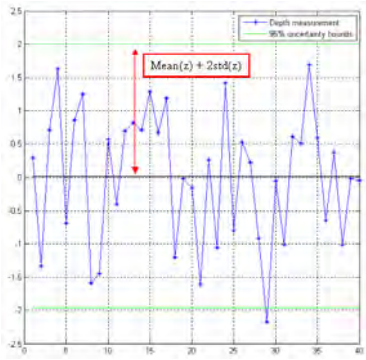

Figure 3-10: measurement uncertainty example

The S44 provides a tolerated uncertainty (Total Vertical Uncertainty) function of the depth:

$$\sigma_{bathyTVU} = \frac{1}{2}\sqrt{1^2 + (0.023z)^2}$$

The figure 3-11 is the implementation of this vertical uncertainty

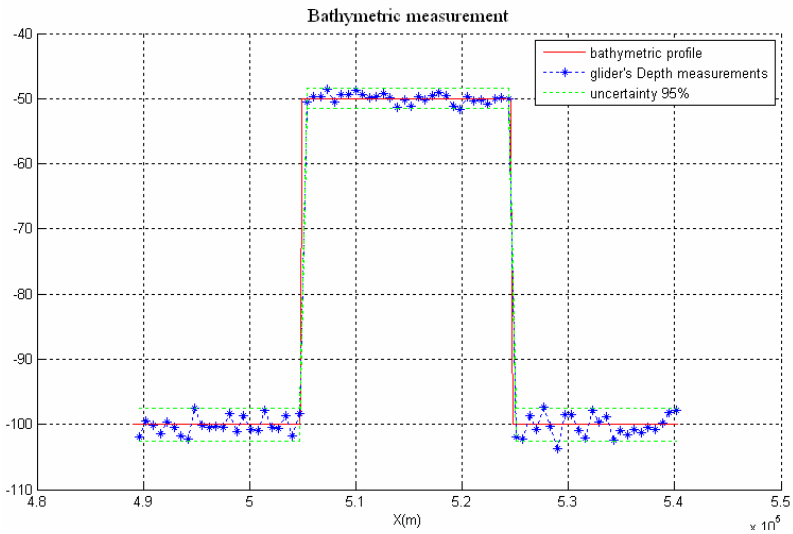

Figure 3-11: Glider's depth measurement with addition of an uncertainty

However, due to the beam footprint we have also a horizontal uncertainty that can lead to a vertical uncertainty. The figure 3-12 illustrates this idea:

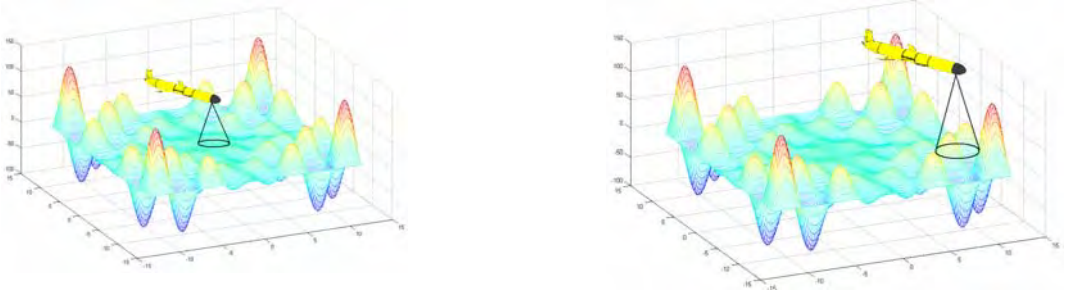

Figure 3-12: low vertical uncertainty due to the beam footprint - high vertical uncertainty due to the beam footprint

The idea consists in saying that if we are pinging on an almost flat area, even if the footprint is "quite big" we are almost confident on the depth measurement. However, if we are pinging on an area that is not

"smooth", we must consider an increasing measurement noise. Given this consideration, we have now to link the horizontal uncertainty with the gradient chart of the area in order to generate a "new" vertical uncertainty. According to the S44 order 2, the horizontal uncertainty is defined as:

$$\sigma_{bathyTHU} = \frac{1}{2}(20 + 0.1z)$$

The bathymetric gradient map, which highlights rough areas, is defined as:

$$gradient_{map} = \sqrt{(\frac{\delta z}{\delta x})^2 + (\frac{\delta z}{\delta y})^2}$$

Figures 3-13 and 3-14 outline the link between the bathymetric and gradient chart on the same area (Ligurian Sea).

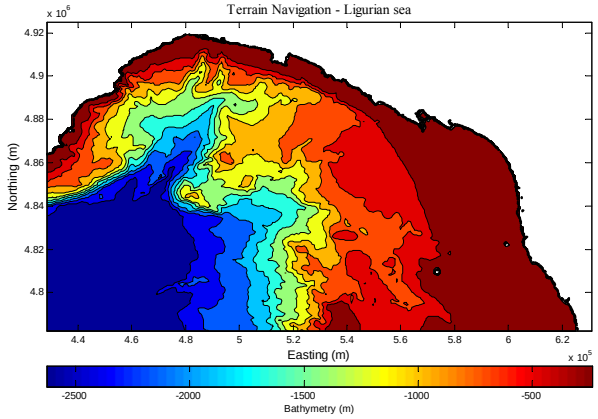

Figure 3-13: bathymetric chart

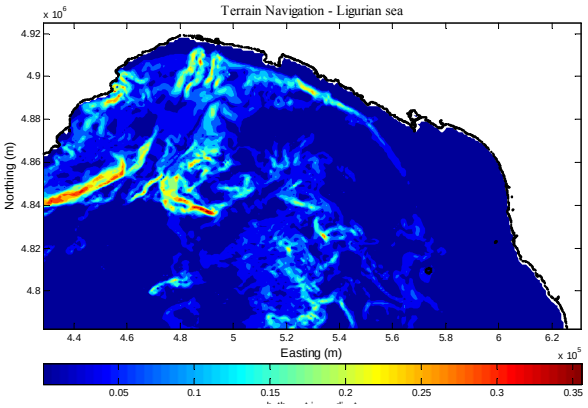

Figure 3-14: Gradient chart

In this context we are now able to define the total measurement uncertainty as:

$$\sigma_{bathy} = \max(\sigma_{bathyTVU}, \sigma_{bathyTHU} \cdot gradient_{map})$$

The figure 3-15 illustrates contributions of both TVU and THU on the total measurement uncertainty:

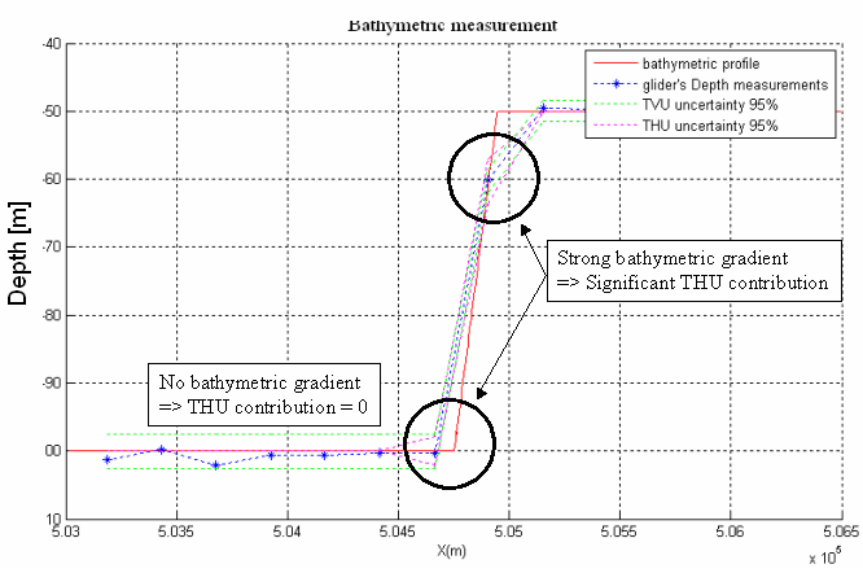

Figure 3-15: Total Vertical Uncertainty and Total Horizontal Uncertainty contributions

3.1.2.3 Weight distribution illustration

Examining the likelihood function, weight distribution is more accurate when the confidence on bathymetric measurement is high (small σ^2_{bathy}). This idea is illustrated on the following example.

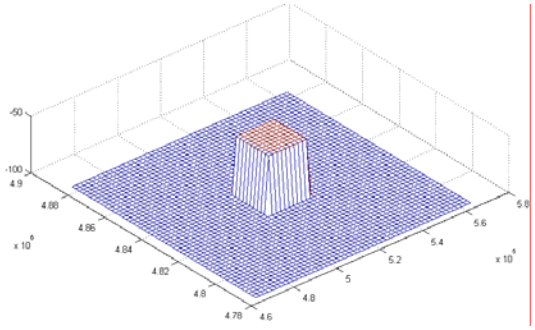

Figure 3-16: DTM to test the weight distribution

The figure 3-17 highlights the idea that with a weak confidence on depth measurement, the shape of the likelihood function has been smoothed. This smoothing of the likelihood function really handicaps the weight distribution as the particle cloud illustrates it.

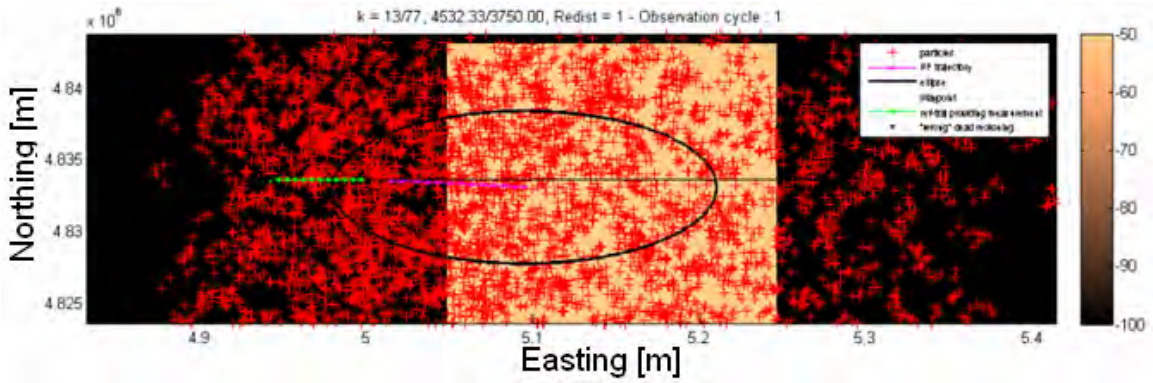

Figure 3-17: particle cloud on a "cubic" bathymetry – low confidence on measurements

But now if we trust our depth measurements, we can observe a much more coherent an accurate weight distribution as illustrated on figure 3-18. Thanks to the likelihood function, particles have now a weight that stands for the confidence we have in it.

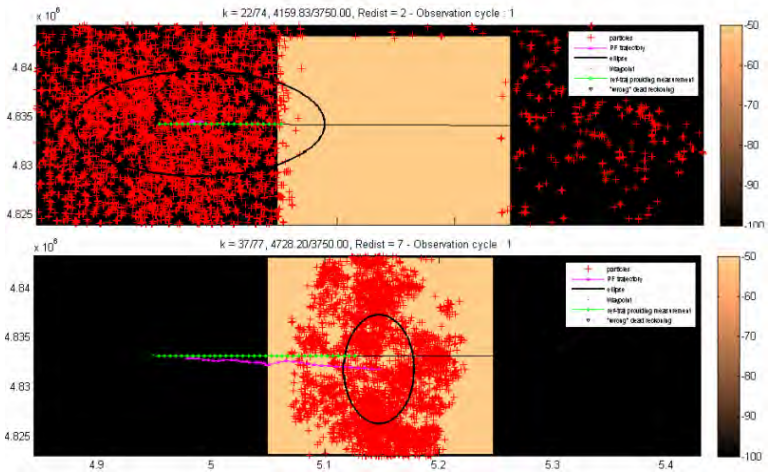

Figure 3-18: particle cloud on a "cubic" bathymetry- high confidence on measurements

3.2 *Outcome: Simulation principle*

- Generation of a reference trajectory with specified waypoints and pitch angle. As seen in the section 3.3.1.1, the user also defines the pinging policy (for example 1 ping every 3 dives on the figure 3-21) and if he wants the glider to go back to the surface at each waypoint.

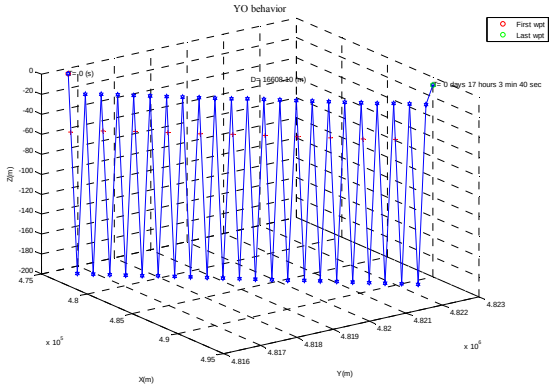

Figure 3-19: desired glider's trajectory

- The algorithm retrieves parameters from this trajectory of reference:
    - Instantaneous pitch and heading angles
    - Indices of bathymetric observations (red dots of the figure above)
    - Indices of surface behavior

- Generation of a global dead reckoning trajectory with "virtual" speed measurements every N seconds, "virtual" pitch and heading angles. This dead reckoning process is not able to detect the sea current and leads both glider and particles.

- Generation of a trajectory constrained by currents. This trajectory will provide depth measurements that feed the particle filter.

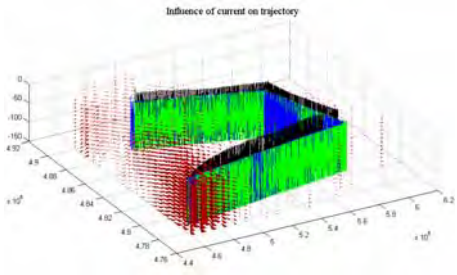

Figure 3-20: Trajectories used for the simulation

- blue line: desired trajectory
- black line: trajectory constrained by currents
- green line: Dead reckoning estimation
- red cones: current

- The glider Dead reckons during the first dive from the last GPS fix to the first bathymetric observation

- The particle filter is applied on the whole underwater cycle, with a sequence of prediction/update.
    - From the last dead reckoning position
    - Glider's dynamic is applied to particles between two consecutive depth measurements (blue step on the figure above)

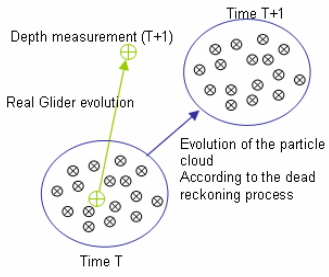

Figure: Simulation principle

- Finally, the glider dead reckons to the surface waypoint.

4 TBN-PF parameters sensitivity and simulation results

4.1 *Simulation Framework*

4.1.1 Bathymetric chart

Bathymetric navigation depends on the availability of a sufficiently accurate map. Two different possible deployment areas have been considered: the Ligurian Sea and the Arctic Ocean.

4.1.1.1 Ligurian Sea

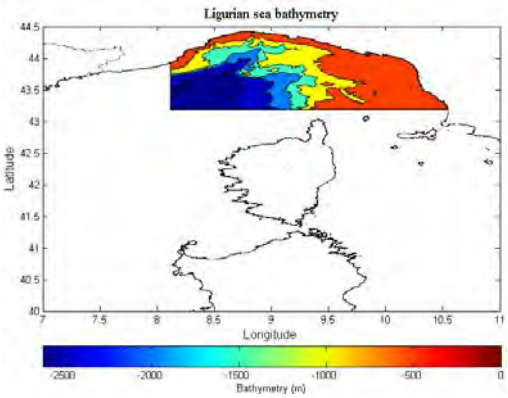

Figure 4-1: Bathymetric data localization

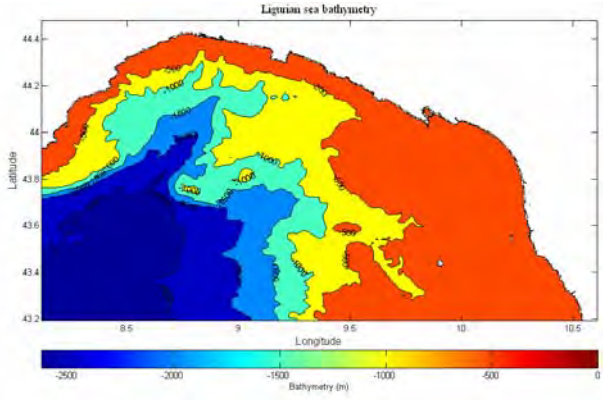

Figure 4-2: Ligurian Sea bathymetry (resolution 700x1000 m) – source: NURC - N.A.TO.

The algorithm works in Universal Transverse Mercator (UTM) coordinates, see annex 1 for coordinates conversion principle.

4.1.1.2 Arctic Ocean

The bathymetric chart of the Arctic Ocean has been provided by the **International Bathymetric Chart of the Arctic Ocean (IBCAO).** The IBCAO pieces together data from the following four archives:

1. the US National Geophysical Data Center
2. the US Naval Research Laboratory
3. the Canadian Hydrographic Service
4. the Royal Danish Administration of Navigation and Hydrography

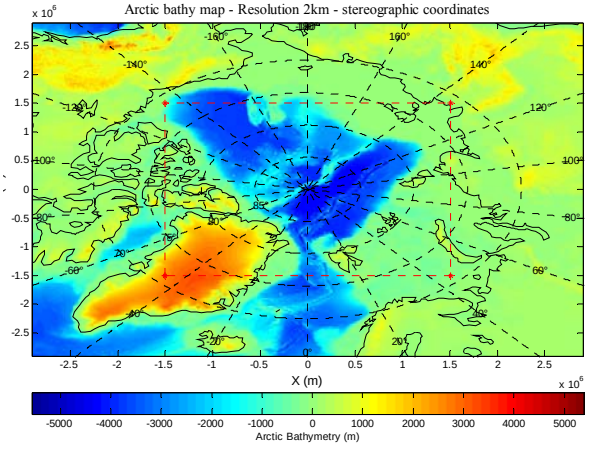

Figure 4-3: Bathymetric chart of Arctic Ocean – resolution 2km – stereographic coordinates
Source: http://www.ngdc.noaa.gov/mgg/bathymetry/arctic/

The algorithm works in stereographic coordinates, see annex 1 for coordinates conversion principle.

4.1.2 Current data

Considering that a glider evolves at a low speed, it is strongly constrained by currents. This simulation tool includes a current data to be as close as the real environment as possible.

4.1.2.1 Ligurian sea current

Current data used here comes from the Super Ensemble method based on 3 different models (Mercator, Mediterranean Ocean Forecasting System, Navy Coastal Ocean Model). This current data is a mean over 4 days (September 2008), and represents the average current over the first 200 meters.

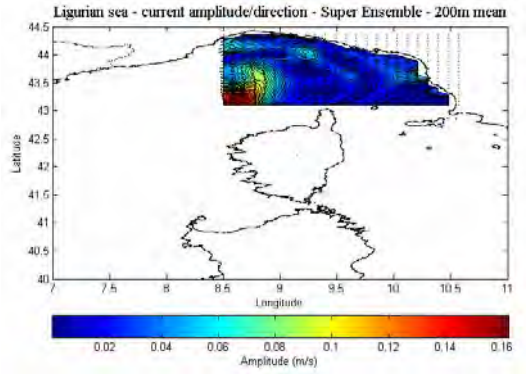

Figure 4-4: Ligurian sea current – data localization

Remark: Super Ensemble method – *source: A review of recent super-ensemble multi-model challenges (Michel Rixen, Baptiste Mourre, Luc Vandenbulcke and Fabian Lenartz)*

To improve forecast skills, data assimilation is generally used to integrate information from satellite and in-situ measurements into the forecasting system. Observations of the ocean surface are routinely provided by Sea Surface Temperature (SST) and Sea Surface Height (SSH) operational satellites. High-frequency coastal radars also measure coastal surface currents in an increasing number of littoral regions. Based on the idea that different models may have different skills in reproducing the ocean state, and these skills probably evolve in time due to the temporal variability of coastal ocean dynamics, multi-model fusion methods have been developed with the aim to improve our ocean forecast skill. One of such method, known as Super Ensemble (SE), produces an optimal weighted model combination which minimizes the mismatch with observations over a specified learning period. This optimal combination is then used to produce an optimal ocean forecast.

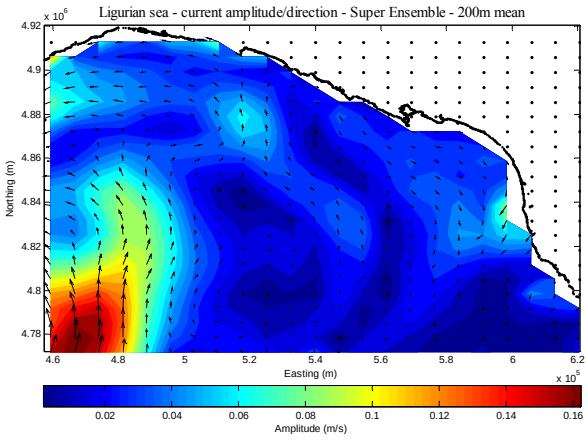

Figure 4-5: Ligurian Sea current – mean 23-26 September 2008

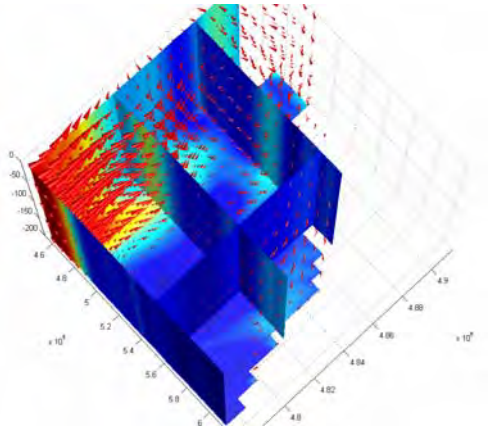

Figure 4-6: Ligurian sea current 3D visualization (using matlab coneplot and slice function)

4.1.2.2 Arctic Ocean circulation

The Arctic Ocean is a semi enclosed sea, constrained by land except for a few connections which establish a link to the Atlantic and Pacific Oceans [14]. These connections are:

- the narrow and shallow Bering Strait (0.8 Sverdrups)
- the narrow but deep Fram Strait (1-2 Sv)
- the broad and shallow Barents Sea (2.2 Sv)
- the small but numerous pathways that make up the Canadian Archipelago.

1 Sverdrup = $10^6 m^3.s^{-1}$
Amazon River debit = 0.2 Sv

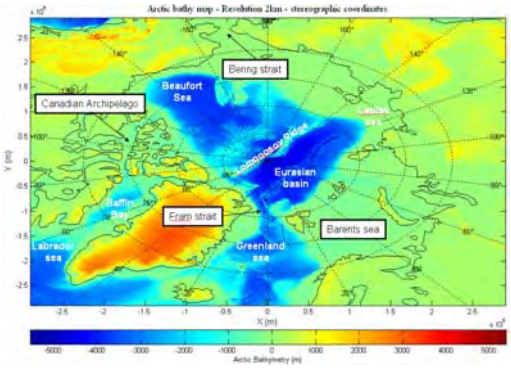

Figure 4-7: Arctic bathymetry - International Bathymetric Chart of the Arctic Ocean (IBCAO)

Although the Arctic occupies 1.5% of the world's ocean surface area, it receives 10% of the river runoff. This large amount of fresh water flux caps the surface of the Arctic with a layer of relatively fresh water which allows the water in the shallow mixed layer to cool to the freezing point.

One third of the Arctic is composed of shallow Eurasian seas (shallower than 200m deep). New ice is usually formed is usually formed in these shallow seas when wind pushes old ice offshore to expose surface water to freezing conditions. In the interior, the large Canadian and Eurasian basins, both reach depths of over 4000 meters. They are separated by the Lomonosov Ridge that transects the Arctic from Greenland to Russia, passing near the North Pole.

Bathymetry is thought to have a large impact on the Arctic circulation. At the shelf break, a rim current travels around the Arctic in a cyclonic direction. At the ridges which transect the interior Arctic, relatively large currents (compared to the basin interiors) have been inferred from the measurements. The deep basins are quiet and sheltered because of minimal of deep convection in the Arctic (aside from a small amount of dense water production from polynyas which are areas of open water surrounded by sea ice). The Canadian Basin is isolated enough so that geothermal heating from the ocean bottom is an important factor for deep mixing [14].

Water masses entering the Arctic from the Pacific and Atlantic have distinct salinity, temperature, and oxygen levels. Those paramaters can be measured to track its progress

throughout the Arctic. The surface waters of the Arctic are relatively cold (below 0°C) and fresh (30-32 psu) compared to Atlantic water (salinity of 35 and temperature greater than 0°C). The water entering from the Atlantic salty enough so that upon entering the Arctic, the warm water mass counter-intuitively sinks below the cold, fresh surface layer of the Arctic.

The end result is an easily tracked warm maximum from about 200m to 800m which is called the Atlantic layer (see figure 4-9). After entering the Arctic through the Fram Strait (east of Greenland) and Barents Sea, the Atlantic layer travels cyclonically around the Arctic and eventually exits back through the Fram Strait. Temperature, salinity and current intensity charts provided by the Mercator model illustrate this statement.

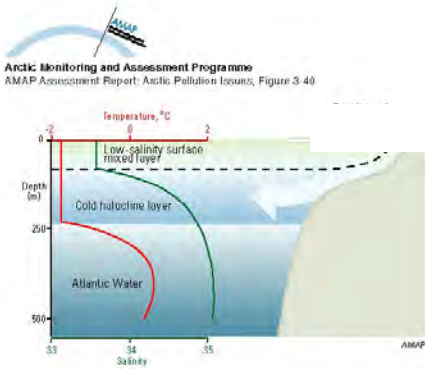

Figure 4-8: Schematic representation of the temperature and salinity structure of the upper Arctic Ocean

At this time, the simulation uses a "virtual" current (figure 4-10) on the area in lack of a real current forecast model of this area.

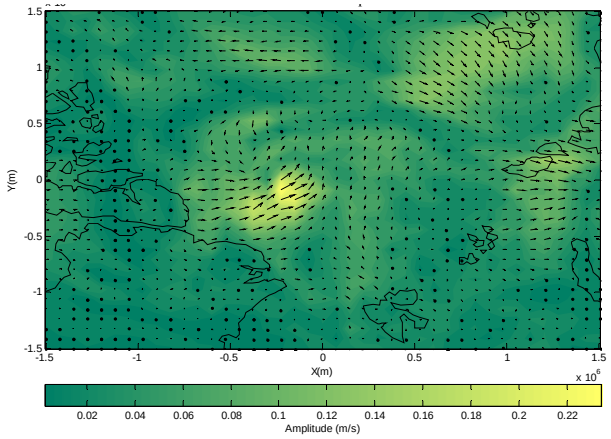

Figure 4-9: Arctic current used in the simulation

Nonetheless, the figure 4-11 highlights the diving entrance of the "warm" north Atlantic water mass, below the cold Arctic water, and resulting in a cyclonic circulation along the border of the Eurasian basin. The figure 4-12 also supports the idea of the cyclonic circulation of a warm and salty North Atlantic water mass below a fresh and cold surface layer. When the Atlantic layer encounters one of the ridges that bisect the Arctic, the current then appears to split with one branch following the bathymetry into the interior and another following the shelf break around the rim towards the Canada Basin.

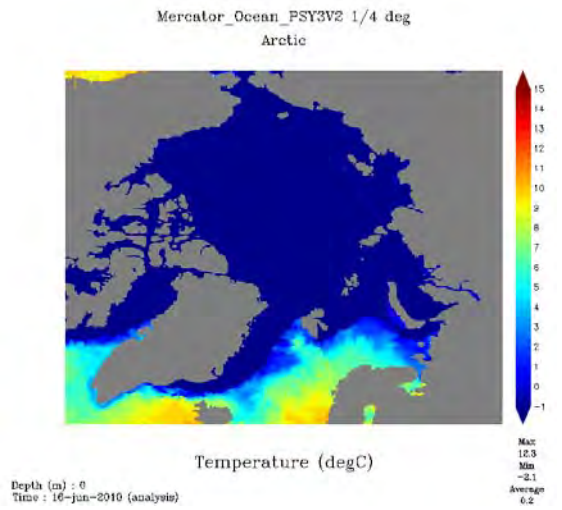

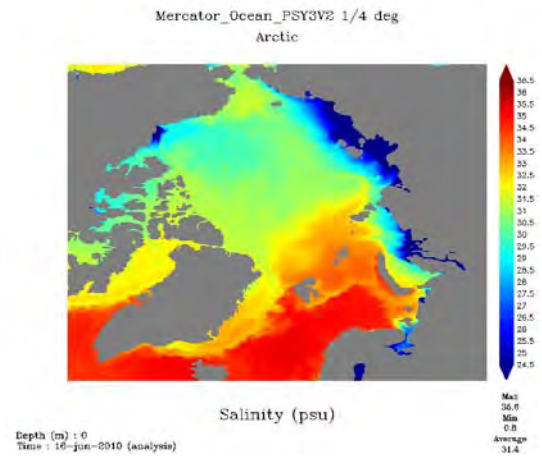

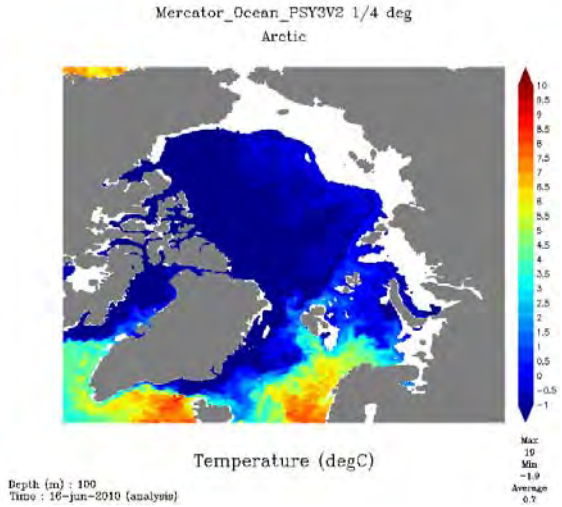

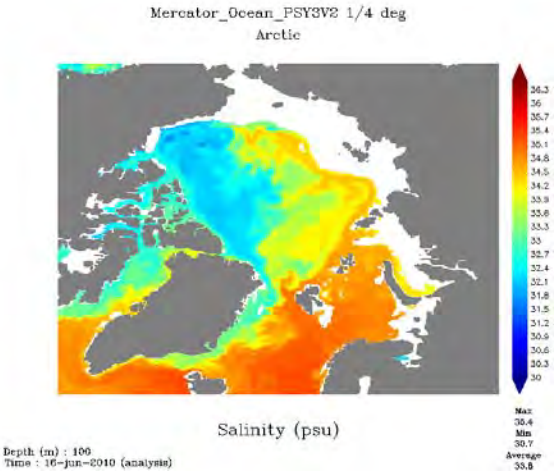

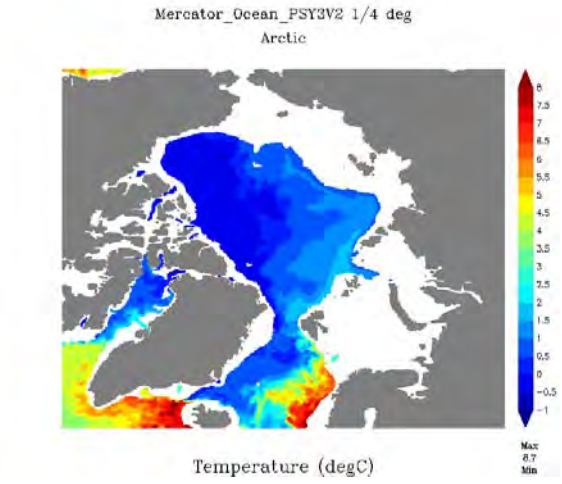

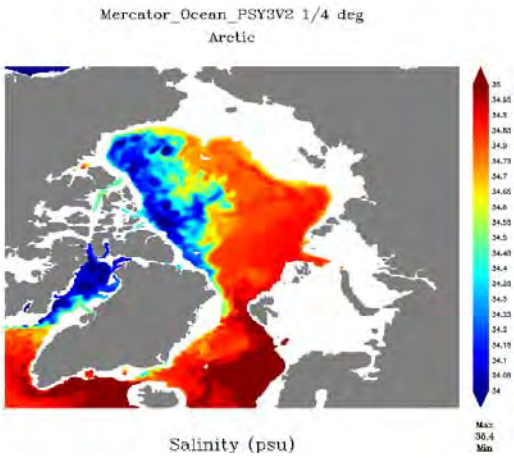

Figure 4-10: Arctic Ocean Temperature - Mercator Ocean model ¼ deg resolution – June 2010

-Surface
-100m
-300m

Figure 4-11: Arctic Ocean Salinity - Mercator Ocean model ¼ deg resolution – June 2010

-Surface
-100m
-300m

4.2 *Influence of bathymetry on positioning accuracy*

Seafloor elevation maps represent a strong source of information that can be used to improve the localization process. Given sufficient information in the terrain structure, observations of terrain elevation provide an external observation of the likely positon of the vehicle. In this context, we should keep in mind that the bathymetric map is the key element that leads the accuracy of the terrain navigation particle filter.

We want to outline here the influence of the sea floor on the positioning accuracy. This is an "empirical study", but it can give an idea of improvement that can be done in trajectory planning. Consequently, some missions may be more successful than others because they may loch more easily to suitable features.

Simulation 1

- smooth sea floor
- trajectory perpendicular to isobaths
- 1 ping per dive / pinging every 2 dive
- Diving target depth 200m
- Climbing target depth 20m

The figure 4-13 illustrates the trajectory used

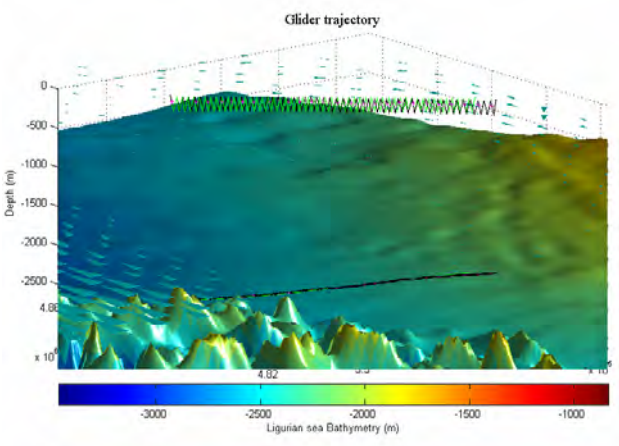

Figure 4-12: trajectory perpendicular to isobaths

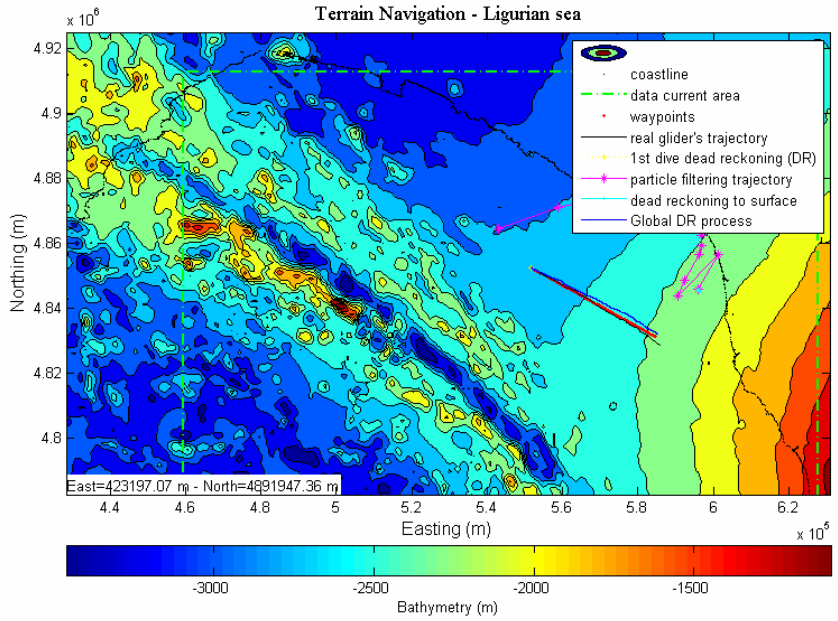

Figure 4-13: particle filter trajectory (magenta) is unable to follow the real trajectory

Variations in terrain elevation are not significant enough to allow convergence of the filter. The cloud of particle is just able to follow the trend of the slope (see figure 4-14).

Simulation 2

- smooth sea floor
- trajectory parallel to isobaths
- 1 ping per dive / pinging every 2 dive
- Diving target depth 200m
- Climbing target depth 20m

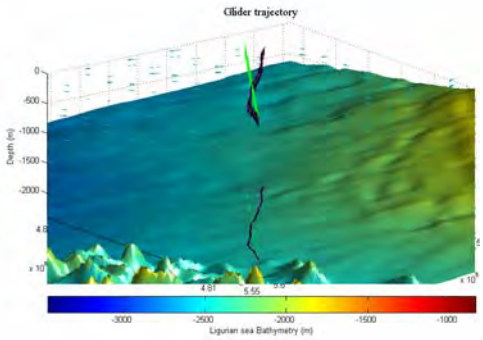

Figure 4-14: trajectory parrallel to isobaths

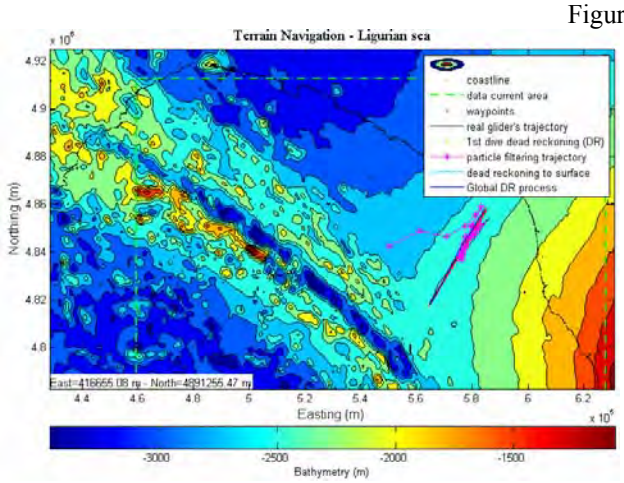

Figure 4-15: particle filter trajectory (magenta) is now roughly able to follow the real trajectory

We can observe a better accuracy in positioning when the trajectory is parallel to isobaths (see figure 4-16).

Simulation 3

- rough sea floor
- 1 ping per dive / pinging every 2 dive
- Diving target depth 200m
- Climbing target depth 20m

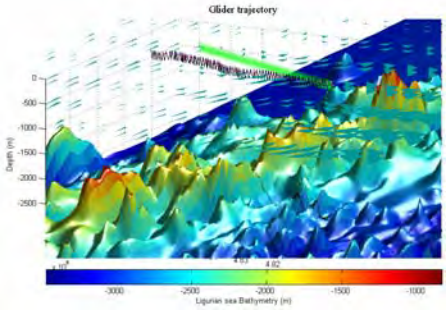

Figure 4-16: trajectory over a rough sea floor

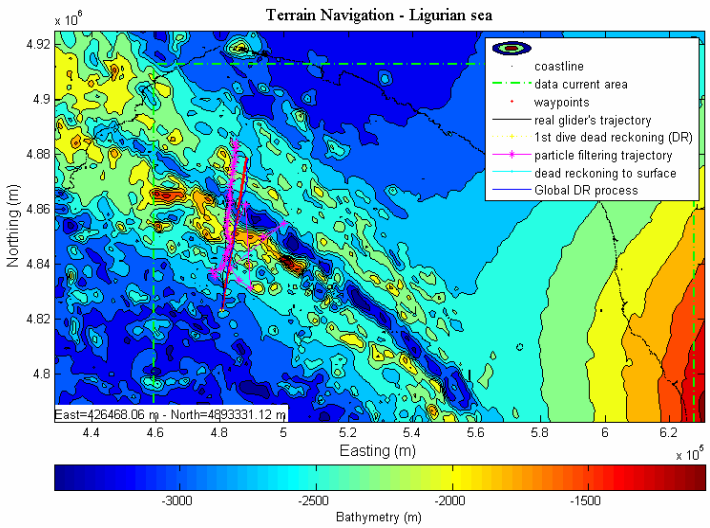

Figure 4-17: particle filter trajectory (magenta) is now able to follow the real trajectory

The unique variability in the seafloor elevation now allows the particle filter to find its position in an accurate and precise way (see figure 4-18).

The figure 4-19 defines how we interpret the accuracy of the terrain navigation particle filer. It can be defined as the distance between the particle filter position estimation (magenta trajectory with uncertainty ellipses) and the position where the depth has been sampled (black trajectory).

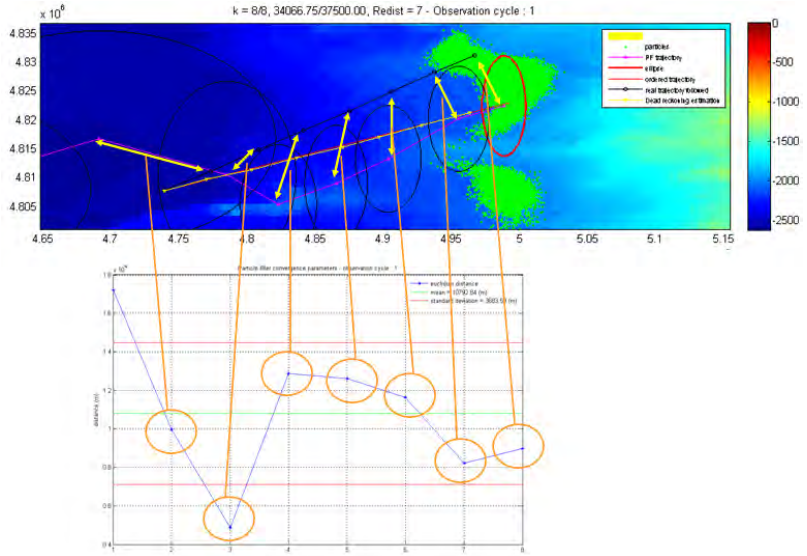

Figure 4-18: TBN-PF navigation accuracy definition

According to the above principle, the figure 4-20 illustrates the filter convergence for those three simulations according to the bathymetric observation number.

As expected, the best terrain condition is characterized by a rough bottom with a glider trajectory that evolves parallel to isobaths.

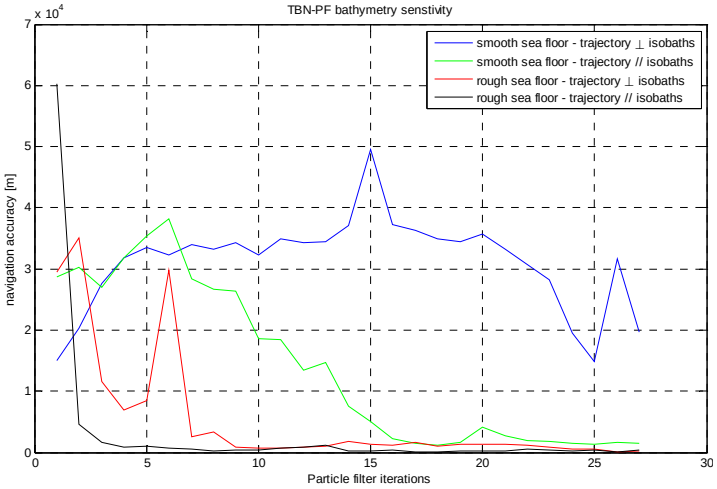

Figure 4-19: Particle filter results – distance between real and estimated positions

	smooth sea floor - trajectory perpendicular to isobaths	smooth sea floor - trajectory parallel to isobaths	rough sea floor perpendicular to isobaths	rough sea floor parallel to isobaths
mean	32 169 m	4 927 m	738 m	430 m
STD	7 851m	5 778 m	496 m	287 m

Table 4.2-1: Filter accuracy from the 10th iteration (bathymetric observation) to the end

Influence of a ridge on the navigation accuracy

Here we want to see the influence of the Lomonosov ridge (figure 4-9) on a possible improvement in positioning accuracy. We have no true values of current, but given a pinging policy and a trajectory scheme (figure 4-22), we can have an idea of the positioning accuracy gain (results on figures 4-11 and 4-12).

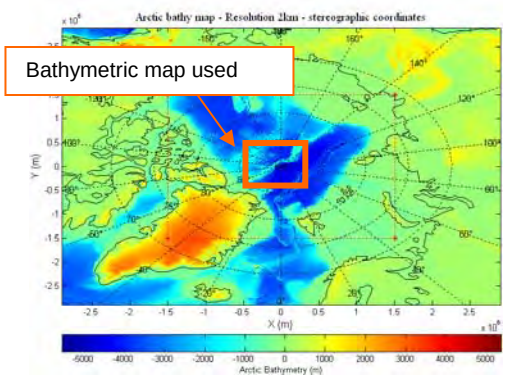

Figure 4-20: Lomonosov ridge

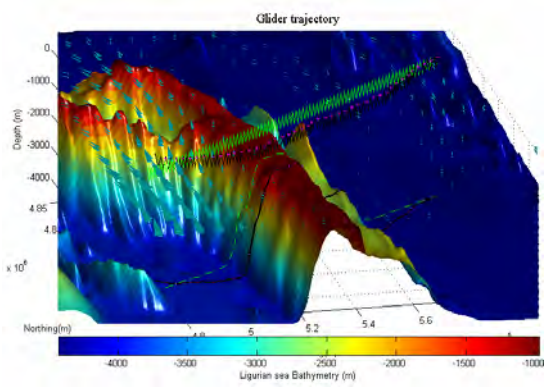

Figure 4-21: trajectory used to test the influence of a ridge

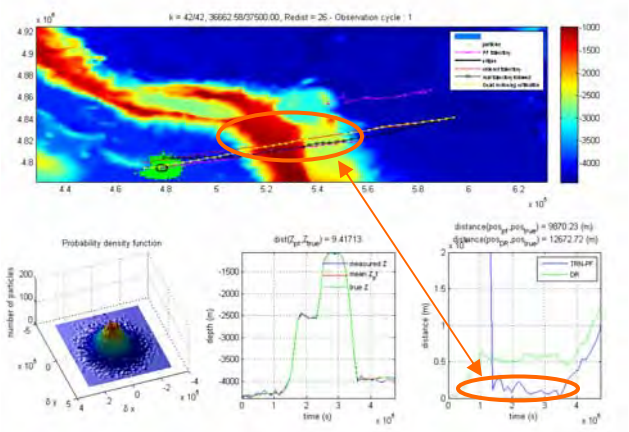

Figure 4-22: Influence of a ridge on the particle filter

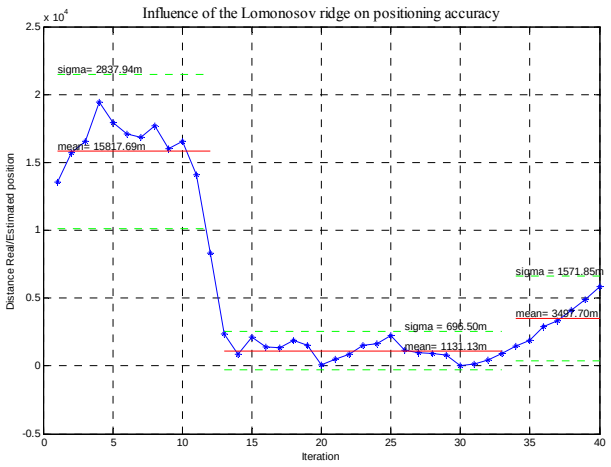

Figure 4-23: Filter's results – the green dotted line represents the uncertainty interval at 95%

This simulation clearly highlights the need to have an area of the seafloor with unique terrain signatures (figure 4-23). It also highlights that a stronger importance is given to the dead reckoning process when the bathymetric measurement uncertainty is significant.

Trajectory optimization

The paper titled *"Planification for terrain-aided navigation"* (S. Paris J-P. Lecadre, IRISA [6]) tackles the trajectory optimization issue. The path optimization problem is equivalent to finding the best decision sequence maximizing an auxiliary convex cost function. A decision is assimilated to an elementary move of the glider between two points of the map. The cost function tends to represent as close as possible the terrain variation information collected during the mobile motion, in other words it measures the terrain elevation variations.

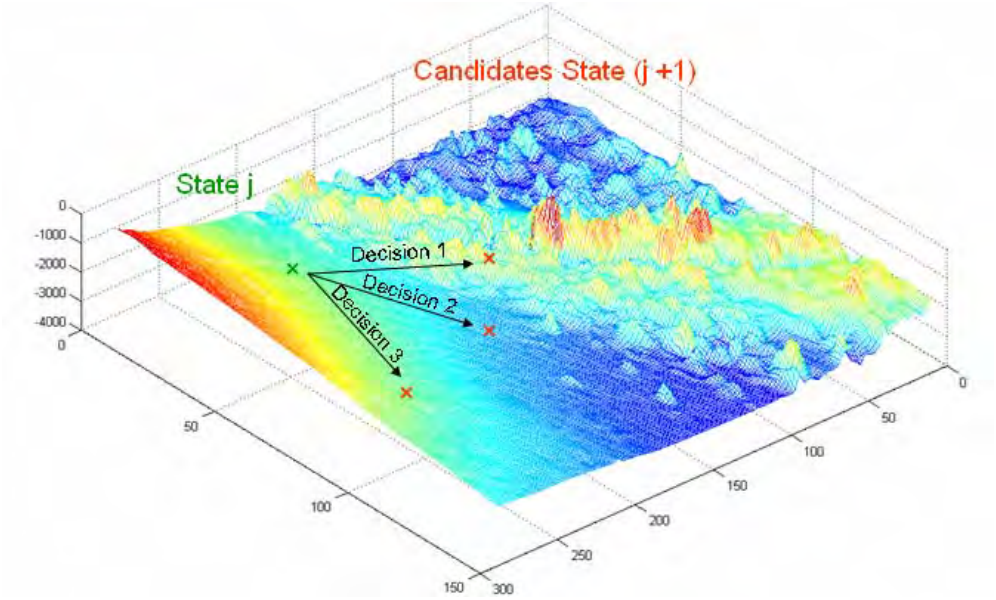

Figure 4-24: trajectory optimization principle – Markov decision process

On figure 4-25, we want to find which one of those decisions is going to maximize the cost function. It can be reminded that the cost function measures the terrain elevation variation. For our example, the decision that would be taken is 1.

However, in the case of a glider mission, where energy is a limiting factor, this kind of "dynamic controlled" trajectory seems difficult to apply. In fact, glider evolves at a low speed with no possibility to wrestle against the current.

Application

In this section we run two simulations. Those two Arctic missions have the same start and end point, but follow a different trajectory to reach the final waypoint. One of those missions tries to stay above a rough seafloor while the other one does not care of the nature terrain elevation evolution (see figures 4-26). To make a relevant comparison, we have to remove the influence of the current.

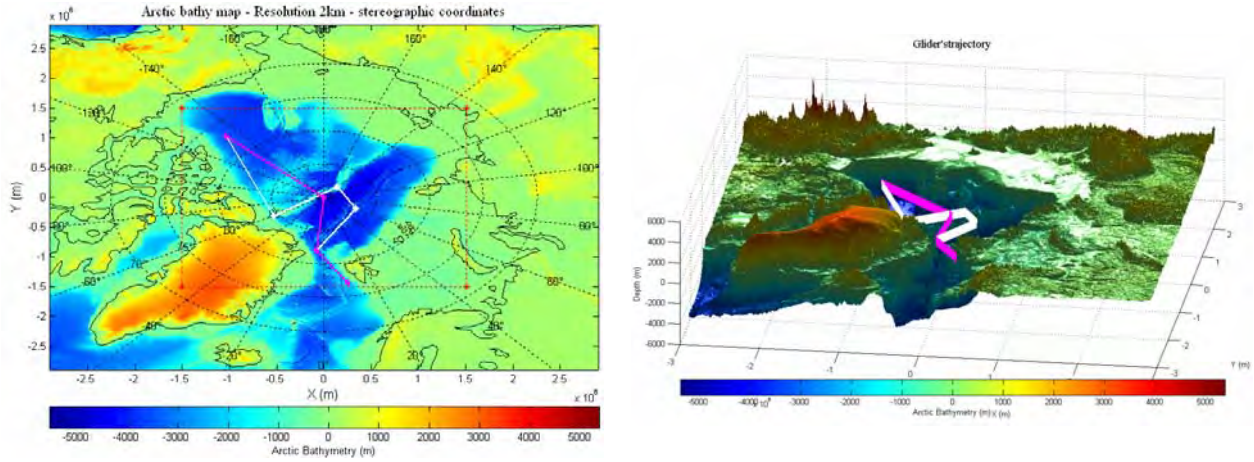

Figure 4-25: Trajectory followed to test the influence of bathymetry (starting point: Fram Strait) – The white trajectory tries to stay above a rough seafloor – The magenta trajectory just tries to cross the Arctic

The figure 4-27 clearly illustrates the influence of the terrain elevation trend on the positioning accuracy. Due to the pinging policy, which consists of one ping every 10 dive, we observe many spikes. Nonetheless the positioning accuracy is clearly improved when the glider flies above a rough sea floor. The two main red peaks appear when the glider has to cross the two deep sea basins (see the magenta trajectory).

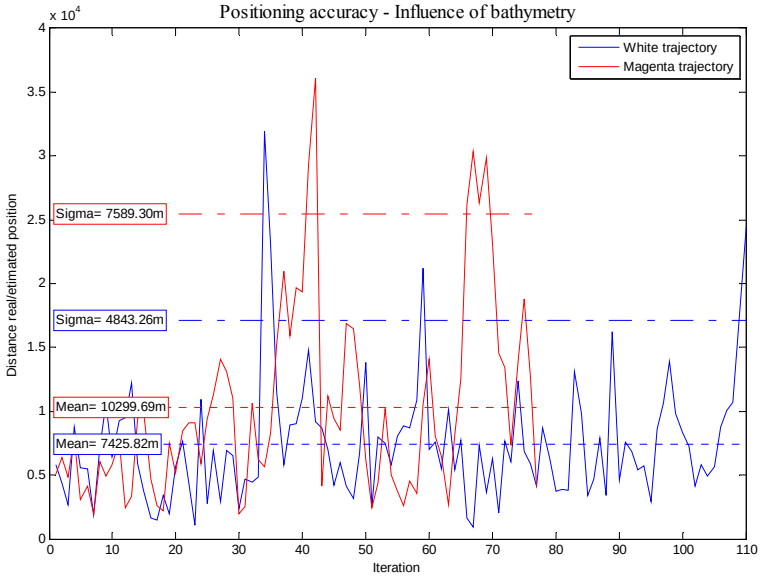

Figure 4-26: Expected range of accuracy given the pinging policy and the trajectory followed – distance expressed in meters

4.3 *Influence of the number of particles*

The number of particles must have an influence on the computation time needed to run the filter. Here, we want to examine the influence of particles number on the navigation accuracy. Various simulations have been run with different number of particles (1000 - 10000 – 25000 – 50000).

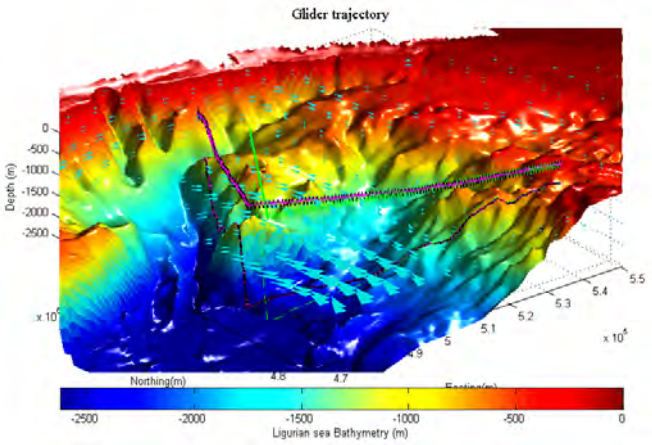

Figure 4-27: Trajectory used for comparison

First simulation: 1000 particles

- 1 ping per dive
- Pinging every dive
- Dive depth target = 200m
- Climb depth target = 20m

Time needed for one iteration of PF: 1.8 ms

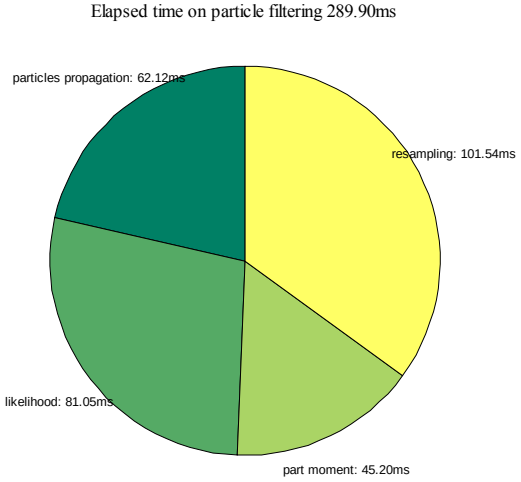

Second simulation: 10000 particles

- 1 ping per dive
- Pinging every dive
- Dive depth target = 200m
- Climb depth target = 20m

Time needed for one iteration of PF: 15.6 ms

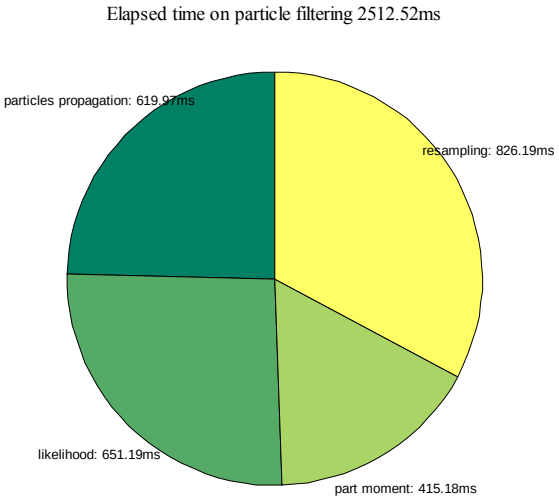

Third simulation: 25000 particles

- 1 ping per dive
- Pinging every dive
- Dive depth target = 200m
- Climb depth target = 20m

Time needed for one iteration of PF: 38.8 ms

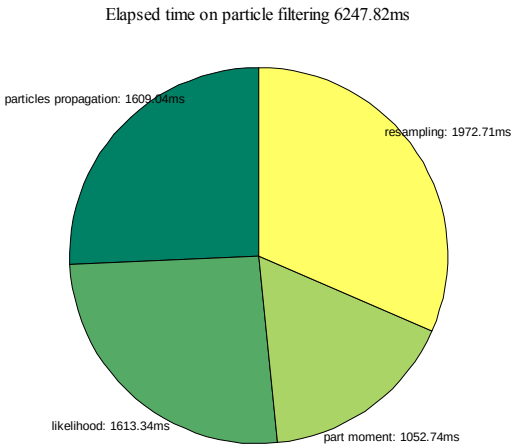

Fourth simulation: 50 000 particles

- 1 ping per dive
- Pinging every dive
- Dive depth target = 200m
- Climb depth target = 20m

Time needed for one iteration of PF: 81.2 ms

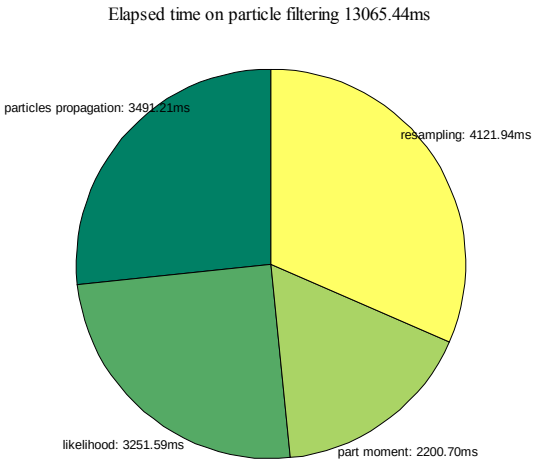

Outcome

If a small number of particles is used, "fake targets" appear or better said some loose in navigation tracking (see spikes around 80 hours on figure 4-29). The particle cloud is not able to cover a wide area, and so the particle filter can be stuck in a false track. Thus, except some computation time saving there is no improvement done by reducing the number of particles.

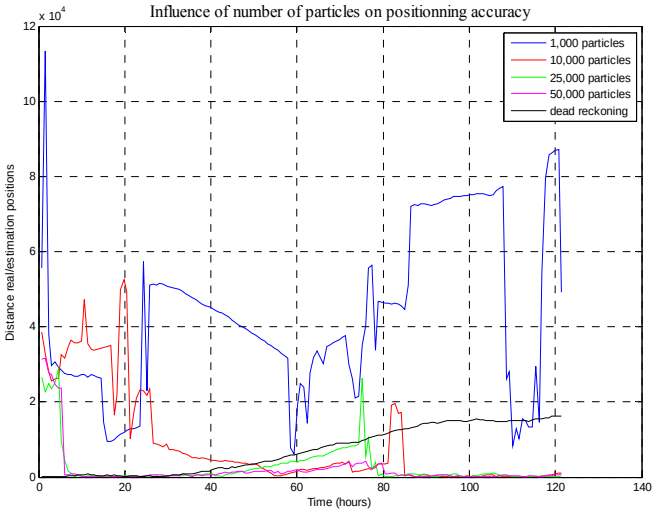

Figure 4-28: Distance between real and estimated position

Moreover, computation time evolves linearly with the number of particles.

4.4 *Influence of pinging policy on positioning accuracy*

In this section we would like to see the influence of the pinging policy on the positioning accuracy. In fact, one of the key parameters that constrains the duration of a glider mission is the energy consumption of each component. Given that broadcasting a ping requires energy, a tradeoff between the desired number of pings and the willing accuracy has to be done.

The particle filter needs observations, however this data has a cost. For example if we consider the Kongsberg EA600 single beam echo sounder, each pulse (12 kHz – 16ms length) has a cost of 32 Joules.

12J	Energy delivered by the flash of a camera (capacitor 220 uF, 330 v)
90J	Kinetic energy of a tennis ball(masse 58g) at 200 km/h.

Table: Energy ranges in everyday life

To see the influence of the pinging policy, different simulations with different broadcasting policies are being run.

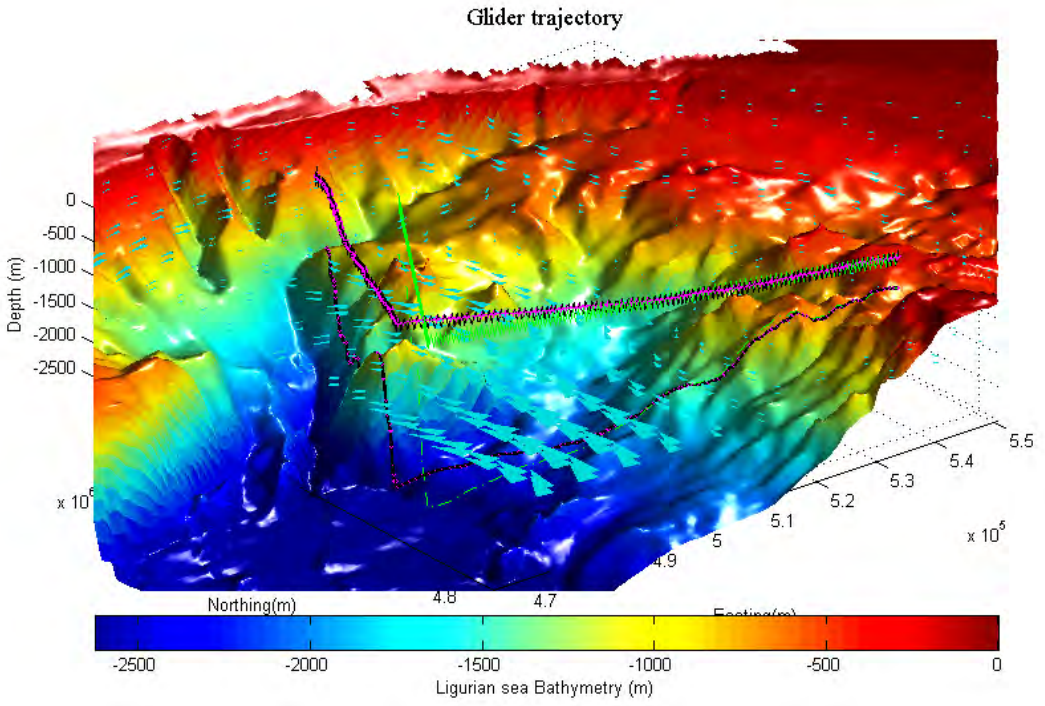

Figure 4-29: Trajectory used for comparison

Simulation 1

- 3 pings per dive
- Pinging every dive
- Dive depth target = 200m
- Climb depth target = 20m

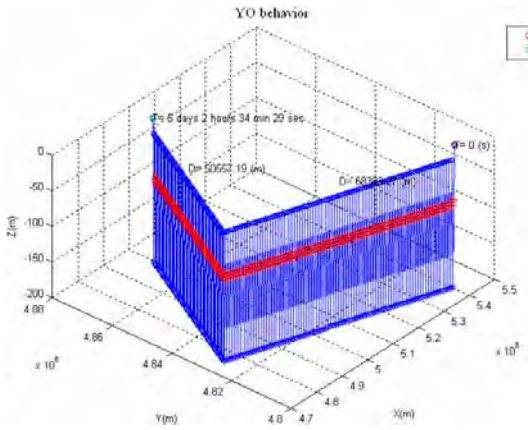

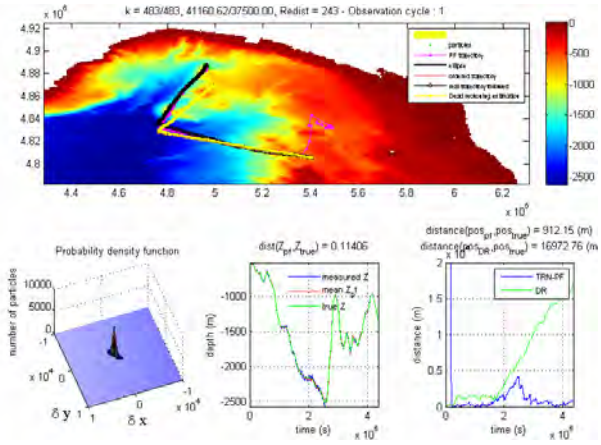

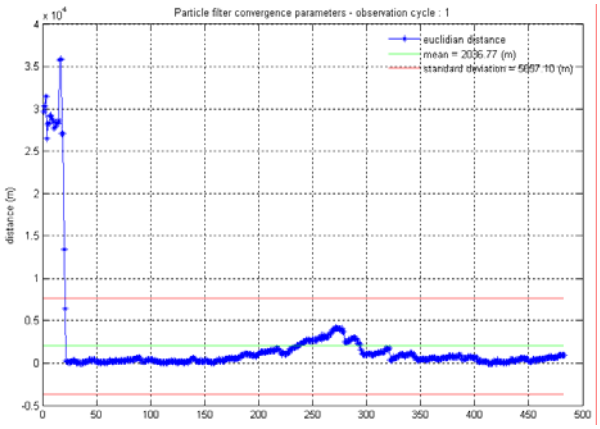

Figure 4-30: results of particle filtering – simulation 1

Simulation 2

- 1 ping per dive
- Pinging every dive
- Dive depth target = 200m
- Climb depth target = 20m

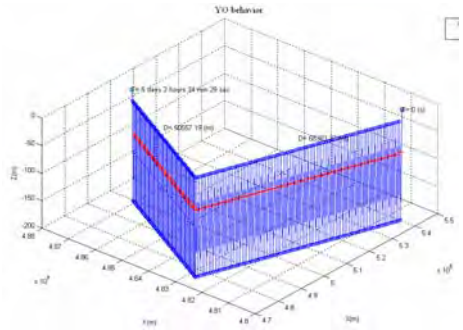

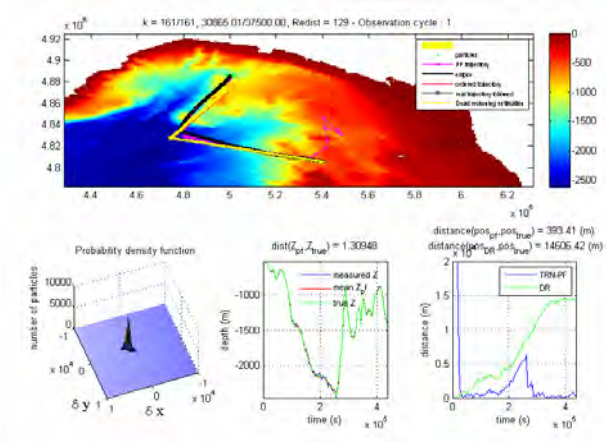

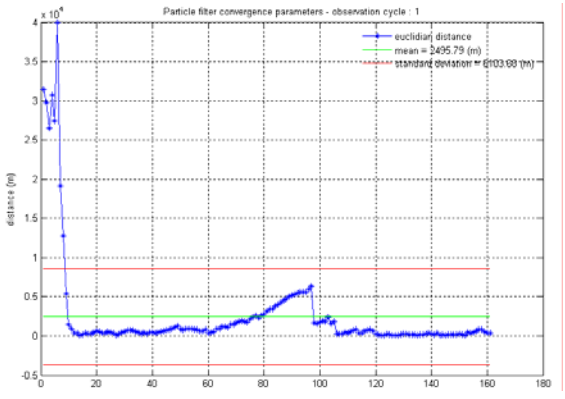

Figure 4-31: results of particle filtering – simulation 2

Simulation 3

- 3 ping per dive
- Pinging every 5 dive
- Dive depth target = 200m
- Climb depth target = 20m

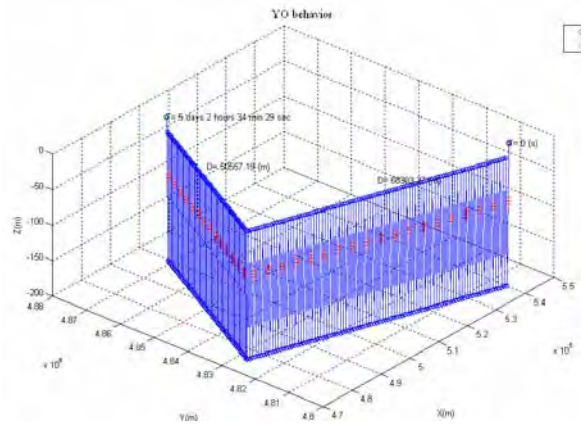

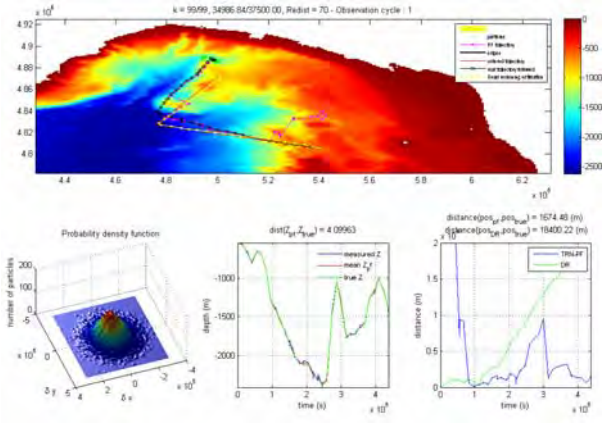

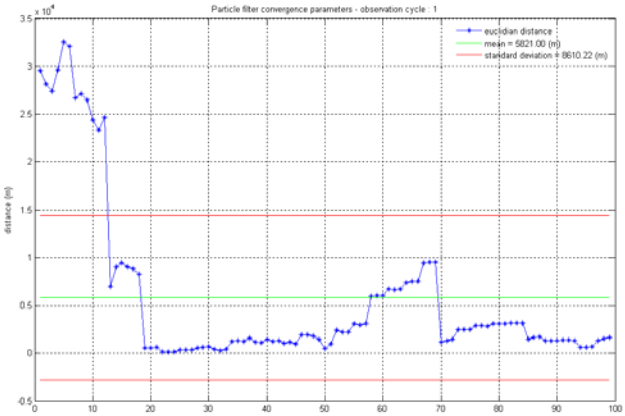

Figure 4-32 : results of particle filtering – simulation 3

Simulation 4

- 1 ping per dive
- Pinging every 5 dive
- Dive depth target = 200m
- Climb depth target = 20m

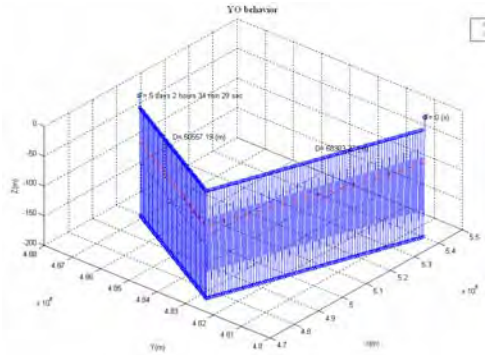

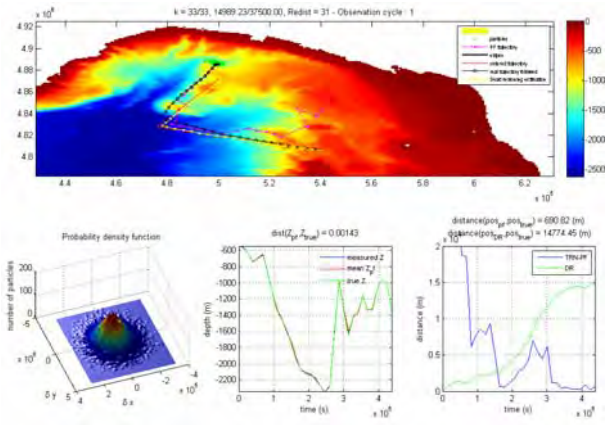

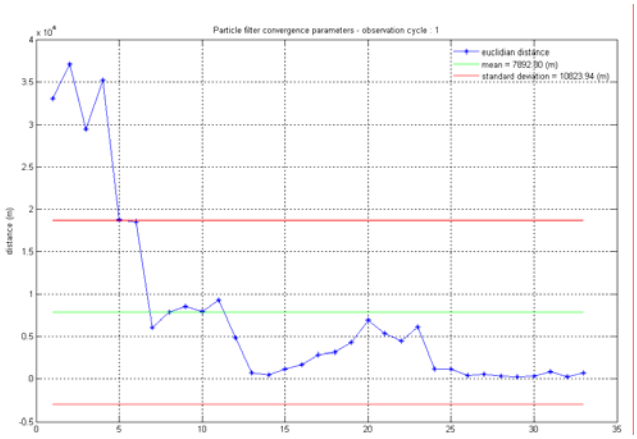

Figure 4-33: results of particle filtering – simulation 4

Conclusion

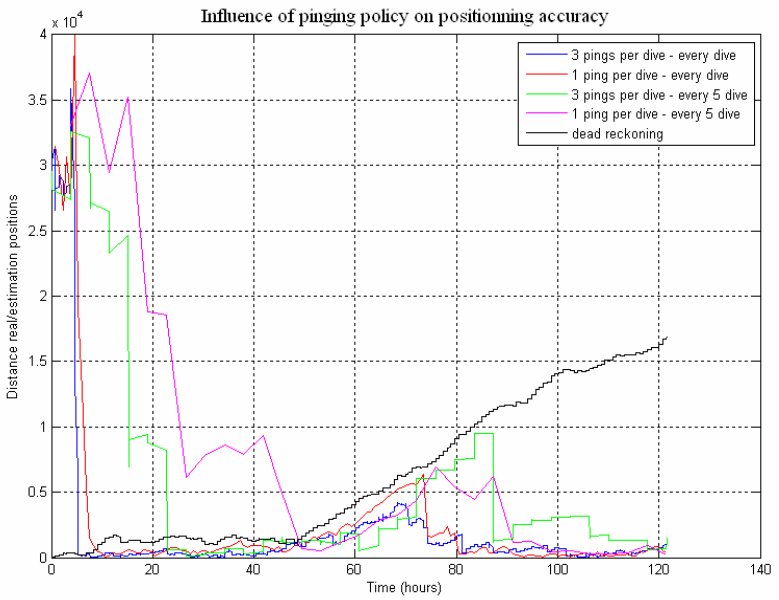

Figure 4-34: global trend of pinging policy influence - evolution according to the dead reckoning with high uncertainty on depth measurements

The figure 4-35 illustrates the behavior of the navigation accuracy according to the number of depth measurements fed to the particle filter.

<u>Some key ideas can be outlined</u>

- Obviously the convergence in time of the filter is faster when the number of depth measurement increases. However it requires much more depth measurements to converge, in fact due to the very low speed of the glider, depth is sampled almost at the same position.

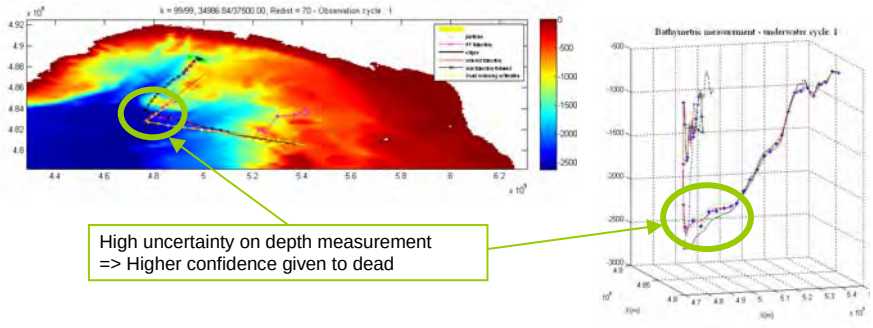

Figure 4-35: uncertainty increasing with depth

- When the glider is over a very deep area, the uncertainty on depth measurements increases. Thus, if this uncertainty increases, the shape of the likelihood function becomes smoother and so the weight distribution is done in a less sharp way (see figure 4-37).

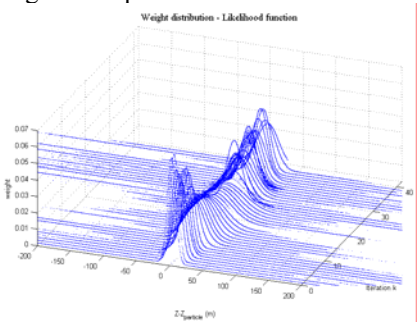

Figure 4-36: evolution of the likelihood function – shape's smoothing around the 20th iteration due to deep water

Consequently, more weight is given to the dead reckoning than to measurement. This trend can be observed on the figure 4-35 between 50 and 80 hours when the distance between estimated and real position is soaring following the same trend than the dead reckoning process.

- After convergence, the filter does not need a lot of depth measurements to keep an "acceptable" accuracy (based here on the user requirements).

Simulation #	Pinging policy	Time needed to "converge"	Number of pings until convergence	Mean distance to real position	Standard deviation distance to real position
simulation 1	3 pings / every dive	5 hours	21	892 m	968 m
simulation 2	1 ping / every dive	10 hours	14	1185 m	1474 m
simulation 3	3 pings / every 5 dive	23 hours	21	2425 m	2344 m
simulation 4	1 ping / every 5 dive	48 hours	13	2076 m	2150 m

Table 4.4-1: Simulations results – mean and standard deviation are computed once the filter has "converged" – we establish that the filter has converged when we get better results with the particle filter than with the dead reckoning process.
Resolution of the bathymetric chart: 0.5' (~926m)

Given those results, what we can imagine in order to save energy while keeping a good positioning accuracy is to set different pinging policies along the trajectory.

- During the first hours of the mission we need a high rate of depth measurements in order to converge quickly. We can first rely on the dead reckoning process that has not drifted too much before giving more weight to the terrain navigation particle filter.

- Once those few hours are spent, the glider does not have to emit a ping at every dive, however if the glider is flying over a rough sea floor, it can be interesting to sample the depth with a high rate in order to improve the positioning accuracy. This would have to be established prior the mission given the desired trajectory.

To conclude, as expected, the pinging policy is a tradeoff between the desired navigation accuracy and energy consumption requirements.

4.5 *Influence of dead reckoning*

In this section the influence of the dead reckoning accuracy on the TBN-PF estimated position accuracy is being studied. This section outlines a comparison between the already existing low cost dead reckoning process and a much more accurate navigation estimation process (for example with the use of a Inertial Navigation System aided with a Doppler Velocity Log). The aim is to see the improvement done in navigation accuracy thanks to the use of INS.

4.5.1 "Low cost" position estimation

Till now we have considered a dead reckoning obtained thanks to:

- hydrostatic pressure measurements leading to the vertical speed of the glider
- attitude measurements : pitch and roll
- heading got thanks to a magnetic compass

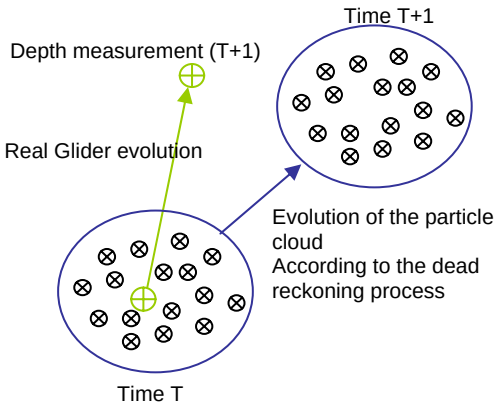

Figure 4-37: simplified principle of the simulation

With such input parameters we underlined the fact that the glider was not able to identify the current. The figure 4-38 synthesizes this idea. So, till now, the idea of the simulation was to submit particles to this "wrong" position estimation (trajectory similar to the green line on the figure 4-39), while the glider was sampling depth, and so providing data to the TBN-PF along the real trajectory followed (black line).

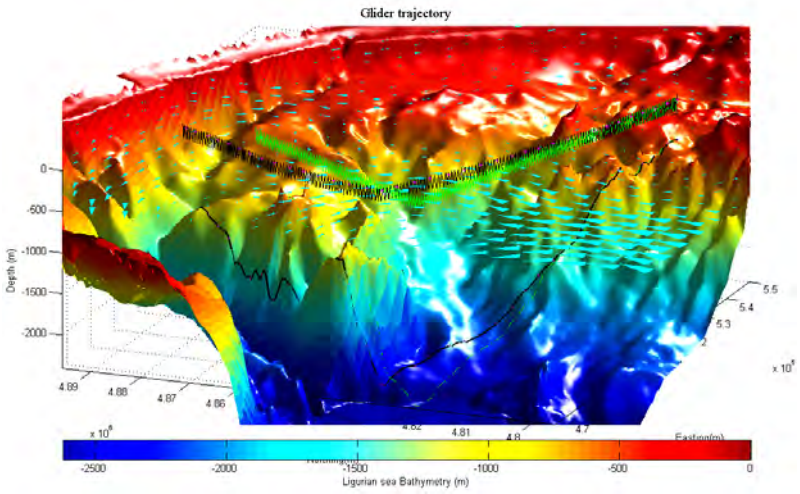

Figure 4-38: Desired trajectory (green) – Real trajectory followed (black)

Application: what is the expected navigation using a low cost navigation process?

We will use a trajectory made of three waypoints:

- Diving target depth = 180m
- Climbing target depth = 20m
- 1 ping every 5 dives

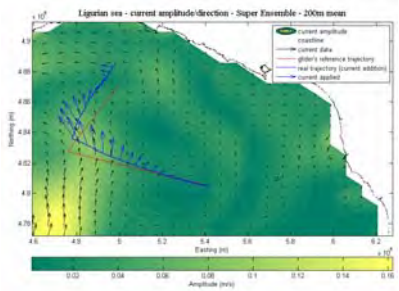

Figure 4-39: Influence of sea currents on desired trajectory

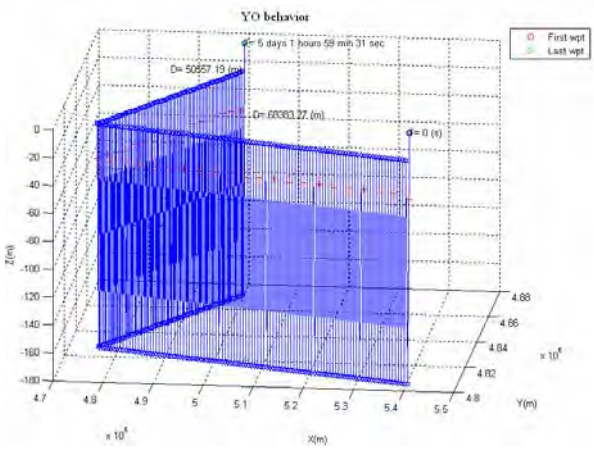

Figure 4-40: Desired trajectory

The figure 4-42 illustrates the particle filtering process. The top figure represents different trajectories followed:

- magenta line: particle filtering result
- black line: real trajectory followed by the glider and providing depth measurements
- yellow line: Dead reckoning process unable to see the current

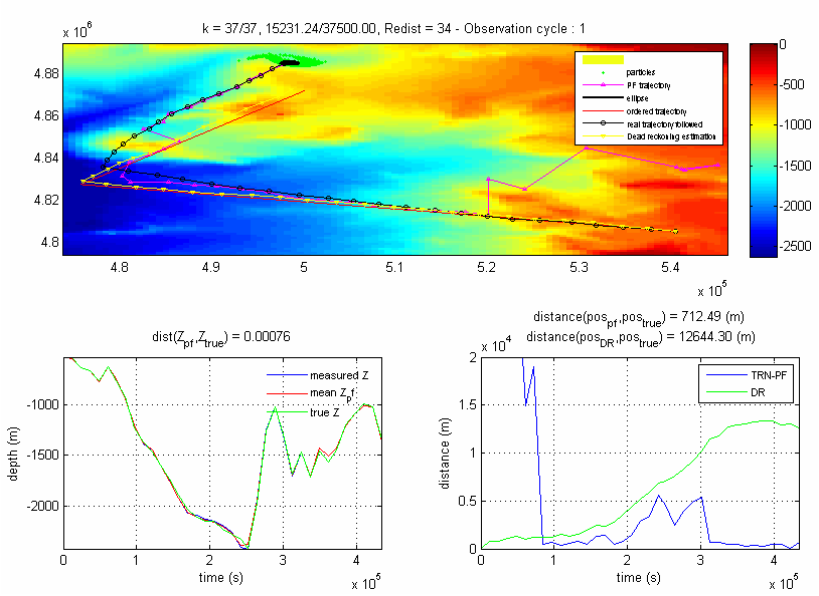

Figure 4-41: Particle filtering process when the glider is not able to see the current

On figure 4-42, the bottom left figure shows the bathymetric profile seen by the glider. The bottom right picture represents:

- green line: distance between the real position and the dead reckoning estimate
- blue line: distance between the real position and the particle filter position.

This simulation clearly highlights the interest of using the terrain navigation particle filter to improve the estimation of the glider position.

4.5.2 Accurate position estimation – use of a DVL aided INS

In fact, in the simulation below, we consider that, thanks to a DVL, the glider is able to see the current and so to exploit it within the dead reckoning process. The figure 4-43 tries to summarize this idea.

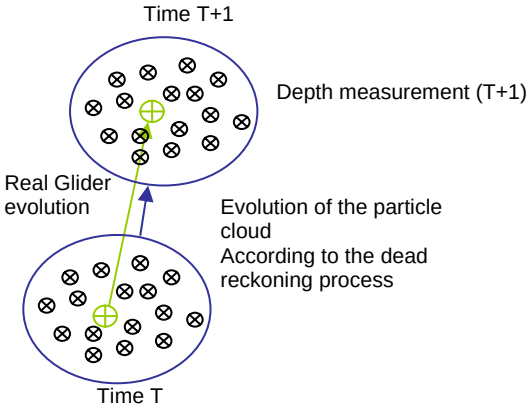

Figure 4-42: Particle's cloud follows the same dynamic than the glider constrained by currents

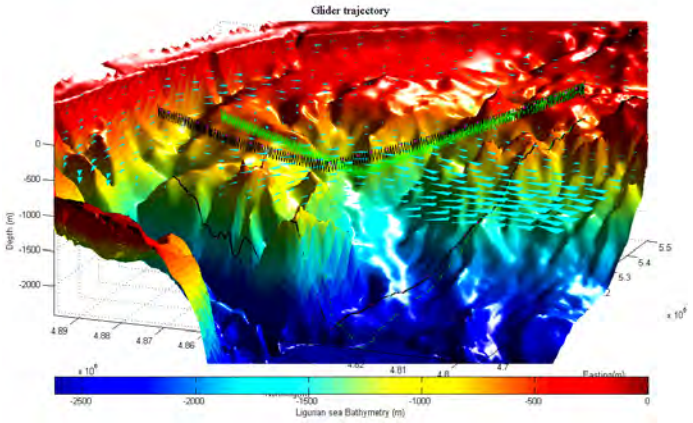

Figure 4-43: The dead reckoning is now able to send the glider back to the real trajectory followed (black)

We use exactly the same simulation parameters, and we obtain:

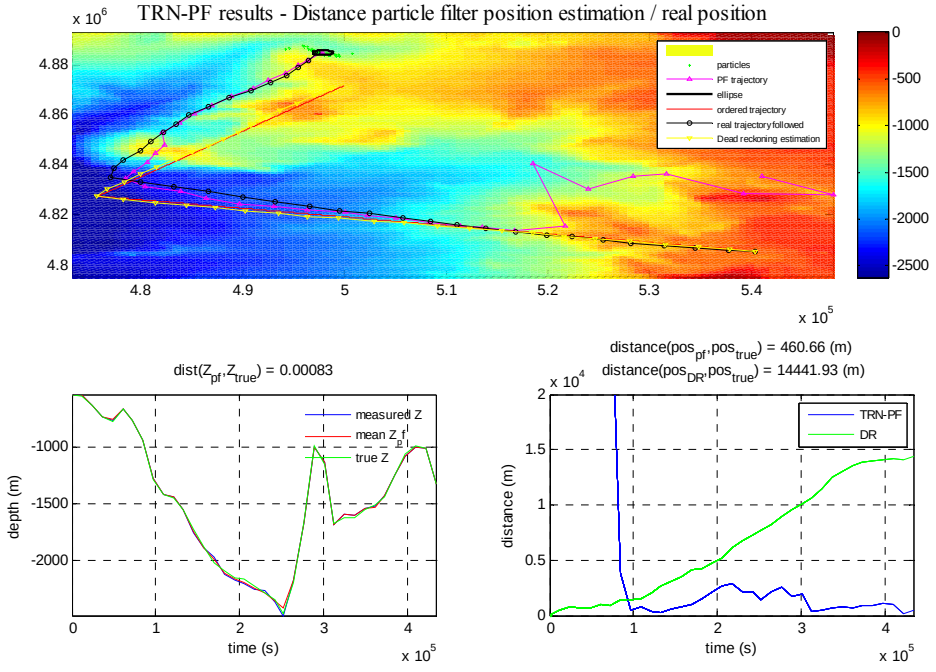

Figure 4-44: Particle filter using an accurate dead reckoning

The figure 4-46 is a comparison of particle filtering results. It represents the distance between this PF position estimation and the real position where the depth measurement has been taken. The blue line refers to a "rough" dead reckoning process as seen in the part 1, while the red line refers to a much more accurate dead reckoning process using for example a DVL aided INS. Those two navigation estimation processes are coupled with the TBN-PF, to feed the prediction step.

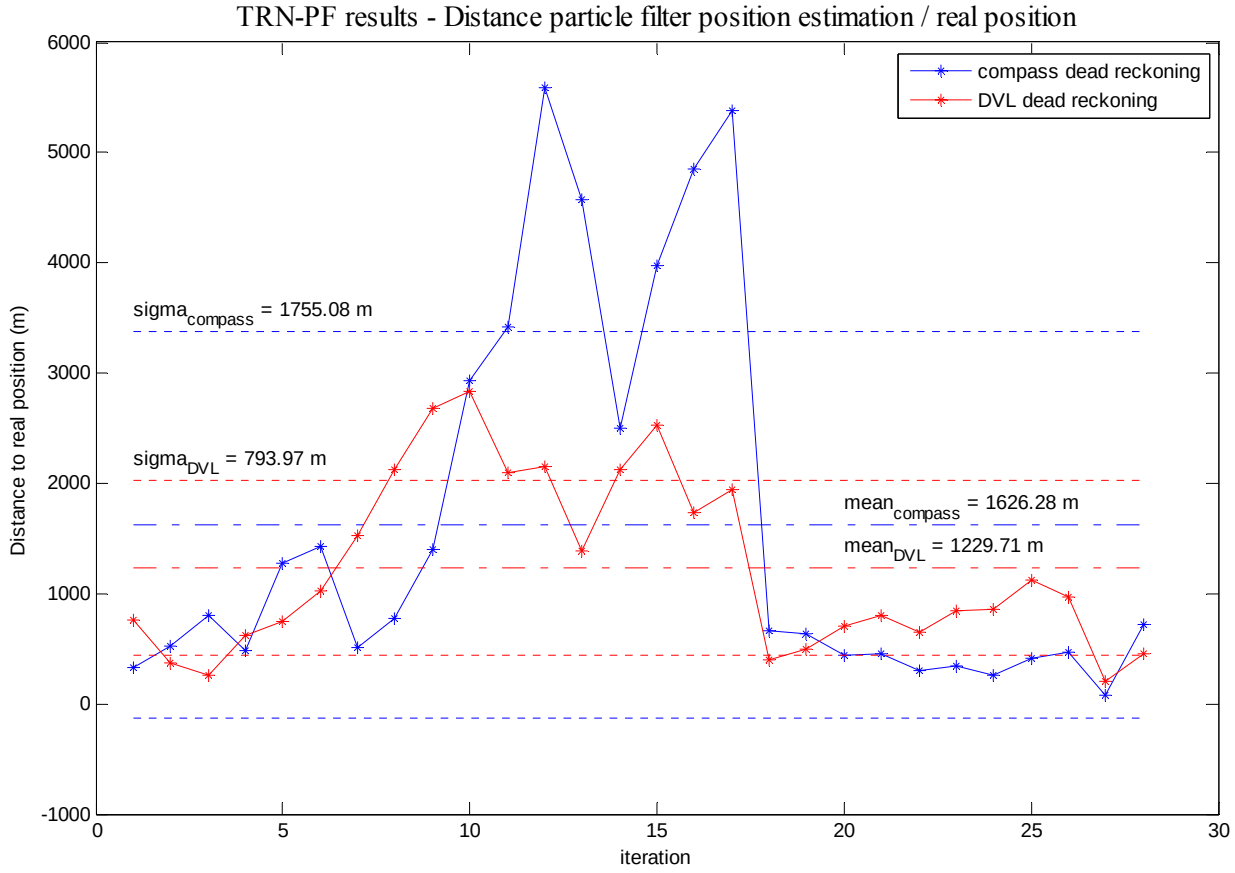

Figure 4-45: influence of dead reckoning accuracy on TBN-PF accuracy - results

Those results outline the idea that a very accurate dead reckoning process is not compulsory to run the terrain navigation particle filter with acceptable results. Thus, despite some spikes, a "low cost" dead reckoning process combined to this TBN-PF seems to reach a satisfying accuracy in the position estimation process.

Glider Mission Simulation

Results of a Ligurian sea mission and of Arctic crossing simulations are presented and examined in Annexes 4 and 5.

5 Inertial Navigation System – Uncertainty estimation algorithm

(based on the paper of Piotr KANIEWSKI – military University of technology, Poland [8]*)*

In this section we would like to see what is the underwater positioning accuracy using an Inertial Navigation System for comparison with the terrain navigation particle filter. There are already many studies on this subject combining an inertial measurement unit (IMU), a Doppler velocity log (DVL), an electronic compass (EC), a depth sensor (DS).

The study of Piotr Kaniewski (Military University of Technology, Poland) is one of those. In his simulation he considers:

- IMU velocity and attitude errors
- DVL velocity errors
- DS depth errors

5.1 *Kalman filter*

We will implement here a Matlab algorithm of a Kalman filter based on the state space model provided by the paper of P. Kaniewski. Thanks to this Matlab algorithm we will be able to see the performance of the inertial navigation system: IMU + DVL.

The figure 5-1 illustrates the velocity uncertainty in m/s of: (sensors specifications in Annex 2)

- IMU Kongsberg MRU-Z (red)

0.05m/s^2 uncertainty on acceleration

- DVL RDI Workhorse Navigator (blue).

0.3 cm/s uncertainty on velocity

Considering:

$$\sigma_{velocity}(k) = \sigma_{velocity}(k-1) + \sigma_{acceleration}\Delta T$$

We can clearly see the drifting nature of the IMU's velocity error due to the integration process.

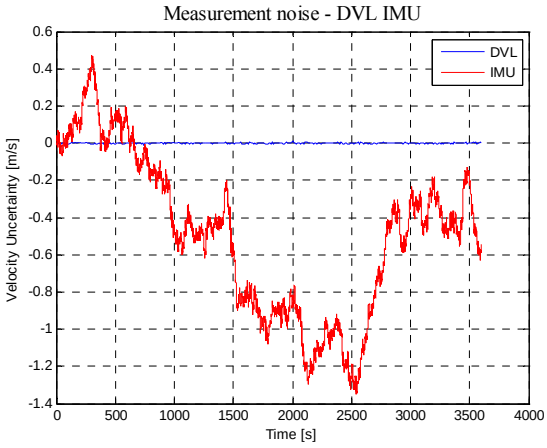

Figure 5-1: Velocity uncertainty of DVL and IMU

uncertainty on positioning: IMU alone

Due to the double integration process, this uncertainty increases indefinitely. This burden is the consequence of the addition of all former uncertainties.

$$\sigma_{velocity}(k) = \sigma_{velocity}(k-1) + \sigma_{acceleration}\Delta T$$
$$\sigma_{position}(k) = \sigma_{position}(k-1) + \sigma_{velocity}(k-1)\Delta T$$

The figure 5-2 clearly outlines the need to combine the IMU data with an extra sensor.

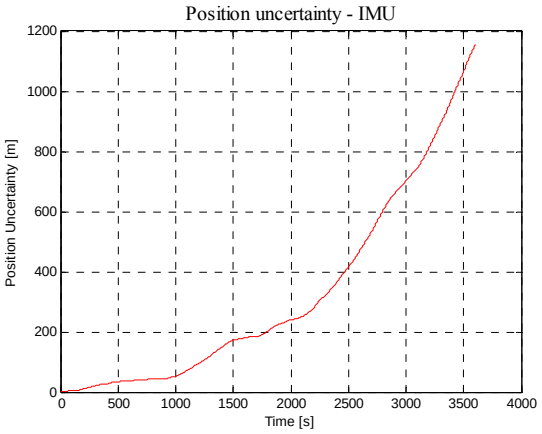

Figure 5-2: Positioning errors of IMU without correction

Ixsea provides for example the following specifications for its Inertial Navigation System ROVINS positioning performance:

- With DVL: 0.2% of traveled distance
- No aiding for 1 min/2 min => 1.5 m/6 m

The figure 5-3 is the Matlab implementation of the noise that confirms those performances.

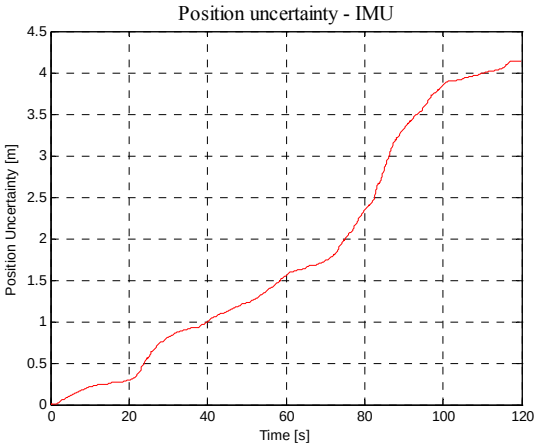

Figure 5-3: IMU stand alone performances

Thus the idea to improve underwater navigation performance is to use an integrated positioning system that combines data from an IMU and a DVL.

Discrete model of the system: dynamic model and observation model

$$x(k+1) = A(k+1,k)x(k) + w(k)$$
$$z(k) = H(k)x(k) + v(k)$$

x - state vector to be estimated via Kalman filter
$w(k)$ - vector of random process disturbances
A - state transition matrix
z - measurement vector
$v(k)$ - vector of measurement noises
H - observation (measurement) matrix

The Kalman filter used in the positioning system for AUV estimates error of IMU and provides for correction of IMU velocity components.

The state vector is made here of IMU uncertainties.

$$x(k)=\begin{pmatrix}\delta v_N(k)\\ \delta\phi_E(k)\\ \delta v_E(k)\\ \delta\phi_N(k)\\ \delta v_Z(k)\end{pmatrix}$$

δv_N - IMU velocity uncertainty along the North axis

$\delta\phi_E$ - IMU attitude uncertainty around the East axis

δv_E - IMU velocity uncertainty along the East axis

$\delta\phi_N$ - IMU attitude uncertainty around the North axis

δv_Z - IMU velocity uncertainty along the Down axis

Dynamics model:

$$\begin{pmatrix}\delta v_N(k+1)\\ \delta\phi_E(k+1)\\ \delta v_E(k+1)\\ \delta\phi_N(k+1)\\ \delta v_Z(k+1)\end{pmatrix}=\begin{pmatrix}1 & gT & 0 & 0 & 0\\ \frac{-T}{R} & 1 & 0 & 0 & 0\\ 0 & 0 & 1 & -gT & 0\\ 0 & 0 & \frac{T}{R} & 1 & 0\\ 0 & 0 & 0 & 0 & 1\end{pmatrix}\begin{pmatrix}\delta v_N(k)\\ \delta\phi_E(k)\\ \delta v_E(k)\\ \delta\phi_N(k)\\ \delta v_Z(k)\end{pmatrix}+\begin{pmatrix}w_{v_N}(k)\\ w_{\phi_E}(k)\\ w_{v_E}(k)\\ w_{\phi_N}(k)\\ w_{v_Z}(k)\end{pmatrix}$$

g - gravity acceleration

R - Earth's radius

T - Sampling interval of the discrete model.

w - Discrete random process disturbance

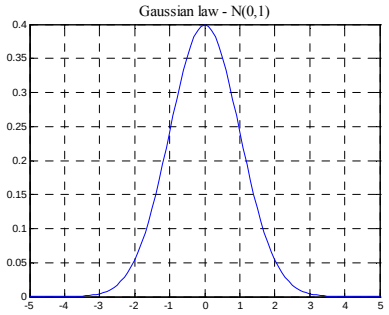

If we consider the Kongsberg MRU-Z, the noise w presents those characteristics.

$$\overline{x}=0 \qquad \sigma_{acc}=0.05 m.s^{-2} \qquad \sigma_{angle}=0.15^{\circ}$$

The covariance matrix of discrete random process disturbance

$$Q=\begin{pmatrix}\sigma^2_{acc_N} & 0 & 0 & 0 & 0\\ 0 & \sigma^2_{angle_E} & 0 & 0 & 0\\ 0 & 0 & \sigma^2_{acc_E} & 0 & 0\\ 0 & 0 & 0 & \sigma^2_{angle_N} & 0\\ 0 & 0 & 0 & 0 & \sigma^2_{acc_Z}\end{pmatrix}$$

Observation Model: Observations consist here in measuring the current velocity uncertainty using a DVL

$$\begin{pmatrix}v_N^{IMU}(k)-v_N^{DVL}(k)\\ v_E^{IMU}(k)-v_E^{DVL}(k)\\ v_Z^{IMU}(k)-v_Z^{DVL}(k)\end{pmatrix}=\begin{pmatrix}1 & 0 & 0 & 0 & 0\\ 0 & 0 & 1 & 0 & 0\\ 0 & 0 & 0 & 0 & 1\end{pmatrix}\begin{pmatrix}\delta v_N(k)\\ \delta\phi_E(k)\\ \delta v_E(k)\\ \delta\phi_N(k)\\ \delta v_Z(k)\end{pmatrix}+\begin{pmatrix}v_{v_N}(k)\\ v_{v_E}(k)\\ v_{vZ}(k)\end{pmatrix}$$

If we consider the RDI Workhorse Navigator DVL, the measurement noise v presents those characteristics.

$$\overline{x} = 0$$

$$\sigma_{vel} = 0.5cm.s^{-1}$$

The covariance matrix of measurement errors:

$$R = \begin{bmatrix} \sigma_{vel_N} & \sigma_{vel_E} & \sigma_{vel_Z} \end{bmatrix} \begin{bmatrix} \sigma_{vel_N} \\ \sigma_{vel_E} \\ \sigma_{vel_Z} \end{bmatrix}$$

Equations of the linear covariance Kalman filter:

Here we just model the behavior of uncertainty using an IMU alone and using both IMU and DVL.

$$\begin{aligned}
x(k+1|k) &= Ax(k|k) \\
P(k+1|k) &= AP(k|k)A^T + Q \\
res(k+1) &= z(k+1) - Hx(k+1|k) \\
R_e(k+1) &= HP(k+1|k)H^T + R \\
K(k+1) &= P(k+1|k)H^T R_e^{-1}(k+1) \\
x(k+1|k+1) &= x(k+1|k) + K(k+1)res(k+1) \\
P(k+1|k+1) &= P(k+1|k) - K(k+1)HP(k|k+1)
\end{aligned}$$

$x(k|k)$ - estimated state vector at a time k after the measurement update,

$x(k+1|k)$ - estimated state vector at a time k+1 - before the measurement update,

$x(k+1|k+1)$ - estimated state vector at a time k+1 - after the measurement update,

$res(k+1)$ - residuals (or innovation) vector at a time k+1,

$P(k|k)$ - covariance matrix of filtering errors at a time k,

$P(k+1|k+1)$ - covariance matrix of filtering errors at a time k+1,

$P(k+1|k)$ - covariance matrix of prediction errors at a time k+1,

$R_e(k+1)$ - covariance matrix of innovations at a time k+1,

$K(k+1)$ - Kalman gains matrix at a time k+1,

Q - covariance matrix of discrete random process disturbances,

R - Covariance matrix of measurement errors.

Application: Kalman filter

In this simulation we will consider an INS made of: - IMU Kongsberg MRU-Z

- RDI Workhorse Navigator DVL

Figures 5-4 and 5-5 present results of a simulation length set to 1 hour with a sampling rate of 5Hz. The uncertainty on velocity is clearly improved thanks to the kalman filter.

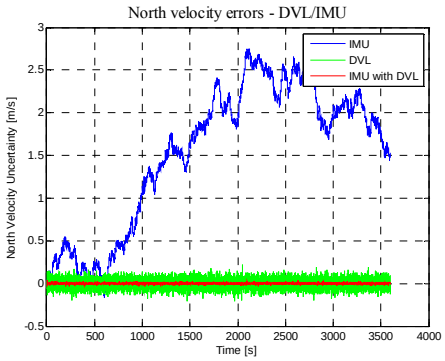

Figure 5-4: Comparison of north velocity errors of IMU, DVL and IMU/DVL

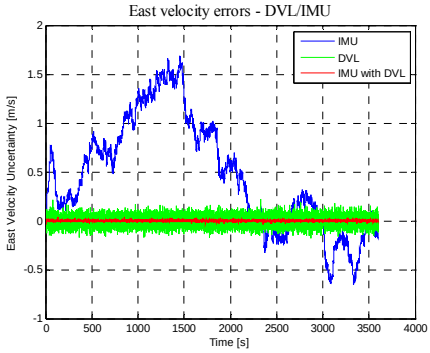

Figure 5-5: Comparison of east velocity errors of IMU, DVL and IMU/DVL

Figures 5-6 and 5-7 highlight the improvement in positioning thanks to the combination of DVL and IMU data.

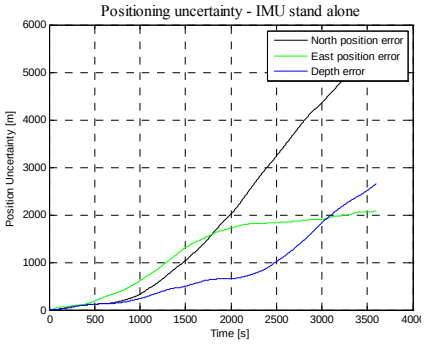

Figure 5-6: Positioning errors of IMU $\sqrt{\delta x^2 + \delta y^2}$ without correction from DVL

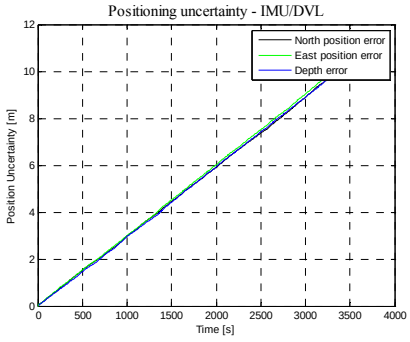

Figure 5-7: Positioning errors of IMU $\sqrt{\delta x^2 + \delta y^2}$ with correction from DVL

The figure 5-8 is another way to illustrate the growth of the positioning uncertainty using a Kalman filter that combines an IMU and a DVL with uncertainty ellipsoid every 30 minutes.

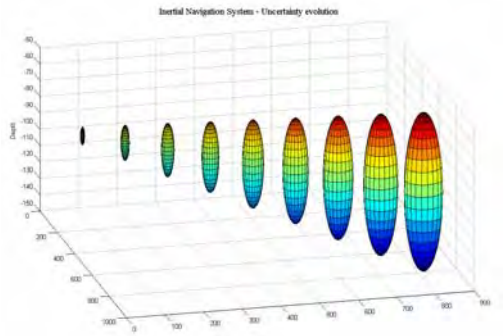

Figure 5-8: uncertainty ellipsoid growth – 5 hours simulation at a 5Hz sampling – ellipsoid update every 30 minutes

The strong vertical uncertainty is then reduced significantly by assimilating depth observations through a complementary filter.

5.2 *Complementary filter*

The use of a complementary filter also allows an improvement on the vertical position. Given that we have now two different estimates of the depth of the vehicle, we can use a complementary filter that combines the z^{KF} obtained from processing IMU and DVL data with the depth sensor data.

A complemtary filter is defined as followed: the filter deals here with uncertainties

$$z(k+1)=\begin{cases} z^{DS}(0) & for \quad k=0 \\ \frac{1}{N}z^{DS}(k+1)+\frac{N-1}{N}\left[z(k)+z^{KF}(k+1)-z^{KF}(k)\right] & for \quad k>0 \end{cases}$$

z^{KF} - depth's uncertainty of AUV from processing IMU and DVL data

z^{DS} - depth's uncertainty of AUV from the pressure meter DS

z - final estimated depth's uncertainty of AUV (output of the system)

N - constant parameter of the complementary filter. More N will be weak and more we will give confidence to the depth sensor measurements.

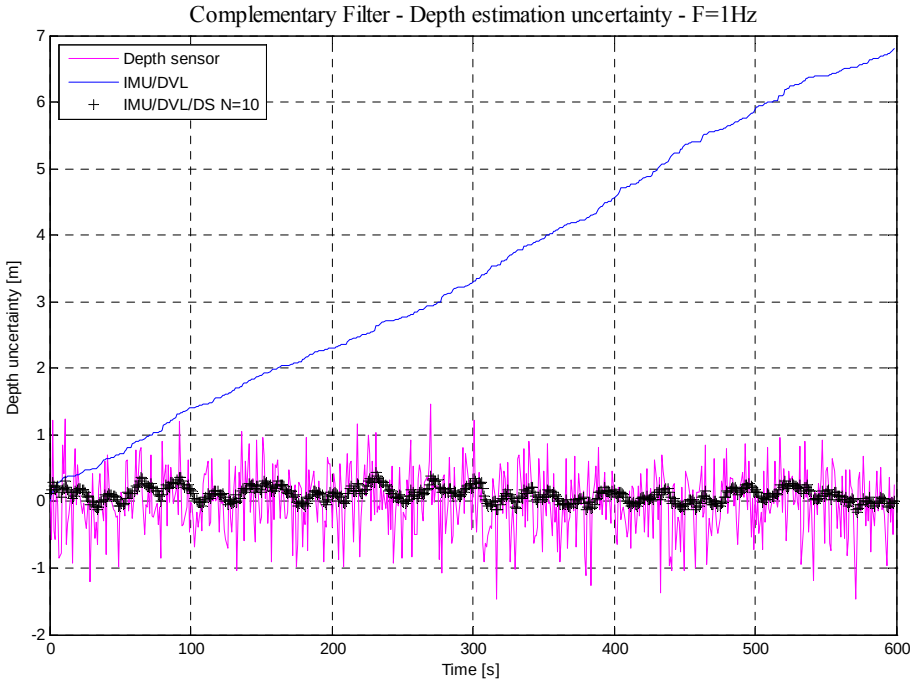

Figure 5-9: Comparison of depth errors of Depth Sensor (DS), IMU/DVL and IMU/DVL/DS – 600 seconds simulation – sampling frequency F=1Hz

5.3 *Energy consumption of an inertial navigation system*

In this simulation we will consider:

- IMU Kongsberg MRU-Z:

consumption 3 Watts

- DVL RDI workhorse Navigator:

consumption 8 Watts

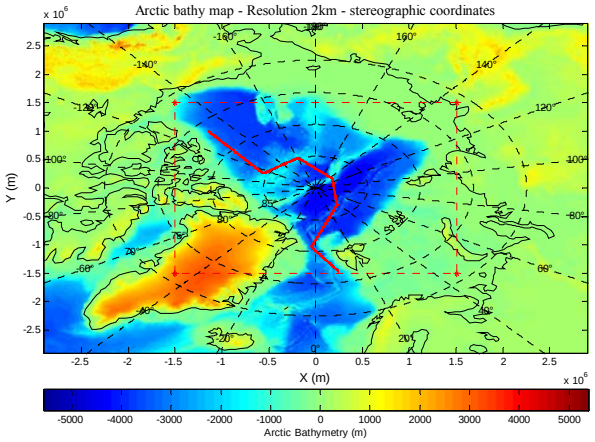

Figure 5-10: Trajectory used to check the Energy consumption of an INS – 158 days trajectory

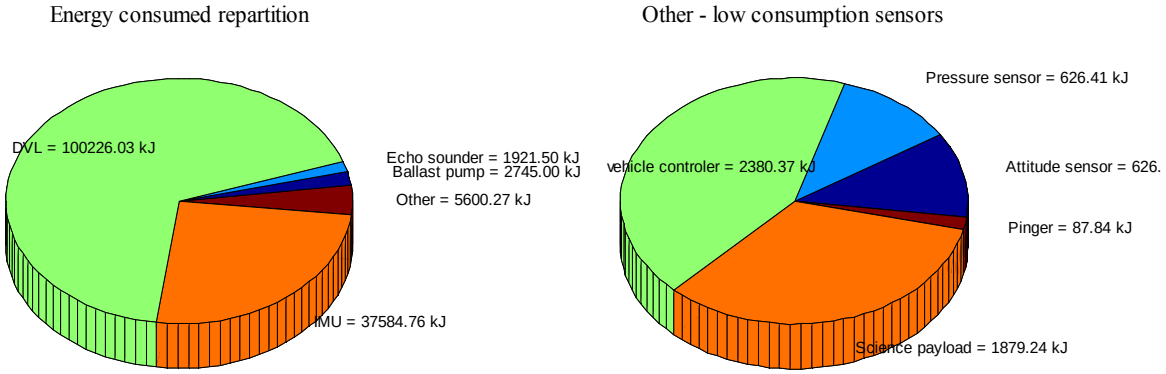

Figure 5-11: Energy consumption repartition among all glider's devices

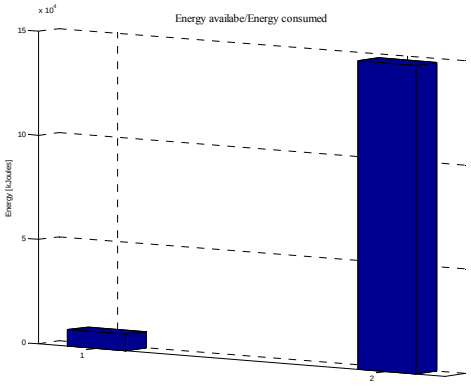

Figure 5-12: overtake of the energy budget

The figure 5-12 clearly underlines that even with low consumption inertial navigation instruments, the use of an Inertial Navigation System remains very "expensive". Thus, the use of such a system on a whole glider's trajectory is above the affordable energy budget with 26 battery packs.

This supports the idea that Terrain Navigation is much more suited to long range glider's missions. The total energy consumption is close to 160 MJoules. In current life, this consumption represents some 37 days of laptop energy requirements, while the glider's battery (7800 KJoules) is only able to provide 1.5 day of autonomy. Nonetheless, thanks to the Inertial Navigation System uncertainty algorithm implemented before, we will be able to compare the accuracy of the Terrain Navigation Particle Filter with a classical INS.

6 Comparison Terrain Navigation Particle Filter (TBN-PF) / Inertial Navigation System (INS)

This comparison of course strongly depends on the pinging policy, the variation in bathymetry, but it allows to give an overall idea of the interest of TBN-PF for long period submerged operations.

In this section, a comparison is performed on estimated position using two different underwater navigation systems:

- TBN-PF
- INS made of the combination of an IMU, a DVL, an EC and a DS.

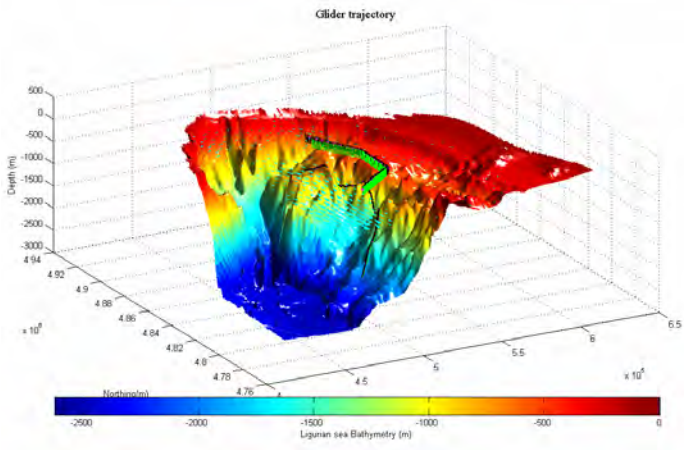

Figure 6-1: trajectory used for the comparison

The figure 6-1 represents the trajectory used to run the terrain navigation particle filter. It is a 3.5 days simulation in the Ligurian Sea, with a pinging policy of 1 ping every 5 dives. (starting point: south west)

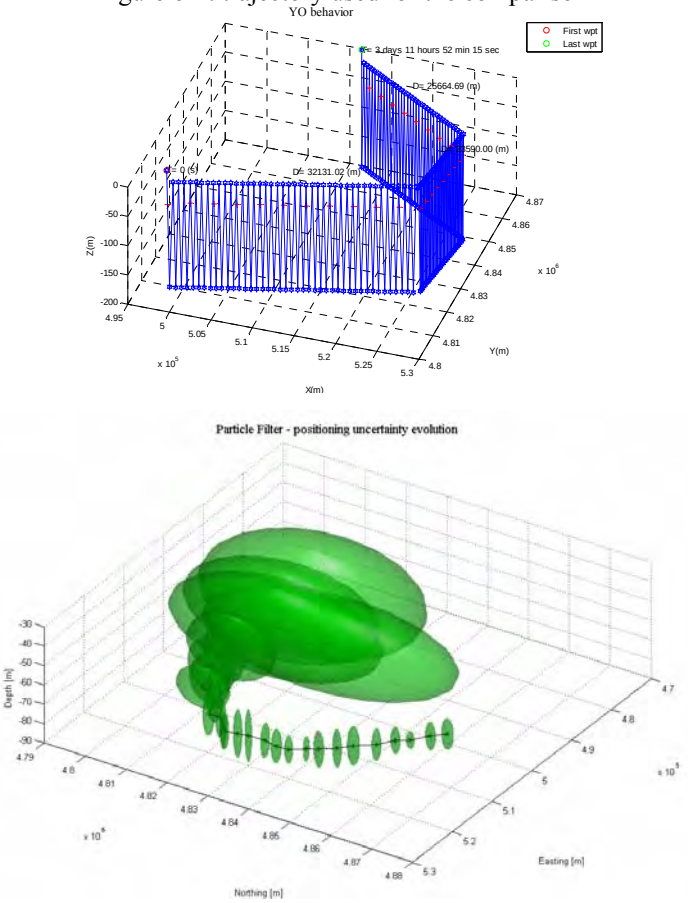

The figure 6-2 illustrates the evolution of the uncertainty ellipsoid we have with the use of the TBN-PF algorithm. The confidence on the estimated position is clearly improved with increasing number of observation.

Figure 6-2: TBN-PF uncertainty ellipsoid of estimated position

Below is the comparison between the TBN-PF and the Inertial Navigation System position uncertainty after 3.5 days of underwater navigation.

The figure 6-3 is the result of the inertial navigation system (INS) uncertainty algorithm at 1Hz which combines:

- An IMU with a DVL using a Kalman filter
- The IMU/DVL kalman filter estimated depth with the depth measured using a depth sensor through a complementary filter.

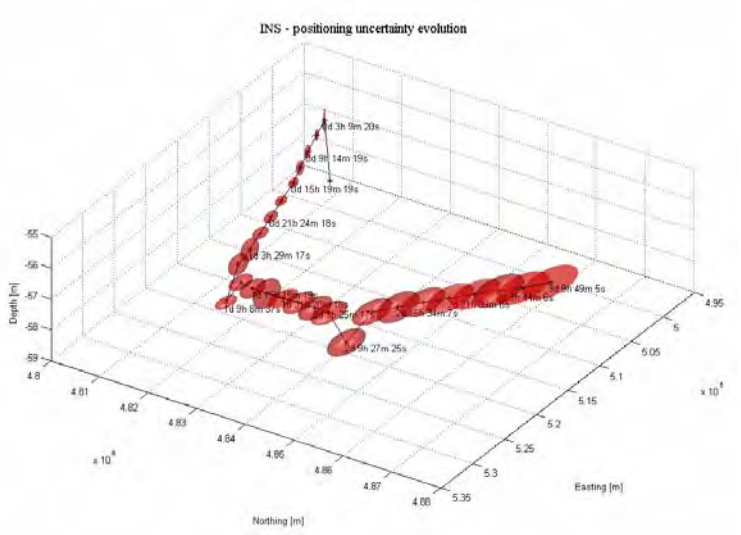

Figure 6-3: Evolution of position's uncertainty along the glider trajectory - We can clearly see the drifting nature of an INS

Thanks to the INS the glider is now able to see the current but its position estimation is burdened by a growing error. Now if we put those two different positioning systems uncertainty results on the same figure, we obtain the figure 6-4.

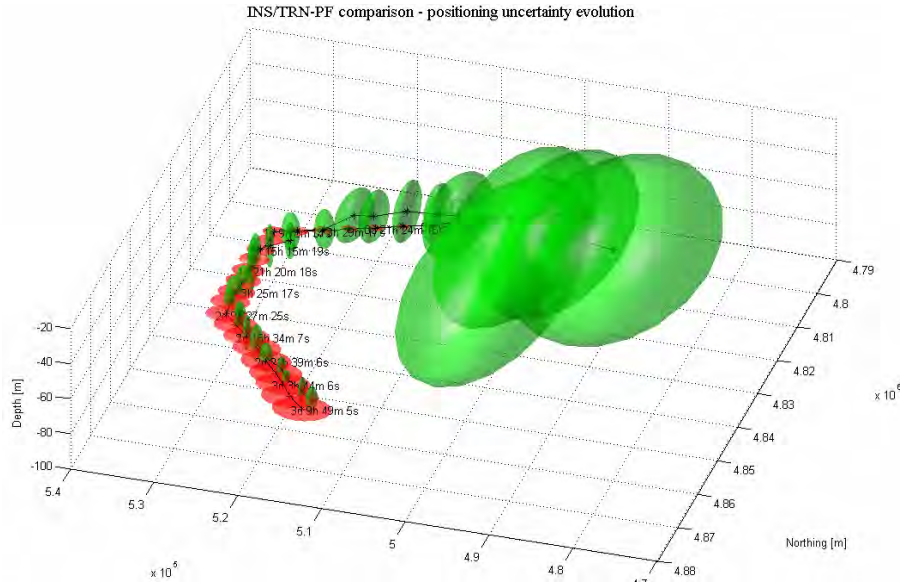

Figure 6-4: comparison TBN-PF (green) / INS (red) - uncertainty on estimated position

This figure supports the idea that after a long range mission, where an INS is burdened by drift, the terrain navigation seems to be a perfect tradeoff to meet:

- an accurate and precise position's estimation
- a restricted energy budget
- a low cost navigation system

Conclusion

As underlined in the abstract, the final objective of this project was to study the feasibility of a glider deployment under ice in the Arctic using Terrain Based Navigation approach. Given results furnished by the TBN-PF simulation development, this conclusion tries to provide clear answers to the fundamental question that has been raised: "Can we use a terrain navigation algorithm for a long range under ice mission in the Arctic Ocean?"

This study has shown that the answer to this question would be yes. In fact, the Terrain Based Navigation principle using a particle filter seems to be a perfect tradeoff to meet:

- an accurate, precise and independent positioning estimation process
- a restricted energy budget
- a low cost navigation estimation process

Those three criteria are the backbone for a successful long range under-ice glider mission.

The TBN-PF: an accurate, precise and independent positioning estimation process

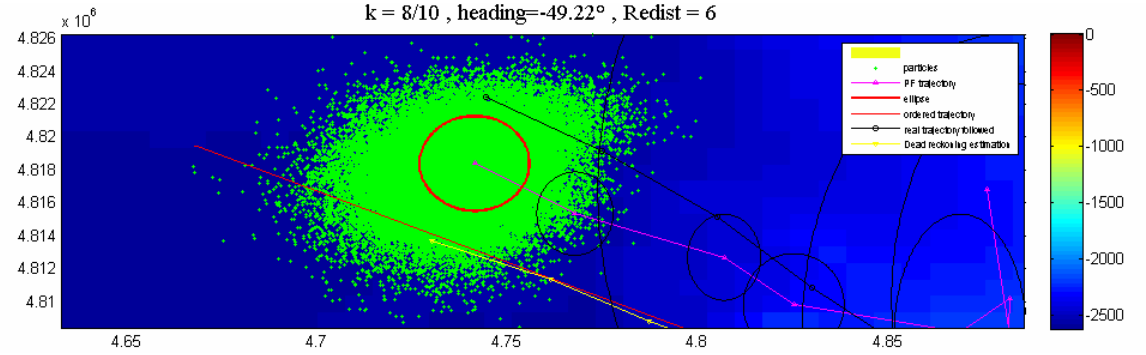

Fig Conclusion 1: accuracy (distance between the estimation and the real position) vs. precision (particles' cloud spreading) for the position estimation process

The particle filter has the ability to track a variable of interest over time thanks to the weight distribution and the re-sampling processes (see fig Conclusion 1). This tracking effect, which is strongly linked to the number of observations, has nonetheless the nice property to be "independent of time". This time independence of the navigation uncertainty, matches perfectly with a long range mission context.

Both accuracy and precision of the particle filter navigation estimation are linked to the resolution of the bathymetric chart and with the unique variability of the seafloor. Thus, for an Arctic crossing where the seafloor elevation presents significant variations, except for flights above Eurasian and Beaufort basins, the estimated position accuracy reaches promising results.

Moreover, the particle filter process presents the nice ability to detect any wrong track by comparing the estimated and measured depth. As soon as a wrong track is followed (this leads to a significant difference between estimated and measured depth), a particle explosion is applied from the last estimated position, and the tracking process restarts.

Finally, the particle filter works in a Bayesian framework, this probabilistic approach allows having some freedom in the dead reckoning process (prediction step) given that we work with a cloud of particles instead of working with a punctual isolated glider. Thus we just need some particles to be at the "right location" in order to converge to the real position.

The TBN-PF: a low energy consumption process

As underlined in Annex 3, Autonomous Underwater Vehicles (AUVs) operate solely on battery power, the mission endurance of today's AUVs depends highly on the capacity and usage of these batteries. It has been also highlighted that the use of an Inertial Navigation System made of an Inertial Measurement Unit and a Doppler Velocity Log would be too expensive for the limited energy budget of a long range glider's mission.

In this context, the use of the terrain navigation seems to be a perfect low energy consumption navigation solution. Moreover, given the tracking principle, the glider does not need to acquire a bathymetric observation at each time step, which allows significant energy savings (as underlined in Fig Conclusion 2). The terrain navigation can be used here to re-initialize the dead reckoning process like the Global Positioning System would do. Thus with a clever pinging policy, the glider would be able to accomplish a long range mission while keeping an acceptable position accuracy, in the range of the bathymetric chart's resolution.

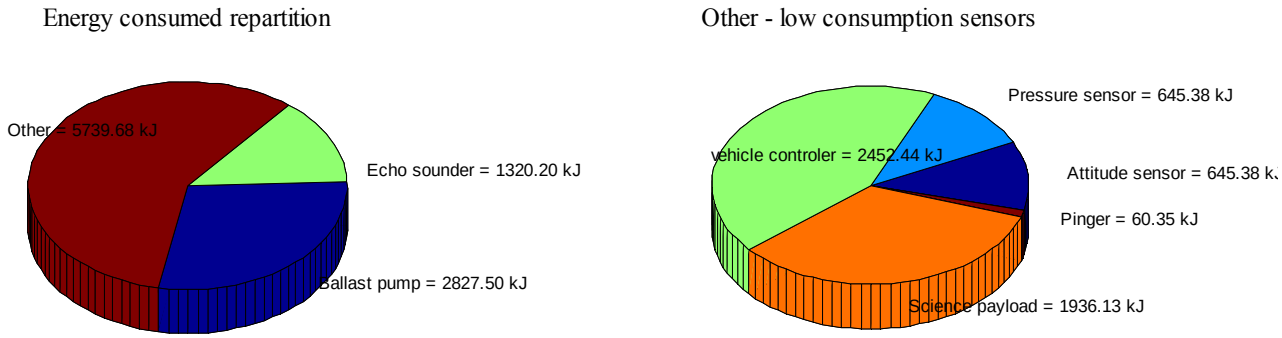

Fig Conclusion 2: Arctic crossing energy budget – thanks to a limited pinging policy, the Kongsberg EA600 Single Beam Echo Sounder (processing unit 75W + pinger 2kW) represents a small part of the global energy consumption

The TBN-PF: a low cost navigation estimation process

Space, ballasting and energy are the limiting factors of a glider mission. It seems difficult to meet with those three requirements at the same time. However the Terrain Based Navigation using a Particle Filter seems to be one of the best alternatives to meet those constraints while keeping accuracy more than acceptable given the cost of navigation instruments used. The Fig Conclusion 3 outlines in a qualitative way the interest in using the TBN-PF.

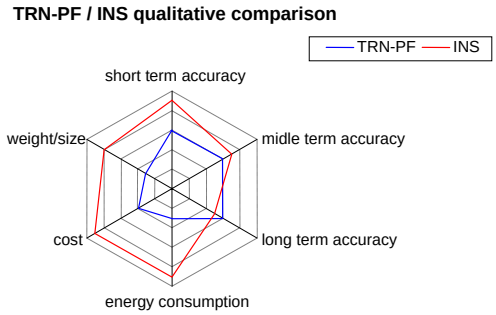

Fig Conclusion 3: qualitative comparison underlying the interest of using the TBN-PF process

Technologic improvements that have to be done before a deployment

The key idea behind using the terrain based navigation principle lies in the acquisition and processing of an accurate bathymetric data. However, for a deep water deployment area, where a low frequency single beam echo sounder (SBES) able to reach 4,000m range has to be used, a problem appears. The size and weight of transducers would not fit onboard a classical deep water Slocum glider.

In order to face this mechanical issue, two alternatives can be imagined:

- increase the payload capability of the actual deep water Slocum glider in order to allow for example the setting up of both the *Kongsberg EA600* transducer (5kg - 11cm x 24cm x 28cm) and science sensors

- develop very deep water gliders

Deep water gliders are now being developed. Those vehicles would be able to reach a depth of some 4000 meters. This capability would allow the use of a smaller and higher frequency SBES such as the *Knudsen mini sounder* (frequency: 24kHz – 210kHz, weight < 3kg - 257mm x 158mmx 89mm). The Annex A5.2 of this paper outlines the Arctic crossing simulation promising results of such a very deep water glider.

Importance of a clever mission planning

The mission planning remains one of the most important tasks for the success of a long range glider's mission. This TBN-PF simulation gives a global idea of the glider's behavior if combined with an adequate current model, but it also provides the expected accuracy in the positioning estimation process given the desired trajectory and the specified pinging policy.

Outcome

The Terrain Based Navigation using a Particle Filter is a promising independent navigation estimation process for a long range under ice mission. However, the bathymetric data collected must be accurate, and till now, due to ballasting constraints, a classical glider has not been able to load a low frequency single beam transducer able to collect accurate deep water bathymetric data.

References

[1] Ioannis M. Rekleitis, "***A particle Filter Tutorial for Mobile Robot Localization***" – Centre for Intelligent Machines, McGill University, Montreal – presented at the International Conference on Robotics and Automation 2003

[2] Stefan Williams, "***A Terrain-aided Tracking Algorithm for Marine Systems***" – Australian Centre for Field Robotics, School of Aerospace Mechanical and Mechatronic Engineering, Sydney - 2006

[3] F. Gustafsson, F. Gunnarsson, N. Bergman, U. Forssell, J. Jansson, R. Karlsson, P-J Nordlund, "***Particle Filters for Positioning, Navigation and Tracking***" – IEEE Transactions on Signal Processing – February 2002

[4] R. Karlsson, F. Gustafsson, "***Bayesian Surface and Underwater Navigation***" – Linkoping University, Sweden – October 2006

[5] B. Jalving, M. Mandt, O. K. Hagen, "***Terrain Referenced Navigation of AUVs and Submarines Using Multibeam Echo Sounders***" – Norwegian Defence Research Establishment (FFI) – 2004

[6] S. Paris, J-P. Le Cadre, "***Planification for Terrain-Aided Navigation***" – IRISA / INRIA / CNRS – 2003

[7] R. R. Beckman, A. Martinez, B. S. Bourgeois, "***AUV Positioning Using Bathymetry Matching***" - IEEE Oceans 2000 Conference

[8] P. Kaniewsky, "***Integrated Positing System for AUV***" – Military University of Technology, Warsaw, Poland – Molecular and quantum acoustic, vol 26, 115-127, (2005)

[9] D. E. Di Massa, "***Terrain Relative Navigation for Autonomous Underwater Vehicles***" – Massachusetts Institute of Technology / Woods Hole Oceanographic Institution, OCEANS '97. MTS/IEEE Conference Proceedings (1997)

[10] R. McEwen, Hans Thomas, D. Weber, F. Psota, "***Performance of an AUV Navigation System at Arctic Latitudes***" – Monterey Bay Aquarium Research Institute / Kearfott Guidance and Navigation Coorporation, Oceans 2003

[11] L. Morel, "***Geodesy ensieta manual***" – ESGT, Le Mans, France, 2008

[12] M. Legris, "***Sonar acoustic censieta manual***" – ENSIETA, Brest, France, 2010

[13] N. Seube, "***Kalman Filter ensieta manual***" – ENSIETA, Brest, France, 2010

[14] P. J. Sugimura, "***Arctic Ocean circulation in an idealized numerical model***" - Massachusetts Institute of Technology / Woods Hole Oceanographic Institution - 2008

[15] R. Grasso, D. Cecchi, C. Trees, M. Rixen, "***Model based decision support for glider operations***" - NURC - N.A.TO. La Spezia, Italy – 2009

[16] I. Nygren, M. Jansson, "**Terrain Navigation Using the Correlator Method**", Department of Signals, Sensors and Systems, Royal Institute of Technology (KTH), Sweden – 2004

[17] D. K. Meduna, S. M. Rock, and Rob McEwen, "**Low-Cost Terrain Relative Navigation for Long-Range AUVs**", Aeronautics and Astronautics Stanford University

[18] R. Karlsson, F. Gustafsson**, "Particle filter for underwater terrain navigation"** – Linkoping University, Sweden. – 2003

[19] P. E. Hagen, **"Making AUVs truly Autonomous" –** Kongsberg Maritime/Norwegian Defense Research Establishment (FFI) - OCEANS 2007

[20] R. Eustice, R. Camilli, and H. Singh **"Towards Bathymetry-Optimized Doppler Re-navigation for AUVs**" – Dept. of Applied Ocean Physics & Engineering
Woods Hole Oceanographic Institution – September 2005

Annex 1: Coordinates conversion

Geographic coordinates to UTM coordinates

(Source: geodesy manual – L. Morel [11])

The Universal Transverse Mercator coordinate system was developed by the United States Army Corps of Engineers in the 1940s. The UTM system divides the surface of Earth between 80°S and 84°N latitude into 60 zones, each 6° of longitude in width and centered over a meridian of longitude.

It belongs to the cylindrical projection family. A cylindrical projection is produced by wrapping a cylinder around a globe representing the Earth (see figure A1-2).

FigureA1-1: passage from the ellipsoid (φ,λ) to the sphere (Φ,Λ) (Gauss–Laborde transformation)

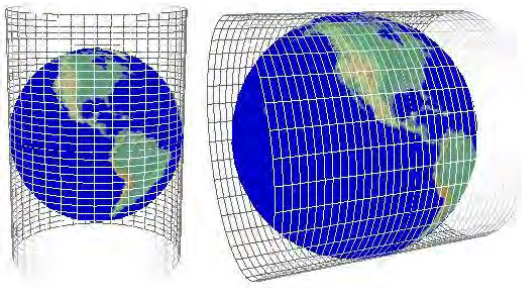

Figure A1-2: tangent cylindrical projection of the sphere

$$V=\sqrt{1+e'^2\cos^2\varphi} \qquad \cos\Phi=\frac{V\cos\varphi}{n_1}$$

$$n_1^2=1+e'^2\cos^4\varphi \qquad \tan\Phi=\frac{\tan\varphi}{V}$$

Coordinates conversion $(\varphi,\lambda)\rightarrow(X,Y)$

$$\begin{cases} X=X_c+\dfrac{k_0 a\sqrt{1+e'^2}}{2V^2}\ln\dfrac{n_1+v\sin\Lambda\cos\varphi}{n_1-v\sin\Lambda\cos\varphi} \\ Y=Y_c+k_0\beta(\varphi)+\dfrac{k_0 a\sqrt{1+e'^2}}{V^2}\arctan\left(\dfrac{\tan\varphi}{V\cos\Lambda}-\arctan\dfrac{\tan\varphi}{V}\right) \end{cases}$$

With:

- β ellipse arc length

$$\beta=a(1-e^2)\int_0^{\varphi}\frac{1}{(1-e^2\sin^2\varphi)^{\frac{3}{2}}}d\varphi$$

$$\beta\approx a(b_0\varphi+\sum_{i=1}^{4}b_i\sin 2i\varphi)$$

$$b_0=1-\frac{e^2}{4}-\frac{3e^4}{64}-\frac{5e^6}{256}-\frac{175e^8}{16384}$$

$$b_1=-\frac{3e^2}{8}-\frac{3e^4}{32}-\frac{45e^6}{1026}-\frac{105e^8}{4096}$$

$$b_2=\frac{15e^4}{256}-\frac{45e^6}{1024}-\frac{525e^8}{16384}$$

$$b_3=-\frac{35e^6}{3072}-\frac{175e^8}{12288}$$

$$b_4=\frac{315e^8}{131072}$$

- (X_c,Y_c) = (500,000 m , 0 m)
- $\Lambda=n_1(\lambda-\lambda_0)$

Geographic coordinates to stereographic polar coordinates

(Source: geodesy manual – L. Morel [11])

The stereographic projection is a mapping function that projects a sphere onto a plane. It is conformal, meaning that it preserves angles. However, it is neither isometric nor area-preserving, in other words it preserves neither distances nor the areas of figures.

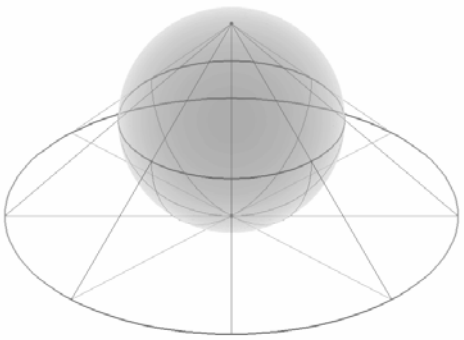

Figure A1-3: stereographic projection of a sphere on a plane

Step 1: passage from the ellipsoid (φ,λ) to the sphere (Φ,Λ)

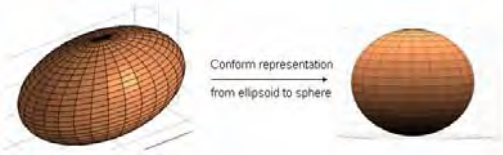

Figure A1-4: passage from the ellipsoid (φ,λ) to the sphere (Φ,Λ)

Isometric latitude and longitude

$$\begin{cases} L_{sphere}(\Phi)-L_{sphere}(\Phi_0)=n(L_{ellips}(\varphi)-L_{ellips}(\varphi_0)) \\ \Lambda-\Lambda_0=n(\lambda-\lambda_0) \end{cases}$$

With:

$$L(\varphi)=\ln\tan(\frac{\varphi}{2}-\frac{\pi}{4})+\frac{e}{2}\ln\frac{1-e\sin\varphi}{1+e\sin\varphi}$$

Step 2: passage from the sphere to the plane

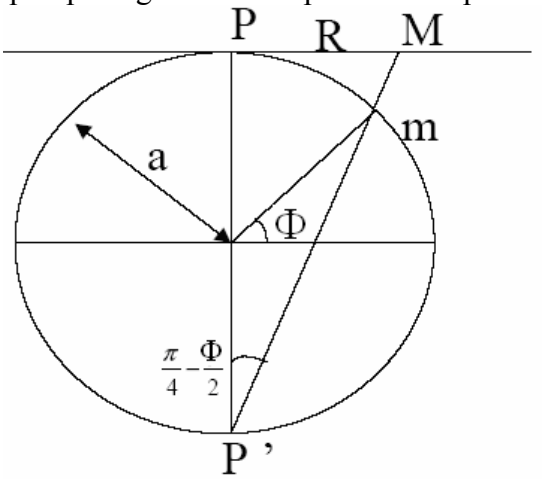

Figure A1-5: passage from the sphere to the plane

$$R=2a\tan(\frac{\pi}{4}-\frac{\Phi}{2})=2a\frac{(1-\sin\Phi)}{\cos\Phi}$$

$$\begin{cases} X=X_c+2a\dfrac{(1-\sin\Phi)}{\cos\Phi}\sin(\Lambda-\Lambda_0) \\ Y=Y_c+2a\dfrac{(1-\sin\Phi)}{\cos\Phi}\cos(\Lambda-\Lambda_0) \end{cases}$$

Annex 2: Product survey

The Slocum glider is already fitted with many instruments such as:

- CTD sensor
- Depth sensor
- Attitude sensor providing heading, pitch and roll measurements. (TCM3)

Both shallow and deep Slocum gliders provide a science payload where many other instruments can be set up.

As underlined in the Slocum glider manual, the payload was designed for easy removal and replacement for calibration needs or sensor type changes, allowing for great ease and flexibility to the user.

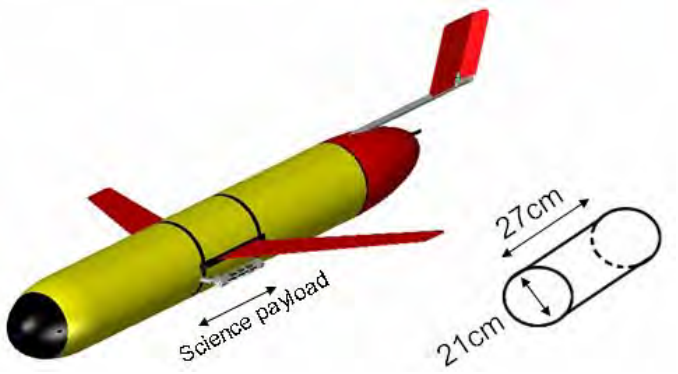

Nominal capacity:

- Shallow water glider: 4 kg
- Deep water glider: 2.5 kg

In this section we want to conduct a product survey of extra navigation sensors that could be used on a glider to improve its position estimation process.

We will focus on sensors such as:
- Single Beam Echo Sounder
- Inertial Motion Sensor
- Doppler Velocity Log

Single Beam Echo Sounder

Before starting the research, we have to define what we want. In order to reduce the research action field the sonar equation can be used.

Sonar equation (source: sonar acoustic manual of M. Legris [12])

Given underwater acoustic theory, we would like to find out the best technologic solution for a glider's mission under the arctic. There are three parameters that have a key influence on system's performances:

- The sonar itself
- The propagation environment
- The target

The sonar itself

As far as sonar is concerned, performances are linked with both source and noise levels, with the antenna directivity both in emission and reception, and with the internal data processing.

SL: *Source Level – Pulse energy of the active sonar*
NL: *Noise* Level – system internal noise (electronic or ambient)
DI: *Directivity Index – antenna lobe directivity*
PG: *Processing Gain*
DT: *Detection Threshold*

The propagation environment

The propagation environment is going to act by generating transmission and absorption losses.

TL: *Transmission Loss – geometric divergence and absorption losses*

RL: *Reverberation Level*
NL: *Noise Level*

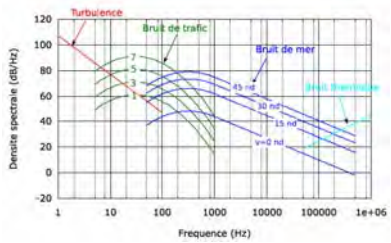

Figure A2-1: Wenz ocean noise model

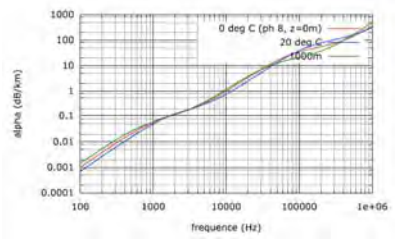

Figure A2-2: sea water coefficient absorption

Given that the coefficient absorption is a function of the square of the frequency, we can have a global idea of some sounders range as the figure below illustrates this.

Sounder frequency	Range
10 kHz	>10 km
50 kHz	5 km
100 kHz	1000 m
500 kHz	150 m
1 MHz	50 m

Table: Global idea of sounders range

The target

The target can be either the sea bottom or a for example a submarine. It can be characterized by two parameters:

TS : *Target Strength – Strength of the echo that goes back to the sonar*

SL : *Source Level – in the case of a passive sonar*

Sonar equation

The aim is to compare the received signal with the global noise (Signal to Noise Ratio SNR), and so to see if the system is able to detect the target.

$$SNR = \frac{signal}{noise} > treshold$$

If we consider active sonar, and if we work in dB, the sonar equation can be written as:

$$SL - 2TL + TS - NL + DI + PG > DT$$

With:

SL: source level
TL: transmission loss
TS: target strength
NL: noise level
DI: directivity index
PG: processing gain
DT: detection threshold

Parameters definition

Source level

If we consider that the acoustic source broadcast an acoustic wave in far field according to a spherical symmetry, the pressure field can be expressed as:

$$p(r) = \frac{A}{r} e^{jkr}$$

In order to define a parameter independent of the distance from the source and to work in dB, we set a reference distance from the source at 1m and we set a reference level at 1 µPa. Thanks to those considerations the source level can be expressed as:

$$SL = 20\log_{10}\frac{p}{p_{ref}}$$

It can be easily shown, considering the acoustic impedance that the expression above can be expressed as:

$$SL = 20\log_{10}\frac{p_{1m}}{p_{ref}}$$

$$SL = 10\log_{10} W_{elec} + 10\log_{10}\beta - 20\log_{10} p_{ref} + 10\log_{10}\frac{\rho_0 c}{4\pi}$$

Then,

$$SL = 10\log_{10} W_{elec} + 10\log_{10}\beta + 170.8 \quad with \quad \beta = \frac{W_{acoustic}}{W_{elec}}$$

Range of this source level is between 170 and 240 dB/1μPa/1m.

Transmission loss

We have to consider two contributions:

- Geometric divergence
- Absorption by sea water due to molecular interactions(viscosity, $Mg(SO)_4, BO(OH)_3$)

A global equation can be found:

$$TL = 20\log_{10} r + \alpha r$$

$$with \quad \alpha : absorption\ \ coefficient(dB/m)$$

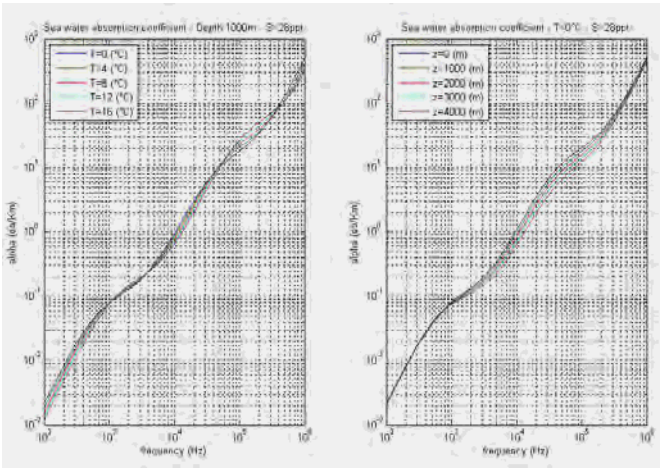

Figure A2-3: Absorption coefficient according to Francois and Garrison model

Target strength or sea floor backscatter

I represents the acoustic wave intensity. TS is expressed in dBm^2

$$TS = 10\log_{10}\frac{I_{backscatter\,1m}}{I_{incident}}$$

The seafloor backscatter can be expressed as:

$$BR = BR_0 + 10\log_{10} S$$

With S: insonificated surface

This backscatter coefficient depends on the kind of impulsion (short or long).

Considering the bandwidth B and the pulse length T, we are in short impulsion if:

$$BT > 1 \ \ or \qquad \frac{Br\varphi^2}{c} > 1 \qquad with \quad \varphi = 0.77\frac{\lambda}{D}$$

Short impulsion

$$BR = BR_0 + 10\log_{10} S = BR_0 + 10\log_{10}\frac{\pi c}{B} + 10\log_{10} r$$

Long impulsion

$$BR = BR_0 + 10\log_{10} S = BR_0 + 10\log_{10}\frac{\pi\varphi^2}{4} + 20\log_{10} r$$

Noise level

Contrary to the popular though, Ocean is not at all a silent world.

$$NL = NL_0 + 10\log_{10} B$$
$$with \quad B : \text{bandwidth}$$

Here NL_0 is the ambient noise

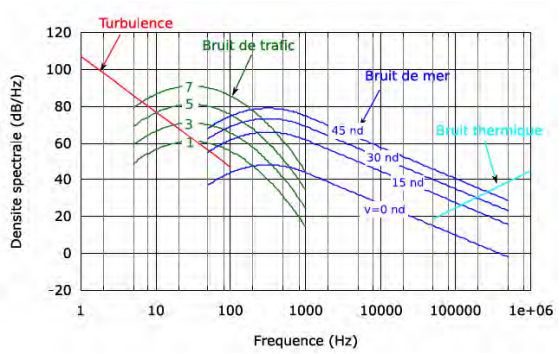

Figure A2-4: Wenz ocean noise model

Directivity index

For a circular antenna, both emission and reception gain can be expressed as:

$$DI_r = DI_e = 10\log_{10}\left[\left(\frac{\pi D}{\lambda}\right)^2\right]$$

The opening at 3dB is defined as the angular sector that contains more of one half of global signal intensity, for a circular antenna, it can be defined as:

$$2\theta_{-3dB} \approx 42.3\frac{\lambda}{D}$$

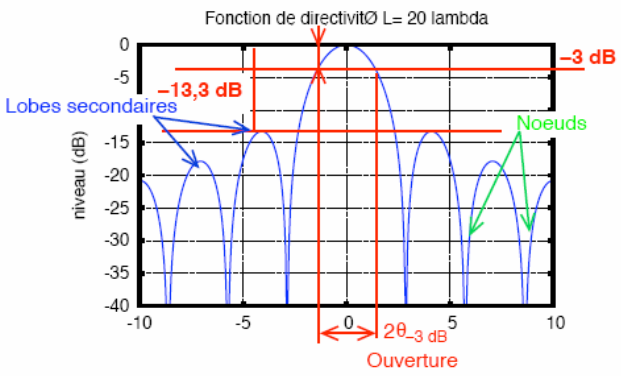

Figure A2-5: Directivity function for a linear antenna

Processing gain

$$PG = 10\log_{10} BT \qquad with \quad B : bandwidth$$
$$T : pulselength$$

Application: the idea is here to find the sounder range given frequency and sounder's power thanks to the sonar equation.

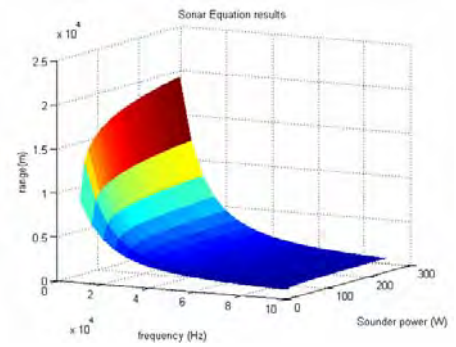

Figure A2-6: Ligurian sea conditionsT=10 C–S=35 ppt

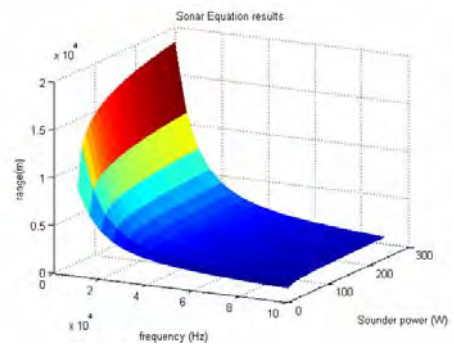

Figure A2-7: Arctic Ocean conditionsT=0 C–S=28 ppt

The sonar equation can allow us to dimensionalize the sounder:

- Find the beam opening
- Find the frequency
- Find the size of the antenna that would fit into the glider
- Find the power needed
- Find the bandwidth

In the case of an Arctic mission, we can expect that the maximum depth will be around 5,000 meters, this threshold is set on the figure below as a red surface.

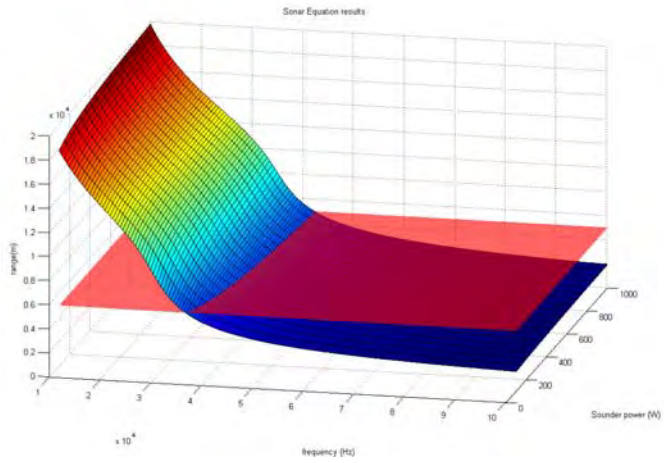

Figure A2-8: sonar equation range results => find the frequency range and the power range that allows the sounder to detect the seafloor (red surface: 5000m)

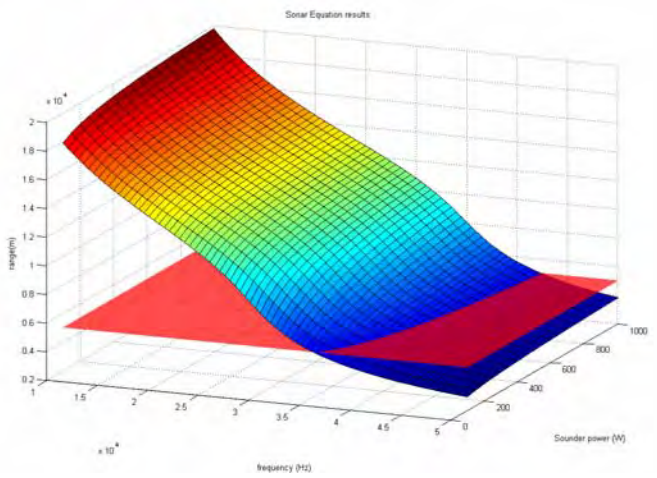

Figure A2-9: frequency range [10-50 kHz] – power [100-1000 W]

Outcome: Thanks to the figure A2-9, we are now able to have an idea and so to select a frequency range and a power emission policy for our sounder. We can also underline that even with a significant power, high frequencies waves are not able to propagate far away in the environment. In this context, if we choose a sounder that emits at 30 kHz or less we should be able to detect the Arctic sea floor without using a huge amount of energy.

Sounder selection

The echosounder has to collect accurate information about the sea bed in order to provide data to the terrain navigation particle filter.

Figure: AUV multi beam echo sounder survey

A broad range of sonars and echosounders exists:

- Multibeam echo sounders
- Wide-swath systems
- Singlebeam echo sounders
- Sidescan sonars
- Imaging Sonars
- Sub bottom profilers
- Synthetic Aperture Sonar

Each one of this system is dedicated to a specific mission. Here we have to do a compromise between the accuracy we need and the energy consumption.

For a long range autonomous mission, given that on the one hand the place is limited, and on the other hand the energy is restricted; the most reasonable choice seems to be the use of a singlebeam echo sounder. The use of a multibeam echosounder for TBN is discussed in paper [16], while the paper [20] tackles the use of the bottom track of a DVL.

On the website: *http://www.hydro-international.com/productsurvey*, we can find a survey of latest single beam echo sounders released on the market.

In this article we can find all parameters of interest that will lead us in the sounder selection. Some of those key parameters are:

- Power consumption
- Weight and dimensions
- Frequency range
- Depth range of operation
- Depth resolution, accuracy
- Power output of transducer
- Pulse length
- Beam angle

Given the sonar equation study did before, and given characteristics of those single beam echo sounders, we are able to find some systems that would fit with our mission.

Deep sea application (depth > 5000m)

- Kongsberg EA 600:

One of the single beam echo sounder that seems to match with our mission is the EA 600. It supports low frequencies and is suited for deep water operation. Frequency range is from 10 kHz to 710 kHz which allows to detect the seafloor from extreme shallow to 10,000m water depth.

Transducer's weight / dimensions:

5kg – 11x24x28cm

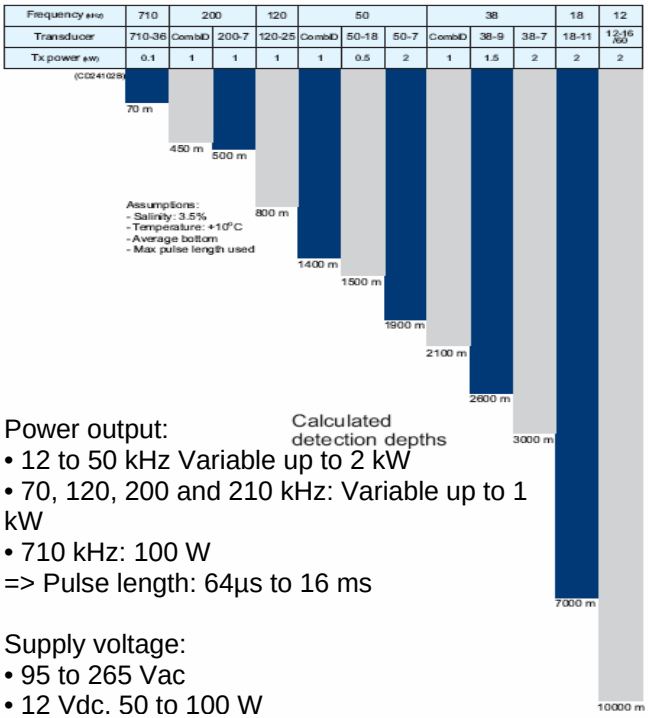

Power output:

- 12 to 50 kHz Variable up to 2 kW
- 70, 120, 200 and 210 kHz: Variable up to 1 kW
- 710 kHz: 100 W

=> Pulse length: 64µs to 16 ms

Supply voltage:

- 95 to 265 Vac
- 12 Vdc. 50 to 100 W

- Atlas Hydrographic GmbH – DESO 30

The DESO 30 from Atlas would also match with our mission. The high frequency channel covers a frequency range from 100 kHz to 750 kHz and is mainly used for survey applications in shallow water and for sidescan operation. The low frequency channel between 3.5 kHz and 50 kHz has a higher depth range and can also be used for sediment investigation.

Transducer's weight / dimensions:

4.5kg – 18cm ∅ x 17cm height

Company	ATLAS Hydrographic GmbH
Year of initial development	2002
Product	ATLAS DESO 30, 210kHz SW6014 & 33kHz SW6028
Physical description	
Max. power consumption (W)	50
Power (DC, AC)	11-28VDC or 115/230VAC
Weight (in air) and dimensions (w x h x d) of transducer/ transceiver	SW6014: 0.7kg without cable, 14.5kg with 33m cable; 11cm Ø, 13cm height SW6028: 4.5kg without cable, 13.5kg with 33m cable; 18.4cm Ø, 17cm height
Weight and dimensions (w x h x d) of display and logging unit	16kg; 44.3cm x 44.4cm x 27.5cm
Portability of logger (rack, desktop, portable)	Desktop
Mode of operation	
Software platform (Windows, other)	Standalone, ATLAS DESO CONTROL (scope of supply)
Depth range of operation (m)	1.0-6,000
Frequency range (kHz)	Low: 3.5-50 High: 100-750 (Manual tuning in 1kHz steps)
Number of frequencies supported simultaneously	2
Power output of transducer at standard frequencies	1.5-2kW @ low; 0.3-1kW @ high
Beam angles (along and across)	18° @ 33kHz; 9° @ 210kHz
Depth resolution, accuracy	18cm ± 0.1% depth @ 12kHz; 10cm ± 0.1% depth @ 33kHz; 1cm ± 0.1% depth @ 210kHz
Max. pulse sounding rate	25Hz
Pulse length	Freely selectable up to 60 circles
Dynamic range (dB)	212

The main problem remains the weight and the size of such single beam echo sounder. Moreover, if we look for light SBES (weight < 2 kg), the range seriously drops below 100 meters. The Atlas Hydrographic GmbH – DESO 30 seems to be the best single beam echo sounder for an Arctic mission. However the buoyancy of the glider would have to be reshuffled.

Inertial Measurement Unit

The glider is not originally fitted with an Inertial Measurement Unit (IMU). Till now, it relies on a low cost position estimation process. In this section we would like to see to what extent it is possible to fit the glider with such a device.

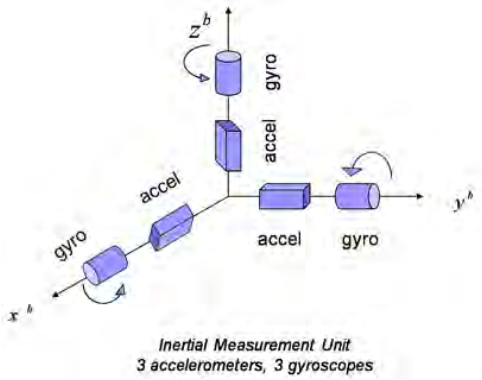

Figure A2 -10: Inertial measurement unit of S3 Missile

On most of AUVs, the IMU is one of the key elements that composes the global Inertial Navigation System (INS). A classical IMU such as the IXSEA octans3000 outputs heading, roll, pitch, surge, sway and acceleration. This data is then sent to the INS that combines all data coming from external sensors. As external sensors we can find for example a Doppler Velocity Log or an acoustic Long Baseline system.

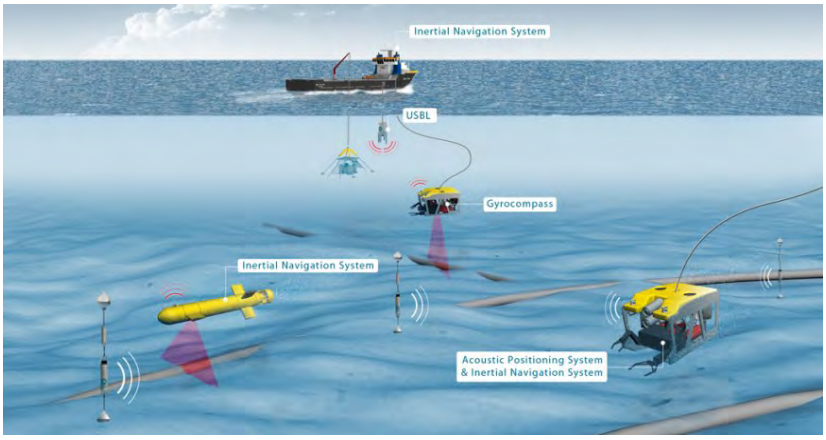

Figure A2-11: Underwater positioning solutions (*source www.ixsea.com*)

A major disadvantage of using IMUs for navigation is that they typically suffer from accumulated error. This leads to 'drift', or an ever-increasing difference between where the system thinks it is located, and the actual location. However when a IMU is combined with an underwater acoustic positioning systems (as USBL), the position of a ROV, AUV or sonar can be determined with robustness and accuracy unequalled by any other system on the market.

Till now, the Slocum glider uses a tilt compensated 3 axes compass module (TCM3)

Features

• High resolution compass heading: 0.1º
• High repeatability: 0.05º
• Extra wide tilt range: +/- 80º
• Calibrated magnetic field measurement range: +/- 80 µT (+/- 0.8 Gauss)
• Extended temperature range: -40º to 85ºC
• Low Power: < 20 mA typical current draw
• Small size: 3.5 x 4.3 x 1.3 cm
• Weight : 12 g
• Compass heading accuracy : 0.5 º
• Pitch Accuracy 0.2°
• Roll Accuracy:
  0.2º for pitch < 65º
  0.5º for pitch < 80º
  1.0º for pitch < 86º

If we do an IMU product survey in order to have an idea of the accuracy we can get with such a device, we can find:

- **Ixsea octans 3000** subsea gyrocompass and motion sensor

OCTANS is a subsea survey-grade gyrocompass and complete motion sensor for water depths up to 3,000m. Based on FOG technology it outputs heading, roll, pitch, surge, sway and acceleration.

Heading

Accuracy 0.1 deg

Resolution 0.01 deg

Roll / Pitch

Dynamic accuracy 0.01 deg

Resolution 0.001 deg

Power consumption 15 W

IXSEA use fibre-optic gyro (FOG) technology in their systems. A FOG is a gyrometer, which is a sensor that instantaneously measures the rotational speed of a mobile platform. The FOG is based on the Sagnac effect, discovered in 1917 by a physicist named Georges Sagnac.

- **Kongsberg Motion Reference Unit (MRU)**

The MRU family is the highest performance model measuring six degrees of freedom.. It outputs absolute roll, pitch and yaw (heading), and relative heave (dynamic). Acceleration and velocity of the linear motions, as well as angular acceleration and velocity, are also outputed. MRU-Z specifications:

- Housing dimensions Ø105x129 mm
- Weight 1.5 kg
- Power requirements 12-30V DC, Max. 3 W

	Roll/pitch	Heading	Heave	Acceleration [m/s2]
MRU Z	0.15°	1.0°	5 cm	0.05

Doppler Velocity Log

Workhorse Navigator DVL

In order to improve the underwater position estimation, we can investigate the possibility to fit a glider with a Doppler Velocity Log (DVL). As specified in the datasheet, Teledyne RDI's highly acclaimed Doppler Velocity Log (DVL) provides precise and accurate velocity and altitude updates for a wide variety of underwater tasks. One of the underwater task can be the determination of a reliable and accurate high-rate navigation and positioning data. Thus, the Workhorse Navigator DVL can be used stand alone to collect high precision velocity data, or can be integrated into an existing navigation system to provide frequent, and crucial, navigation updates.

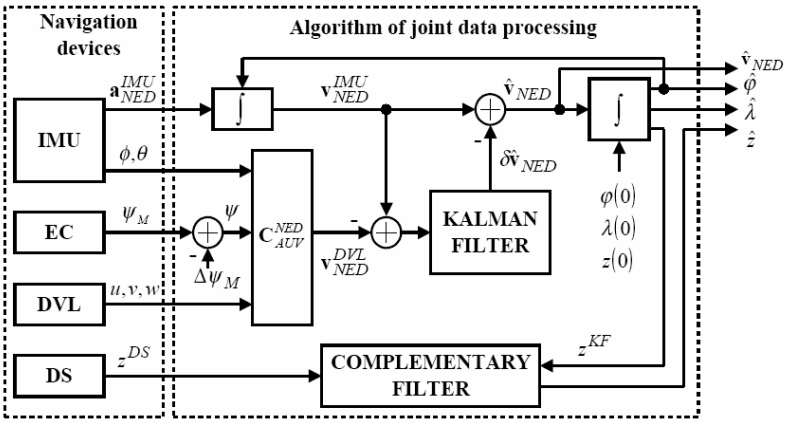

Figure A2-11: Structure of the positioning process for an AUV – source: *INTEGRATED POSITIONING SYSTEM FOR AUV* (Piotr KANIEWSKI, Military University of Technology, Warsaw, POLAND)

As the figure A2-11 highlights it, the velocity data provided by the DVL can be integrated in a complete navigation system in order to correct the Inertial Measurement Unit data from environmental constraints. In other words, the AUV is now able to identify the current to which it is submitted.

The measurements of accelerometers and gyros have various types of errors (biases, scale factor error…), and thus inertial positioning through integration of accelerations is burdened with errors

that increase without bound. For this reason, the combination of IMU and DVL data is usually done thanks to a Kalman filter.

RDI Workhorse Navigator DVL specifications

Technical Specifications

Model		WHN 300	WHN 600	WHN 1200
Bottom Velocity				
Single-ping precision				
Std dev at 1m/s[1]		±0.3cm/s	±0.3cm/s	±0.3cm/s
Std dev at 3m/s[1]		±0.6cm/s	±0.5cm/s	±0.4cm/s
Std dev at 5m/s[1]		±0.8cm/s	±0.6cm/s	±0.5cm/s
Long-term accuracy		±0.4%±0.2cm/s	±0.2%±0.1cm/s	±0.2%±0.1cm/s
Minimum altitude[2]		1.0m	0.7m	0.5m
Maximum altitude[2]		200m	90m	30m
Parameters				
Velocity range[3]		±10m/s	±10m/s	±10m/s
Velocity resolution		0.1cm/s	0.1cm/s	0.1cm/s
Ping rate		7Hz max	7Hz max	7Hz max
Water Reference Velocity				
Accuracy		±0.4% ±0.2cm/s	±0.3% ±0.2cm/s	±0.2% ±0.1cm/s
Layer size		selectable	selectable	selectable
Minimum range		1m	0.7m	0.25m
Maximum range		110m	50m	18m
Environmental				
Operating temperature		-5 to 45°C	-5 to 45°C	-5 to 45°C
Storage temperature		-30 to 75°C	-30 to 75°C	-30 to 75°C
Depth rating		3000m or 6000m		
Weight in air:	3000m	15.8kg	15.8kg	12.4kg
	6000m	20.1kg	20.1kg	18.0kg
Weight in water:	3000m	8.8kg	8.8kg	6.1kg
	6000m	13.6kg	13.6kg	12.1kg
Power				
DC input		20–50VDC, external supply (48VDC typical)		
Current		0.4A minimum power supply capability		
Transmit[4]				
Peak power @ 24VDC		66w	21w	8w
Average power (typical)		8w	3w	3w

Dimensions

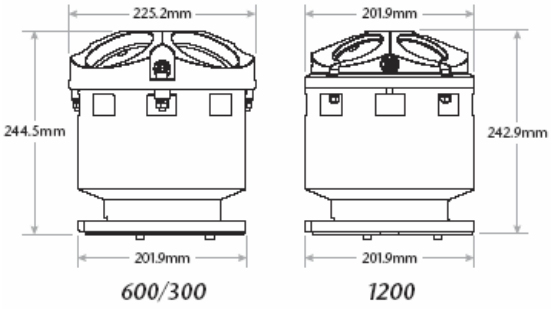

Navigator full suite of capabilities:

- *Bottom track velocity*
- *Water track velocity*
- *Altitude: 4 individual measurements*
- *Error velocity (data quality indicator)*
- *Temperature*
- *Heading/Tilt*
- *Acoustic echo intensity*
- *Pressure and depth (optional)*
- *Current profiling (optional)*

The most problematic issue that appears here is the weight of a DVL. We clearly overtake the nominal weight we are allowed to set on a glider.

Annex 3: Energy budget

Given that Autonomous Underwater Vehicles (AUVs) operate solely on battery power, the mission endurance of today's AUVs depends highly on the capacity and usage of these batteries. Typically, missions for the Slocum Electric Glider last about 30 days. Longer missions, such as the 221 day mission to cross the Atlantic by RU27 from Rutgers University are possible through an increase in the number of batteries and through the careful planning of the usage of the vehicle's devices.

Mission critical tradeoff decisions have to be made between energy consumption and sensing, data processing, and communication activities.

In this context, effective power and energy management requires knowledge about the actual energy consumption of each active component within the AUV. So, to perform more precise mission planning, being conscious of the energy consumption of individual components is necessary.

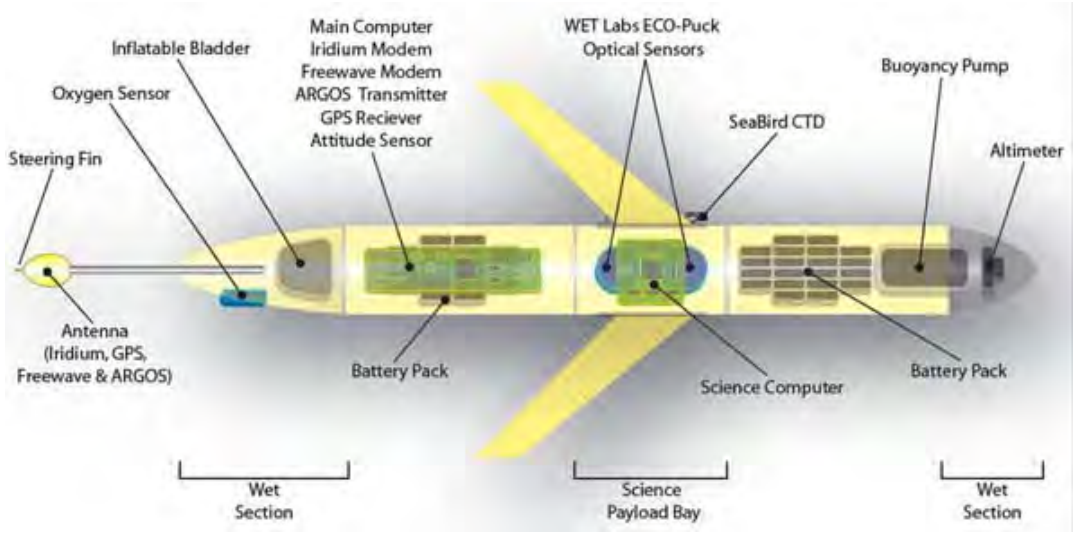

Figure A3-1: Slocum glider structure

Glider's main components requiring energy consumption

Displacement Piston Pump(Buoyancy Pump)

The ballast pump is used to change the buoyancy of the device. A single-stroke piston, using a 90 watt motor and a rolling diaphragm seal, moves 504 cc of sea water directly into and out of a short 12 mm diameter port on the nose centerline.

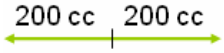

The course of the piston is usually set to displace 200 cc of water.

Thus for each inflection the pump has to move some 400 cc using a 90 Watts motor with a debit of 24 cc/sec.

Pitch Vernier

To trim to the desired dive and climb angles a lead screw drives the forward 8.4 Kg battery pack fore or aft as a vernier. The battery pack is put full forward during surfacing to better raise the tail out of the water for communications.

Altimeter

The transducer is mounted such that it is parallel to a flat sea bottom at a dive angle of nominally 26 degrees. If we consider the use of the Kongsberg EA600, the processing unit requires around 75 Watts, but we can imagine to set up a low consumption "sleep mode", while the transducer requires some 2 kW during 16ms.

CTD

SeaBird is now developing low-power CTD for autonomous gliders with the high accuracy necessary. Those sensors consume only 150 mW while sampling at 1 Hz.

Vehicle Controller

A Persistor CF1, based on a Motorola 68338 processor is used to control the functions of the Glider. In literature, we can find an energy consumption of 0.19 W at a clock rate of 3680 KHz.

Attitude Sensor

The Precision Navigation TCM2-50 provides the bearing, pitch, and roll indications of the Glider with a sampling rate between 1 and 30Hz. These inputs are used for dead reckoning the vehicle while under water. Recalibrating the compass, depending on the magnetic anomalies of the usage area, may at times be necessary.

TCM2-50

TCM2 electronic compass sensor module with tilt compensation of ±50°.

Heading Information	
Accuracy when level:	1.0° RMS
Accuracy when tilted:	1.5° RMS
Resolution:	0.1°
Repeatability:	±0.3°
Tilt Information	
Accuracy:	±0.4°
Resolution:	0.3°
Repeatability:	±0.3°
Range:	±50°

Power Requirements

Supply Voltage: - +5 V-DC regulated or 6 to 18 V-DC unregulated

Current: - Operating standard mode: 15-20 mA
- Operating low power mode: 7-13 mA
- Sleep mode: 2.5 mA

Pressure Transducer

Micron 300 PSIA strain gage transducers are used for vehicle control and dead reckoning. In literature, we can find an energy consumption of 50 mW

ARGOS (source: www.argos-system.org)

Argos locations are calculated by measuring the Doppler shift on the transmitter signals. The processing center calculates an initial estimate of the transmitter's position from the first and last messages collected during the pass and the most recent calculated frequency. In literature, we can find that the energy consumption is close to 1W.

Air Pump System

An air bladder in the flooded tail cone is used to provide additional buoyancy on the surface for bettering communications (the tail fin houses three antennas: ARGOS 401 MHz, RF modem 900 MHz, and a patch with combined GPS 1575 MHz and Iridium 1626 MHz). It is inflated, using air from the hull interior, providing 1400 ml of reserve buoyancy.

GPS

A Rockwell Jupiter engine turned on and while on the surface is used to locate the Glider's position. When the glider is in surface it gets a GPS fix every 5 seconds. In literature, we can find that the energy consumption is close to 975 mW.

Iridium

Iridium delivers reliable, near real-time, mission-critical communications services and creates the vital lines of communication that help improve lives, build businesses, and develop new opportunities.

If we consider The Iridium 9602 SBD transceiver, we can find an average power of 1W

RF modem

Freewave 900 MHz radio modem is used for the local high-speed communications link to the Glider. In literature, we can find that the energy consumption is close to 1W.

Batteries

Battery packs consist of 10 Duracell C-cells in series, diode protected, nominally 15 volts. As indicated below, the number of packs can be adjusted depending on reserve buoyancy after Payload considerations. Given 26 packs (260 C-cells) the battery weight is 18.2 kg and energy available 7,800 kJoules. This battery pack would be able to provide power to a laptop for more than 37 hours.

Evolution of the Energy consumption

The figure A3-2 illustrates the energy consumption evolution on one yo cycle.

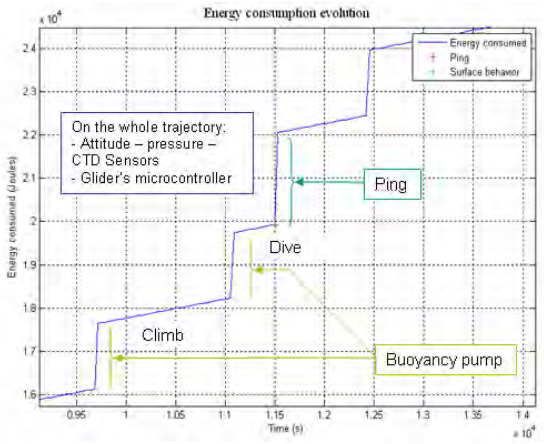

Figure A3-2: Energy consumption evolution on one cycle

Given all those energy consumption requirements we are now able to have an idea of the global energy consumed during a mission (Figures A3-3 and A3-4)

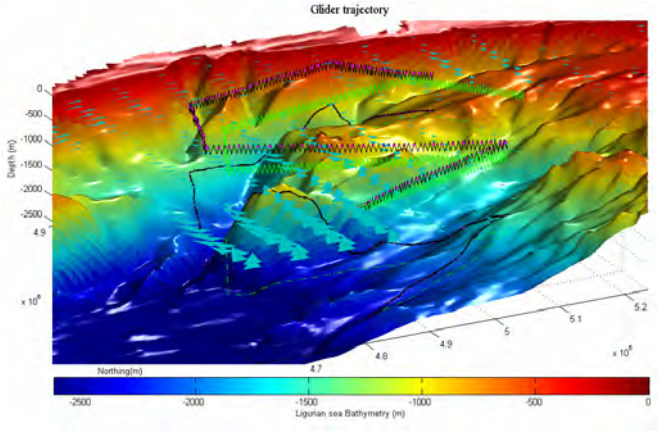

Figure A3-3: trajectory used for the simulation (7 days) – desired trajectory (green) – real trajectory followed (black)

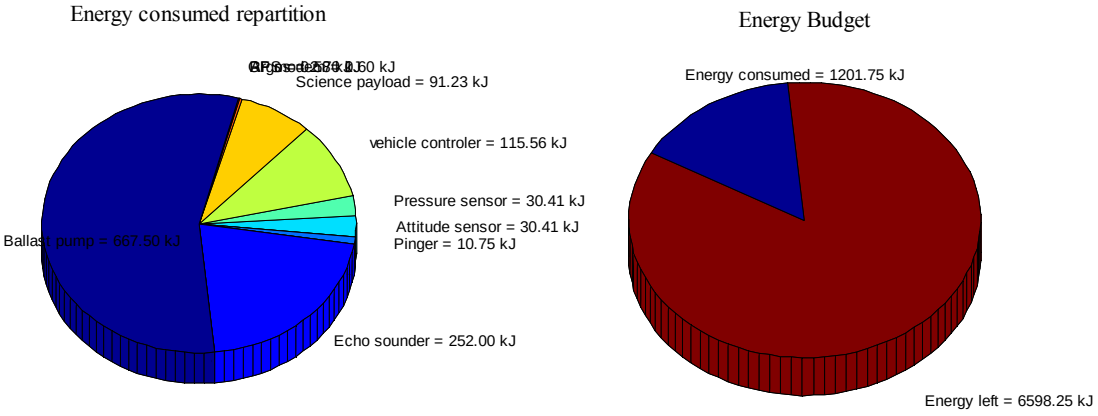

Figure A3-4: Energy budget study on a 7 days trajectory

Annex 4: Ligurian Sea deployment:

During June, a fleet of Slocum gliders has been deployed at sea in order to test their behavior and to train glider's pilots. In the mission planning, the glider has been desired to go back to the surface every 5 hours and every time that its dead reckoning process (black line on the figure A4-2) thinks having reached a waypoint. When it surfaces the glider estimates the current thanks to the difference between its last dead reckoning position estimation and the first GPS fix (blue arrows on the figure A4-2).

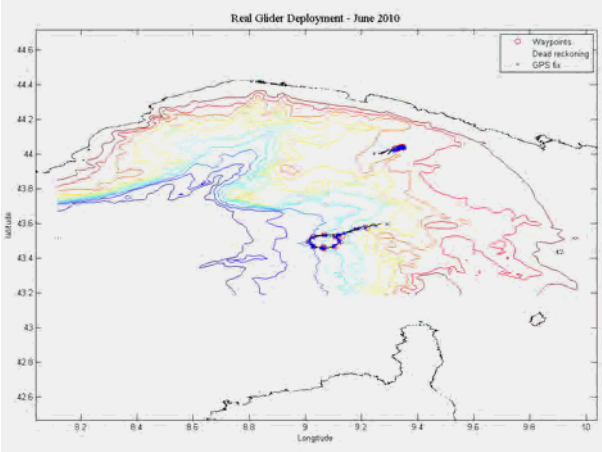

Figure A4-1: Real glider deployment - mission's length: 14 days 21 hours

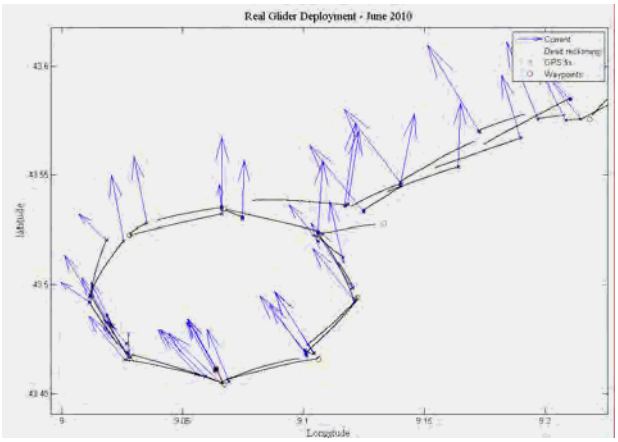

Figure A4-2: zoom in the lower part of the trajectory Glider's navigation data

Given that the gliders is "always" trying to go back to the surface to get a GPS fix, it is not very easy to compare this in situ deployment with the TBN-PF simulation developed in this paper. The idea behind using terrain navigation is to have a low cost positioning estimation process for long period submerged mission, which was unfortunately not at all the aim of this Ligurian Sea deployment.

The simulation that follows is roughly based on the same waypoints but reduced (7 days mission) and illustrates the behavior of a glider using the terrain navigation for its navigation estimation process.

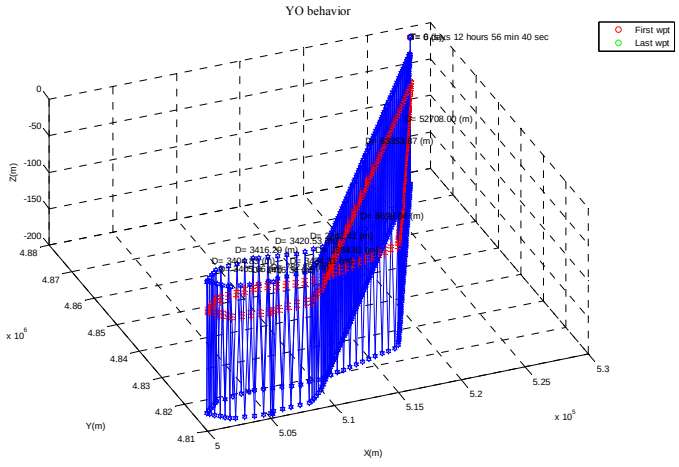

Figure A4-3: pinging policy of 3 pings per dive / every dive

In this simulation, the glider is constrained to remain underwater, without the possibility to acquire a GPS fix. In that case, figures A4-4 and A4-5 illustrate the influence of predicted current on trajectory.

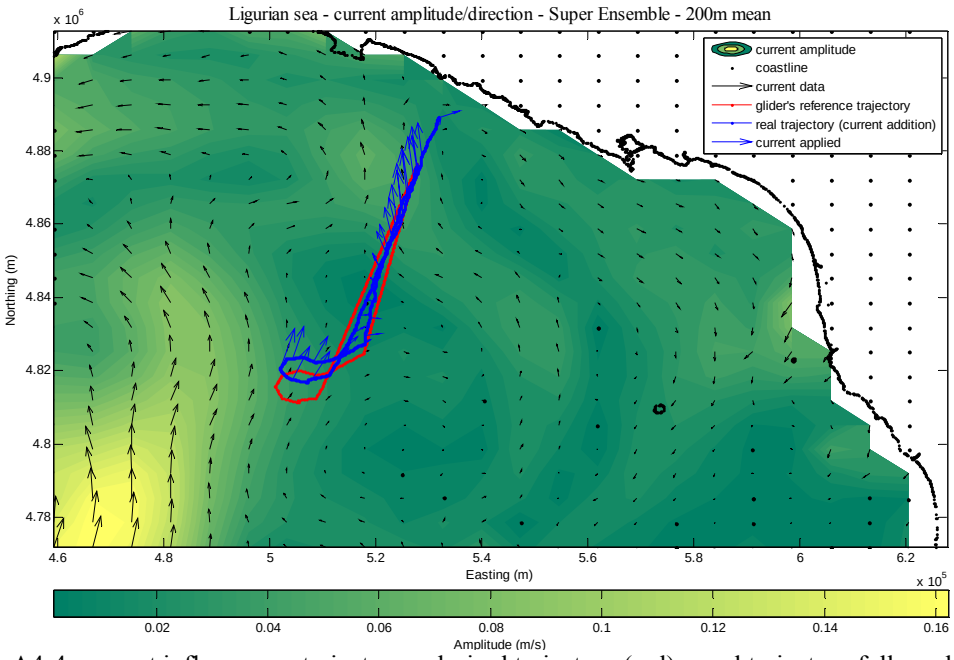

Figure A4-4: current influence on trajectory – desired trajectory (red) – real trajectory followed (blue)

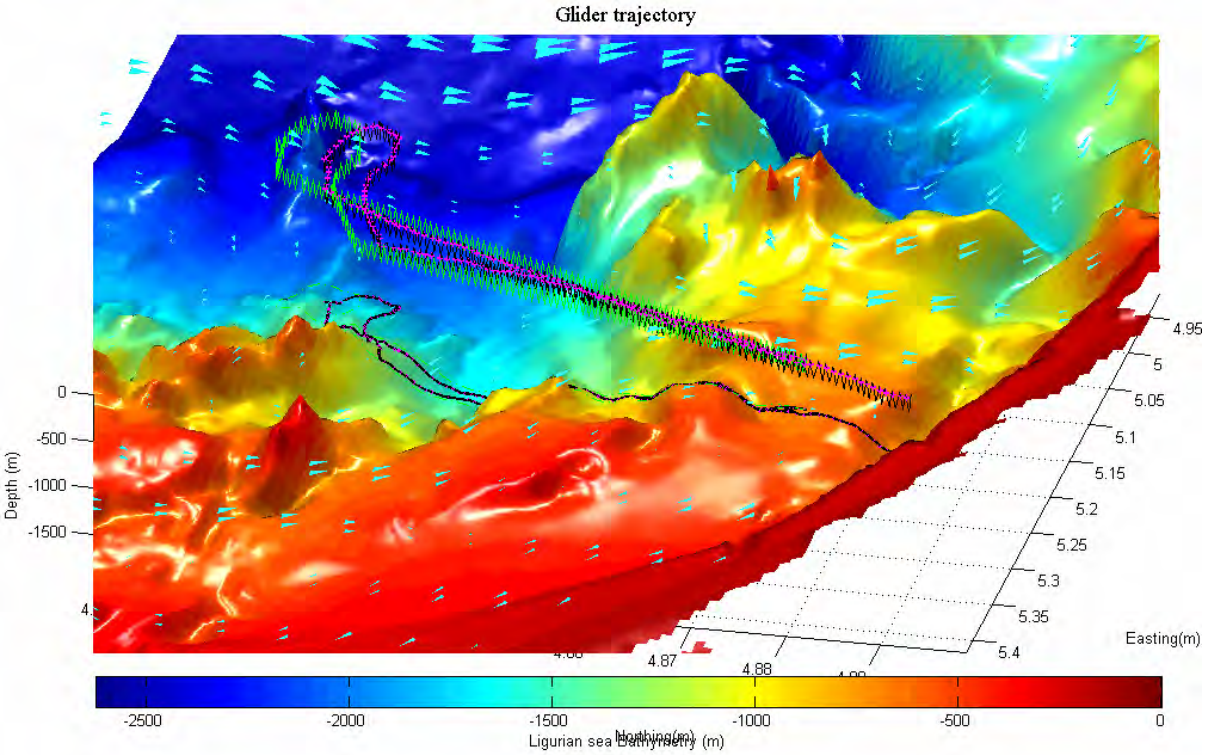

Figure A4-5: current influence on trajectory 3D view with projection on the sea floor of ping location – desired trajectory (green) – real trajectory followed (black)

Terrain navigation results

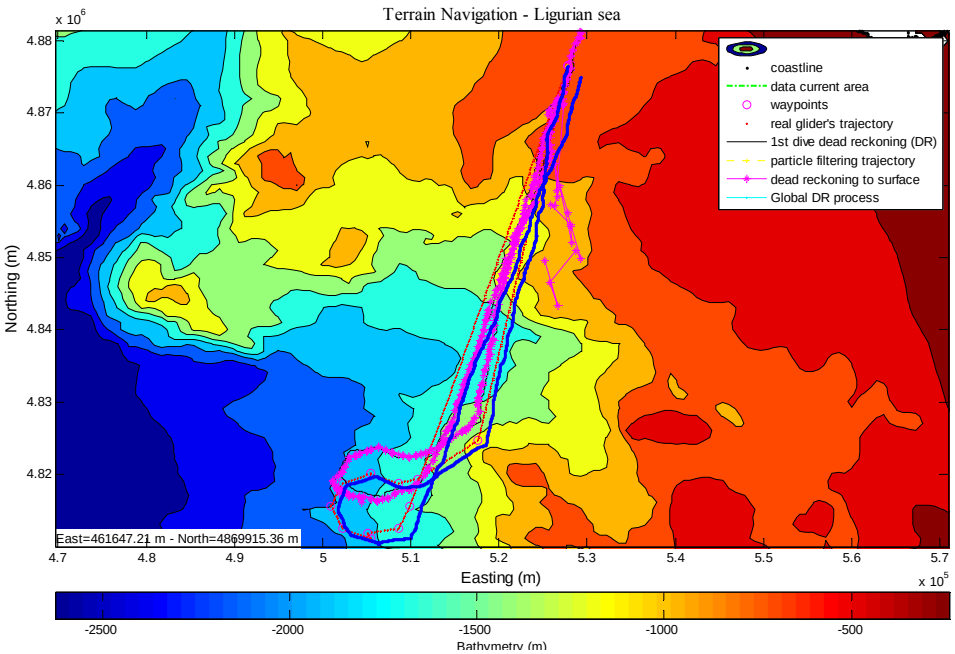

Figure A4-6: Particle filter results - Dead reckoning estimation: blue trajectory
- Particle filter estimation: magenta trajectory

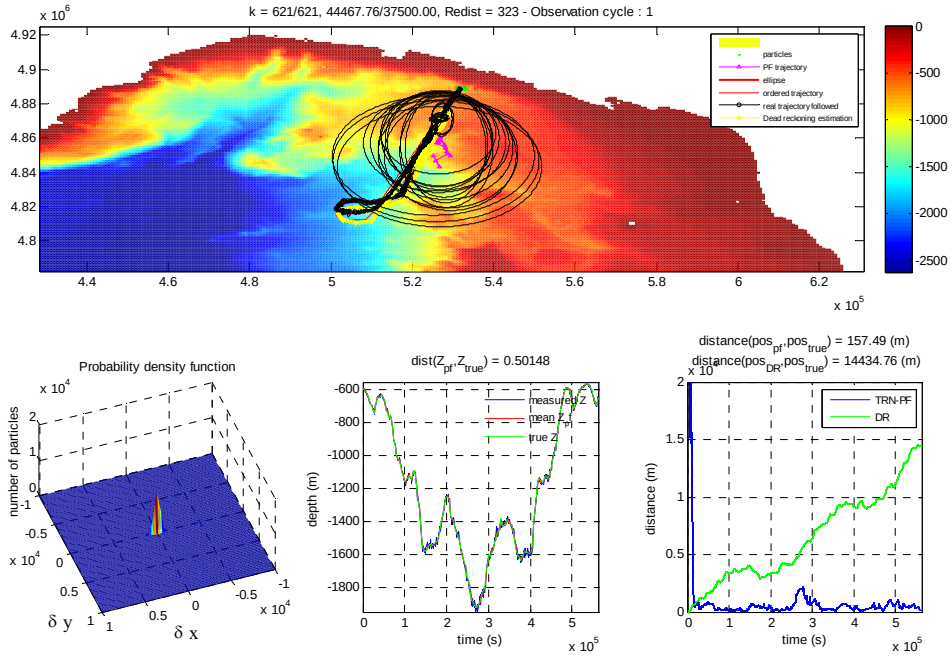

Figure A4-7: Iterative particle filter results

Figures A4-6 and A4-7 underline the ability of the terrain navigation particle filter to track the real position, and this in a much more accurate way than with the simple use of the dead reckoning process.

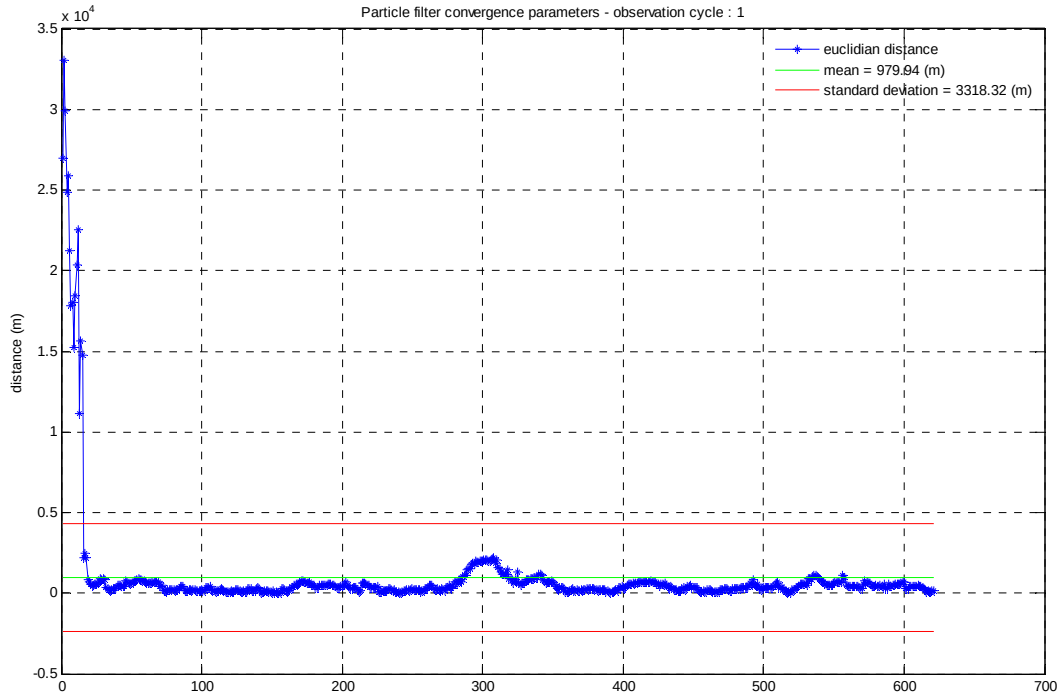

Figure A4-8: TBN-PF accuracy results

The figure A4-8 underlines the idea that TBN-PF is fitted to long range gliders' deployments. In fact, we can clearly see that the TBN-PF is not constrained by a either time or current drift and that the expected positioning accuracy is promising given the low cost navigation process.

Moreover, we can outline that the use of the Terrain Navigation is not expensive as far as energy consumption is concerned. However, given that the backbone of the TBN-PF is a reliable bathymetric data, the main issue remaining is the size and the weight of a long range low frequency single beam echo sounder.

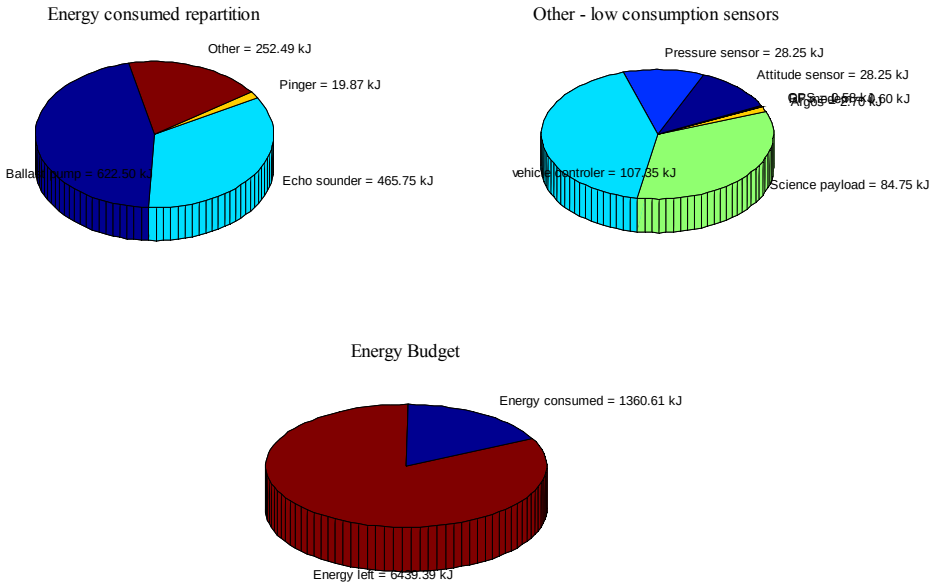

Figure A4-10: Energy budget using

Annex 5: Arctic crossing simulation

Annex 5.1: Deep water Slocum glider simulation (1000m)

In this section, a Arctic crossing simulation using a deep water Slocum glider (1000m) is run. To perform such a crossing, we define:

- 4 waypoints
- pitch angle: 26 degrees
- diving target depth: 1000 meters
- climbing target depth: 100 meters
- pinging policy: 2 pings per dive performed every dive

The figure A5-1 illustrates the desired trajectory pattern used for this simulation. It would represent some 149 days of submerged mission under the ice with neither the possibility to acquire a GPS fix nor to use any other device to retime the dead reckoning process. In this context, the terrain navigation seems perfectly fitted for such a mission.

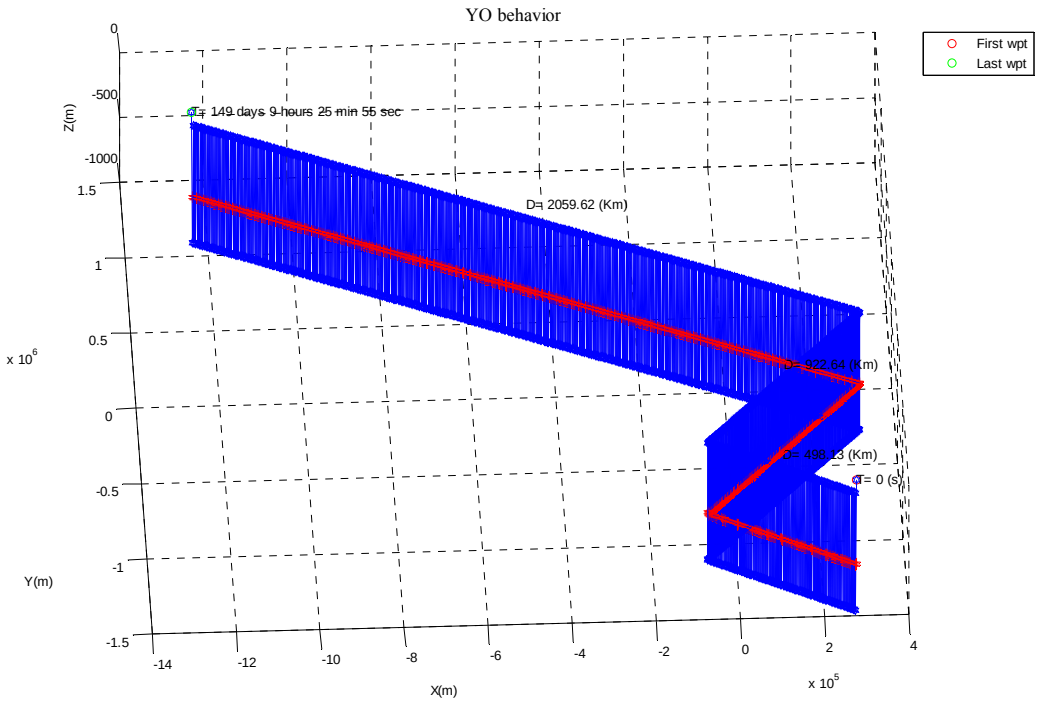

Figure A5-1: desired trajectory for the Arctic crossing simulation

We set a "predicted" model of current on the deployment area. The blue line on the figure A5-2 represents the trajectory that the glider is going to follow because of the current constraint, while its dead reckoning process will think to follow the red trajectory.

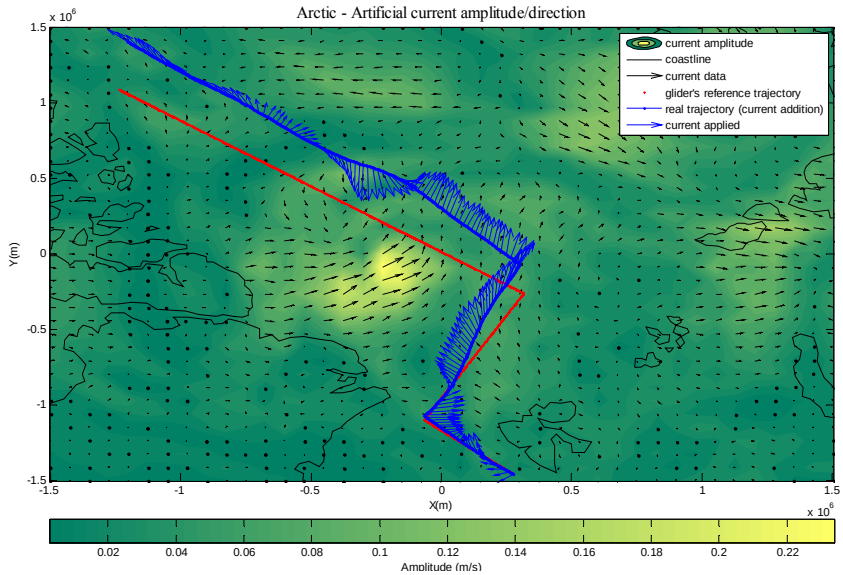

Figure A5-2: Trajectory constrained by currents

The figure A5-3 also illustrates those two trajectories that lead the simulation. It also highlights that, due to the implemented current, the glider has drifted towards the two main Arctic basins.

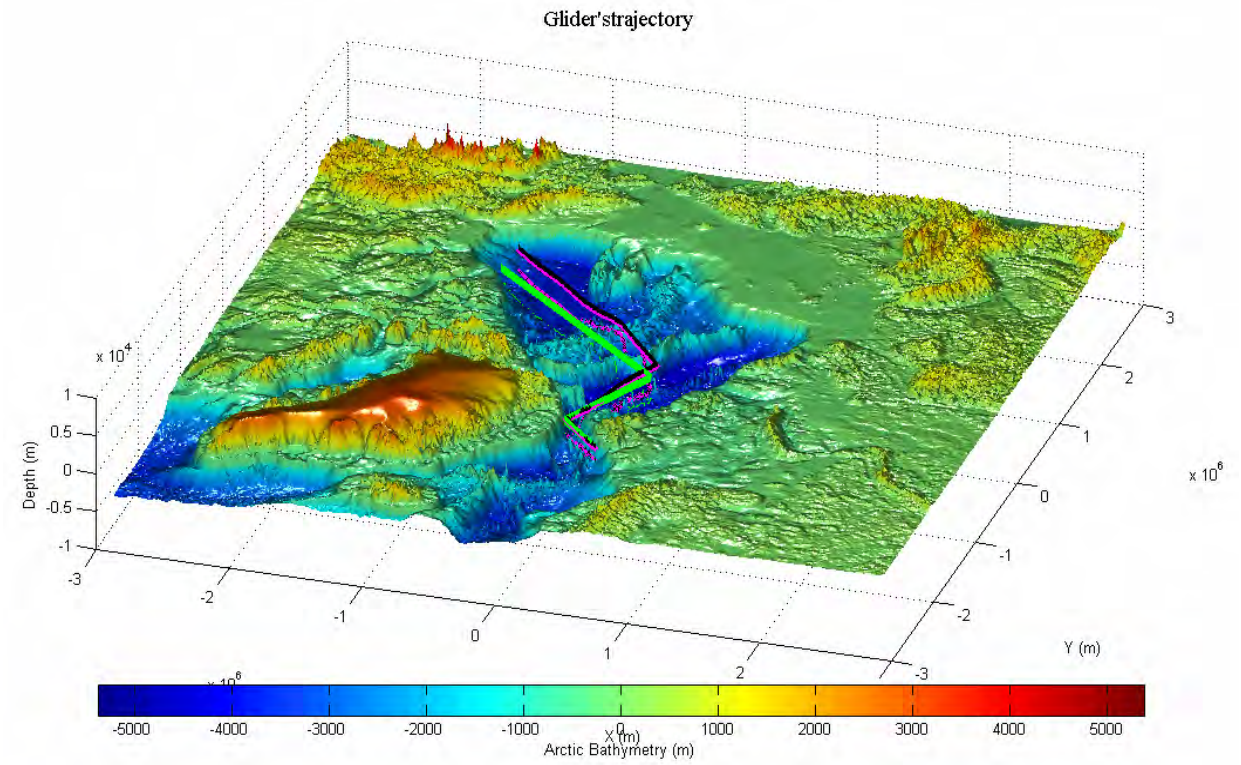

Figure A5-3: Arctic crossing – desired trajectory (green line) – trajectory constrained by currents with bathymetric measurements (black line)

Particle filter results

- The Terrain Navigation Particle Filter presents promising results for long submerged glider missions. As underlined in section 4.1, the position accuracy depends on sea floor elevation variability. However, the glider's drift toward the two deep sea basins implies that it struggles retrieving its real position in an accurate and precise way. Those difficulties are due to the strong uncertainty on bathymetric measurements but also to the lack of variability of the sea floor. This idea is illustrated in figure A5-4 (see magenta and red circles).

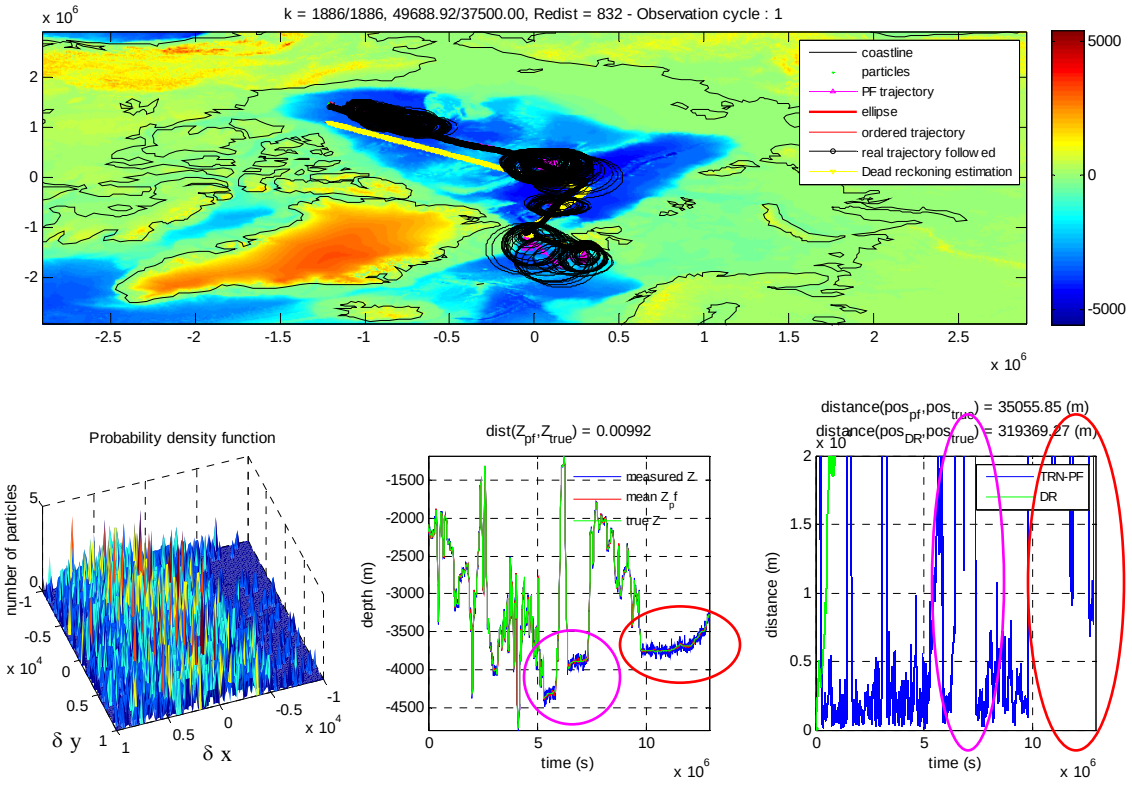

Figure A5-4: TBN-PF simulation

- However the TBN-PF has the ability to detect that it is following a false track, and so to correct for it. To do so, the TBN-PF computes at every time increment the difference between the bathymetric measurement and the depth of the estimated position (see section 2.4.5 for statistical estimations of the particle cloud). If the difference between those two depths is too significant, it means that the TBN-PF estimated position is stuck in a dead end. In such case, a kind of particle explosion is applied to "restart" the convergence process of the particle filter. This particle explosion is based on the last position estimation and tries to enclose a large area. The figure A5-5 illustrates a particle explosion performed during this simulation and the restart of the tracking process.

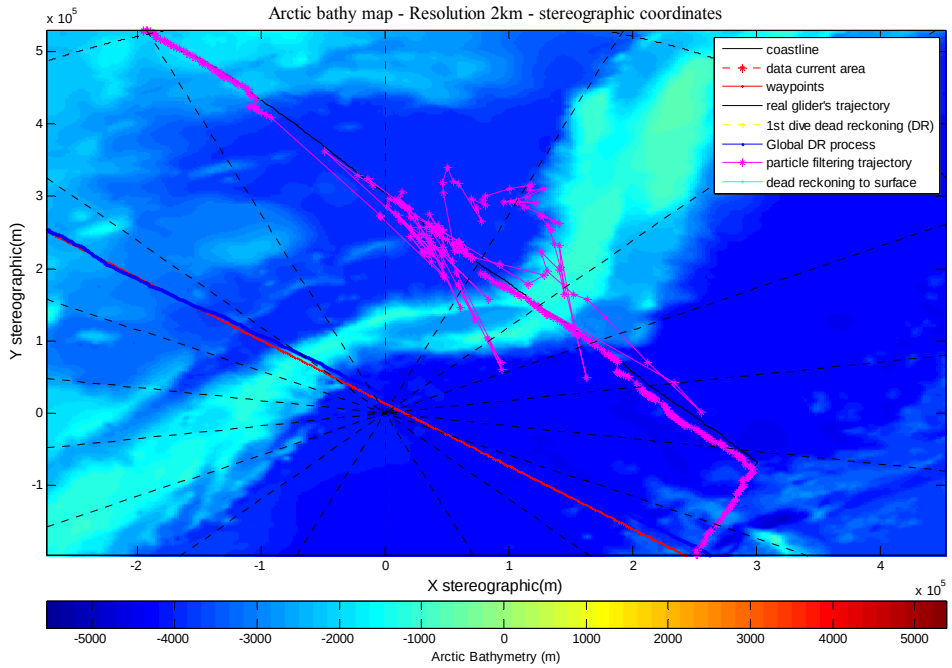

Figure A5-5: "Particle explosion" when the filter is "lost" – the tracking process restarts

- Despite difficulties faced in crossing the deep water basins, the TBN-PF shows encouraging results and clearly overtakes the dead reckoning accuracy. The figure A5-6 outlines the TBN-PF positioning accuracy on the whole trajectory. Given the resolution of the IBCAO Arctic chart (2 km resolution grid) and accuracy results obtained, the TBN-PF seems to be a perfect low cost positioning estimation process.

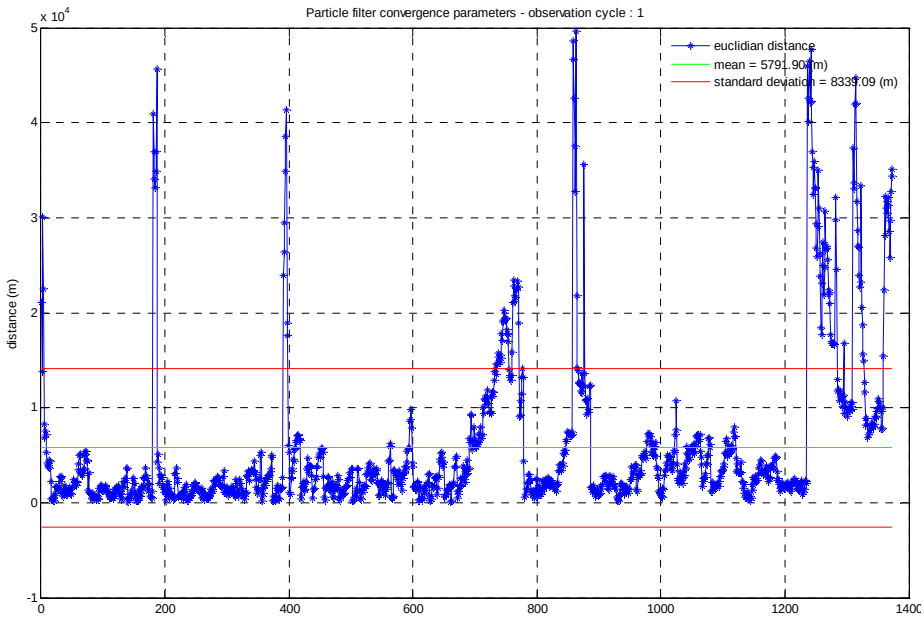

Figure A5-6: Particle filter estimated position accuracy – it represents, according to the iteration i, the Euclidian distance between the position where the depth has been sampled and the estimated position

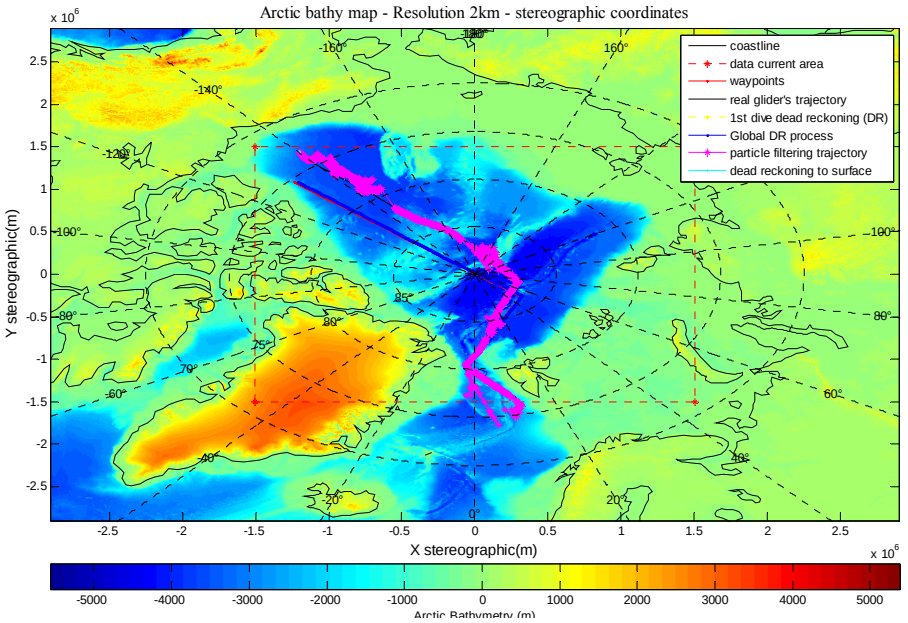

Figure A5-7: Global particle filter trajectory – ability to track the real position

- Now if we focus on the energy aspect, the use of a low frequency single beam echo sounder (SBES) does not burden the energy budget of the glider (the energy budget is detailed in Annex 3). The energy consumption of such sensor is reasonable; moreover, here the pinging policy would allow the SBES to work only for short periods of time, ensuring energy savings. The figure A5-8 summarizes the energy budget repartition.

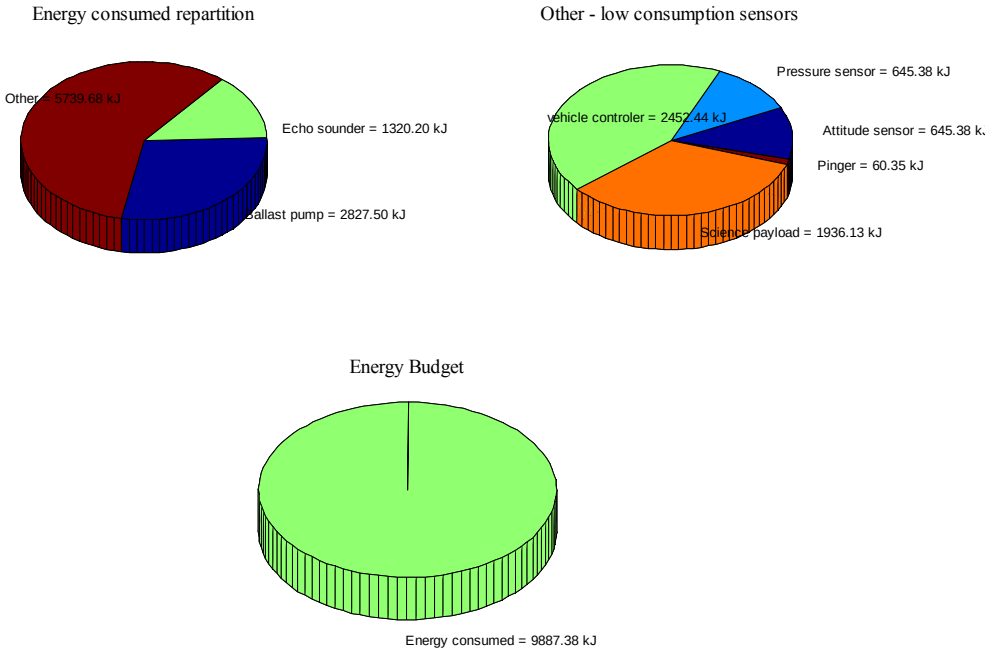

Figure A5-8: Energy consumption of this mission. The energy budget is more burdened by the glider classical components than by the SBES consumption.

Annex 5.2: Very deep water glider simulation (4000m)

A glider capable of reaching very deep waters is considered here. Such a glider can go down to 4000 meters. As far as the desired trajectory is concerned, the glider is here asked either to reach 4000 meters depth or when this is not possible, to stay 500 meters above the sea floor (see figure A5-9 for the desired trajectory).

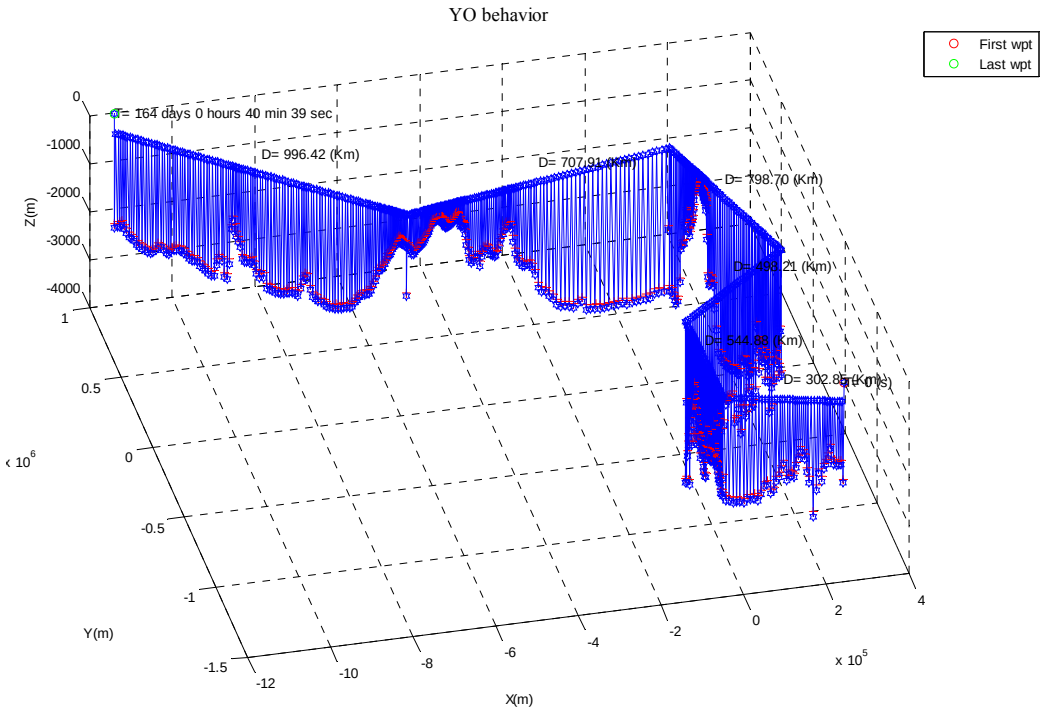

Figure A5-9: Desired trajectory with "obstacle avoidance" – pinging policy of 1 ping per dive every dive

Such a glider allows the integration of a "smaller" high frequency Single Beam Echo sounder. Moreover, given that we are pinging closer to the seafloor, we are increasing the measurement confidence. This decrease in measurement uncertainty also implies a sharper particles weight distribution for the particle filter process.

Thus, there are some *a priori* benefits using a very deep glider:

- Use of a smaller and lighter SBES
- Energy savings (small power requirements to generate a pulse)
- Higher confidence on bathymetric measurements, which should allow improvements on both estimated position accuracy and precision.

The figure A5-10 illustrates both the desired trajectory (green) and the real trajectory followed, constrained by currents (black line with bathymetric measurements location symbolized by magenta dots). The desired trajectory tries to fly above a rough seafloor, avoiding a long deep water basin crossing. The objective of this simulation is to see to what extent the glider is able to find its real position (black trajectory) using the TBN-PF. The TBN-PF principle is to retime the dead reckoning process that tends to drift over time using bathymetric measurement sampled along the black trajectory.

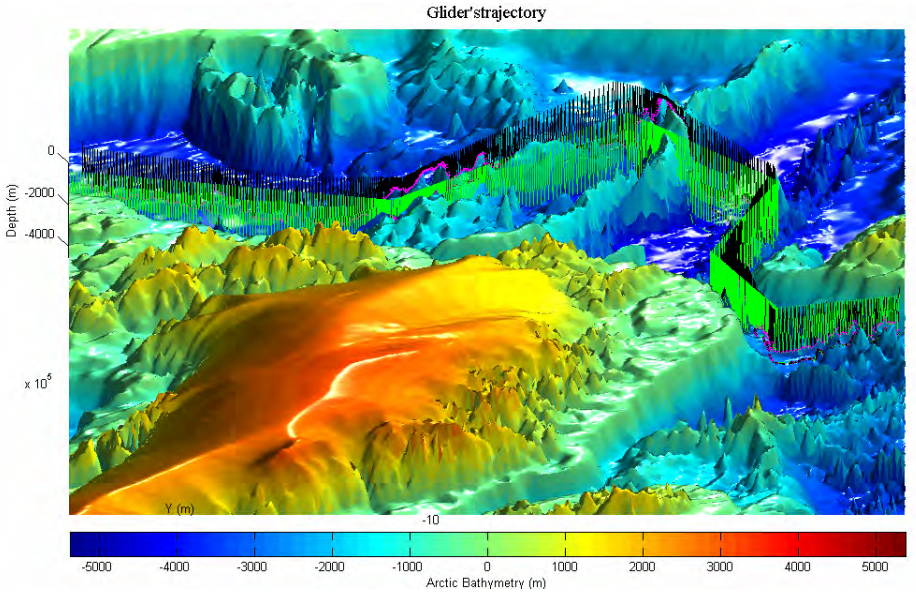

Figure A5-10: Simulation trajectories – desired trajectory (green) / real trajectory followed (black)

Accuracy and precision of the particle filter estimated position on the whole trajectory

Before showing simulation results, the figure A5-11 reminds what is inferred by the estimated position accuracy and precision concept.

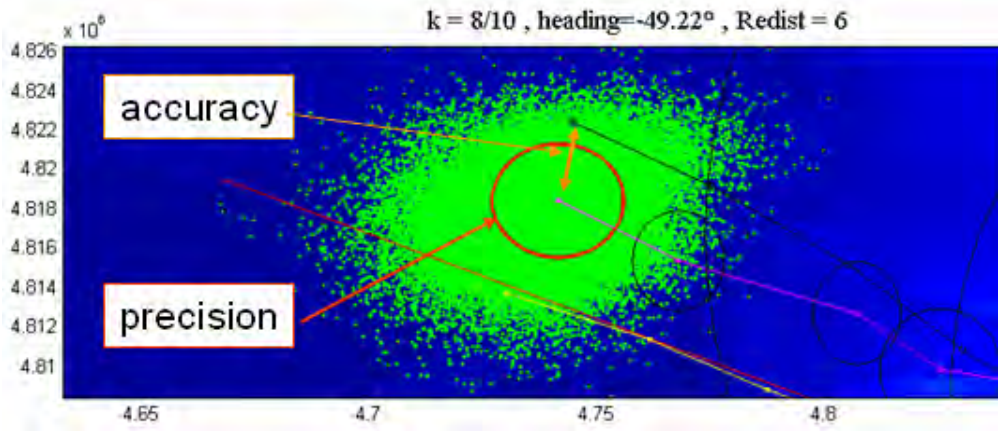

Figure A5-11: Particles' cloud illustrating accuracy and precision concepts – PF estimate (magenta line), real trajectory (black), desired trajectory (red)

Figures A5-12 and A5-13 underline that a particles explosion has been applied after the Eurasian basin crossing. On the one hand, due to the depth of this basin and on the other hand, due to the lack of variability of the seafloor elevation, the particle filter estimated position tends to trust more the dead reckoning process than bathymetric measurements. So, after this crossing, when the glider encounters the Lomonosov ridge, particles are to far away to follow the right track, and so the estimated position is stuck in a dead end. As a consequence a particle explosion is applied. We can easily imagine asking the glider not to retime its dead reckoning process with the particle filter estimated position when such an explosion is applied.

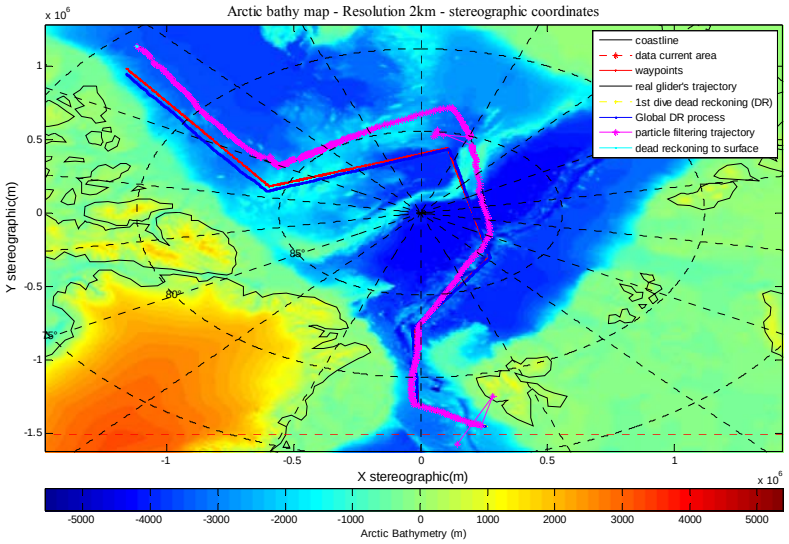

Figure A5-12: Particle explosion after the Eurasian basin crossing

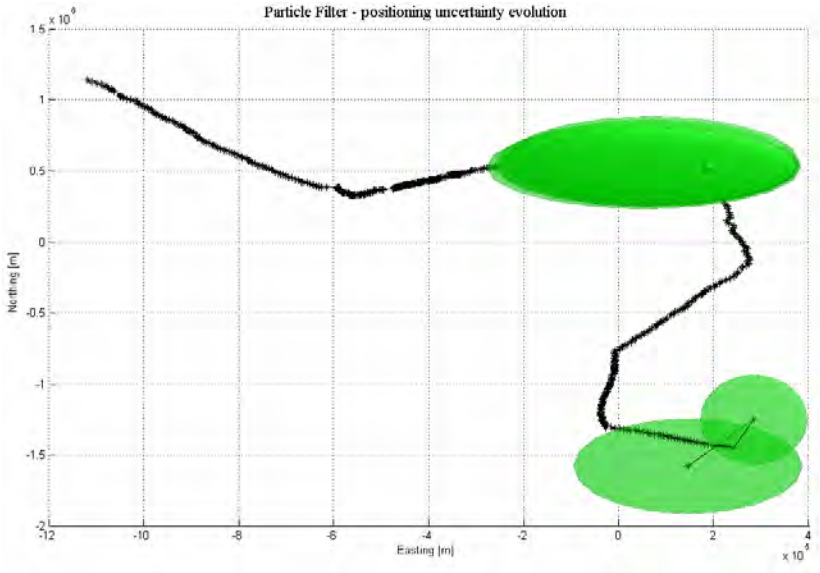

Figure A5-13: Influence of a particle explosion on the filter's precision ellipsoid

Figures A5-14 and A5-15 outline TBN-PF results on the whole trajectory. The accuracy is here burdened by this particles explosion. However, this explosion allows to restart the tracking process when the glider is "lost".

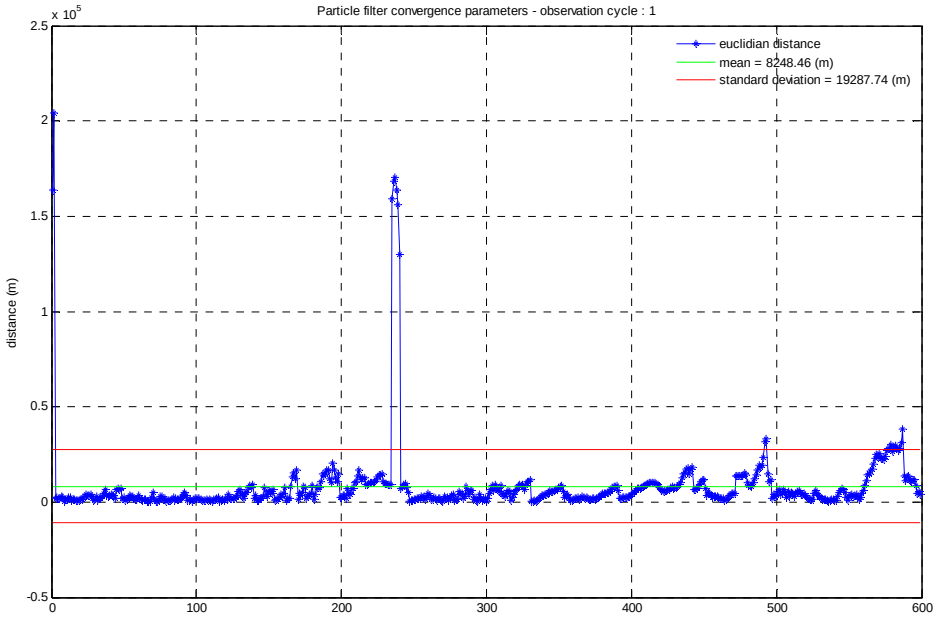

Figure A5-14: Accuracy of the TBN-PF estimated position

Those accuracy results have to be correlated with the precision *i.e.* the confidence we have in the TBN-PF estimated position.

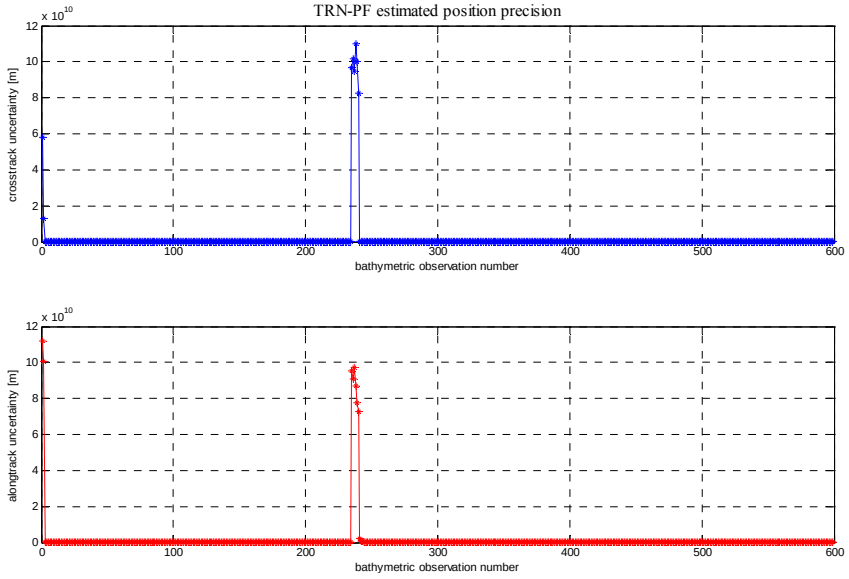

Figure A5-15: Cross-track and along-track precision of the TBN-PF estimated position

A particle explosion is characterized by a strong uncertainty on position and a wide particles' cloud. This idea is illustrated on figure A5-15 where a drop in the estimation confidence, *i.e.* an explosion of position uncertainty, can be seen around the 240th bathymetric observation.

Figures A5-16 and A5-17 now illustrates the particle filter estimated position accuracy and precision when the "explosion" influence has been removed (giving more weight to the dead reckoning process when the estimated position uncertainty is too high for example).

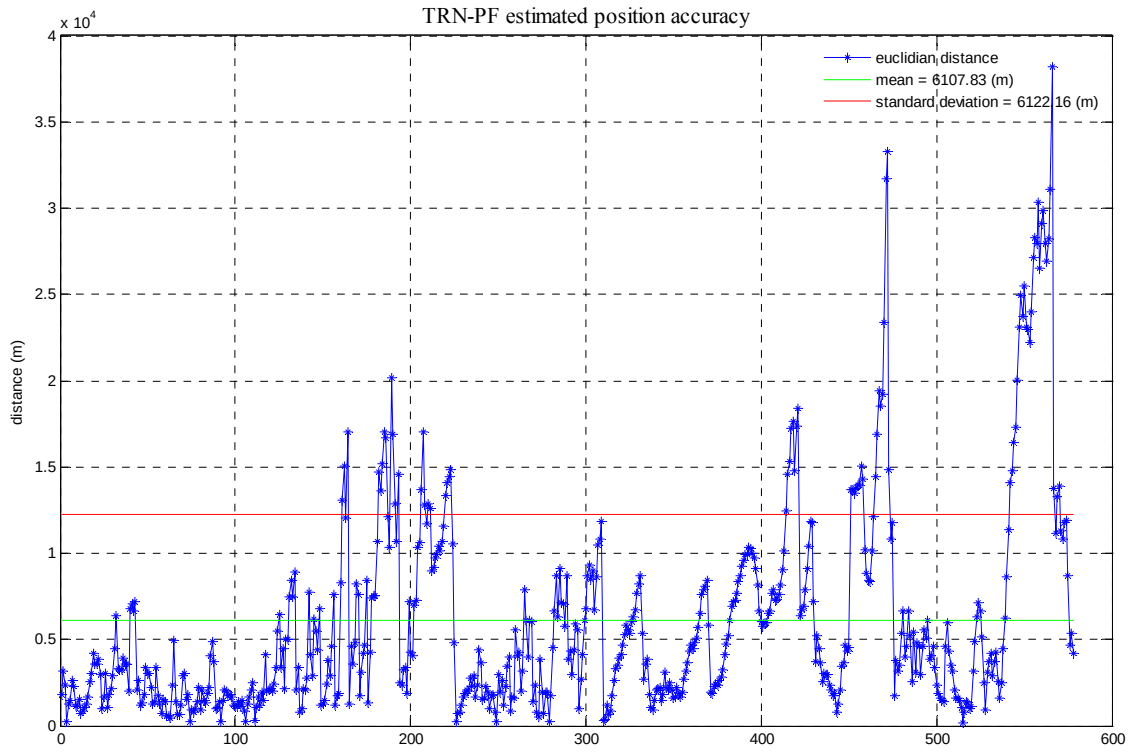

Figure A5-16: Accuracy of the TBN-PF estimated position – corrected from the particles explosion influence

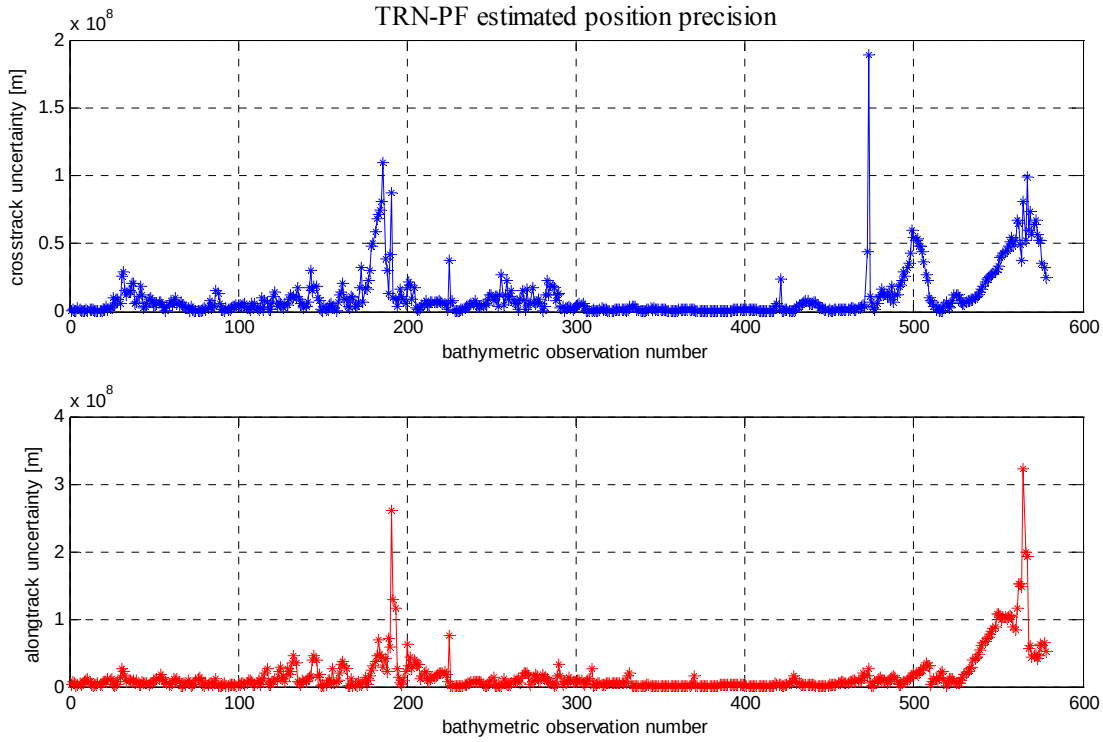

Figure A5-17: Cross-track and along-track precision of the TBN-PF estimated position – corrected from the particles explosion

Those accuracy and precision results (see figures A5-16 and A5-17) can be correlated with the seafloor elevation variations seen in figure A5-18 or with the figure A5-19 that replaces bathymetric observation numbers in their geographical context. The first accuracy decrease is due to the Eurasian basin crossing.

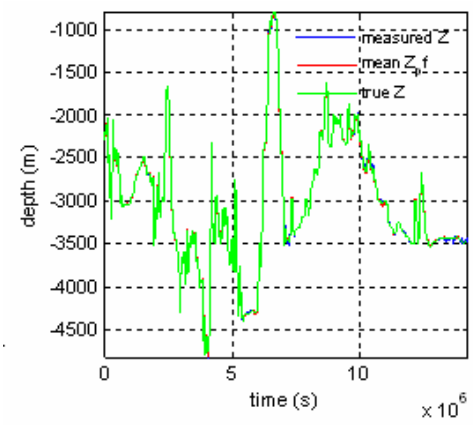

Figure A5-18: bathymetry seen by the glider

Then, the lack of variation of the Beaufort basin is responsible for the final drop of both accuracy and precision of the TBN-PF estimated position.

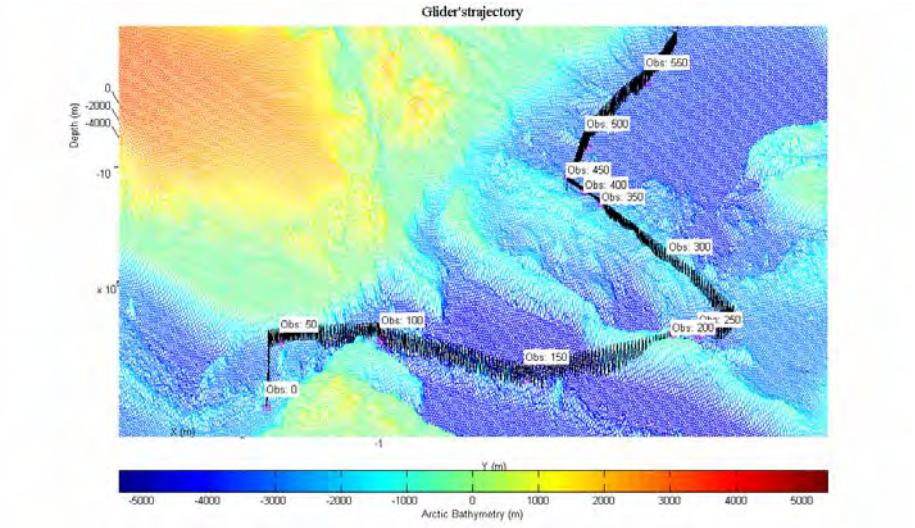

Figure A5-19: bathymetric observation localization

Thus, this “very deep water” glider simulation underlines the potential of the TBN-PF as a navigation estimation process. The expected positioning accuracy has been improved thanks to the increase in bathymetric measurement confidence. The figure A5-20 also underlines one more time the low energy consumption of such a process.

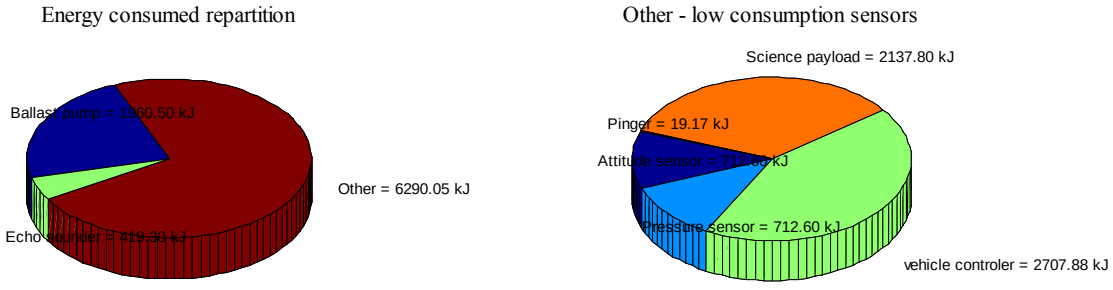

Figure A5-20: Energy consumed during this long range mission (165 days)

Annex 6: Performance of an Inertial navigation system at Arctic Latitudes

This section is based on the paper "*Performance of an AUV navigation System at Arctic Latitudes*" [10] which synthesizes results of engineering tests in preparation for the Atlantic Layer Tracking Experiment (ALTEX). Navigation at Arctic latitudes remains a challenge.

A compass has difficulty determining heading because of the Earth's magnetic field inclination (see figure A6-1). Thus heading determination is strongly linked with the pitch angle of the glider. Inertial instruments have difficulties to align to north. This ability is inherently reduced as a function of secant latitude. If we consider the Ixsea Octans 3000, the heading accuracy reaches 0.1 deg secant latitude, which implies that at 85° North, the heading accuracy is worth:

$$\sigma_{compass} = \frac{0.1}{\cos(latitude)} = \frac{0.1}{\cos(85^\circ)} = 1.15^\circ$$

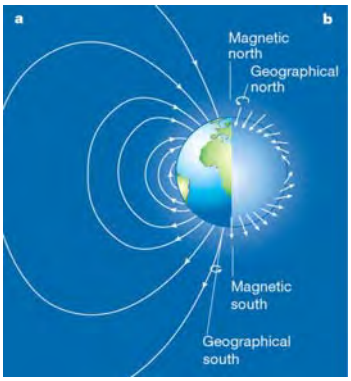

Figure A6-1: Earth's magnetic field inclination (*source: www.nature.com*)

At lower latitudes, the integrated system (IMU providing an ideal heading reference, DVL with bottom track) provides accurate position estimation with a position error growth less than 0.05% of distance traveled. However, at Arctic latitudes, in the case where the INS uses its gyrocompass algorithm for alignment, both the alignment-to-north accuracy and the navigation accuracy decrease proportional to the secant of latitude. For a gyrocompass alignment:

- at 80° North: position error growth reaches 0.3% of the distance traveled
- at 85° North: position error growth reaches 0.6% of the distance traveled

Moreover, the DVL, which is pointing upward to measure velocity with respect to the ice, can loose the track, implying drops in navigation accuracy.

If we consider an Arctic crossing performed by a glider:

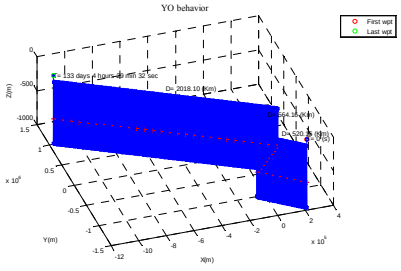

Figure A6-2: Arctic crossing trajectory

Distance traveled	Expected accuracy in positioning using a INS	
	45° North Latitudes (0.05% DT)	Arctic Latitudes (0.5% DT)
some 3 450 km	1 725 m	17 250 m

One the one hand given those accuracy results and those of the TBN-PF Arctic crossing simulations (see Annexes A5.1 and A5.2), and on the other and given that, as seen in section 4-4 with the study of the dead reckoning influence on terrain navigation results, the TBN-PF does not need a perfect dead reckoning process to reach an acceptable accuracy, the terrain navigation process seems perfectly suited to long range under ice missions.

Annex 7: Magnetic compass data assimilation – TBN-PF improvement

Ligurian Sea

Figure A7-1: magnetic declination on a nautical chart

We have to define:

True North: the direction of a meridian of longitude which converges on the North Pole.

Magnetic North: the direction indicated by a magnetic compass.

Magnetic declination: The horizontal angular difference between True North and Magnetic North. The declination is positive when the magnetic north is east of true north.

Heading determination

(x_k, y_k) represents here the iterative coordinates of the desired trajectory.

$$\theta_k = \arctan\left(\frac{x_{k+1} - x_k}{y_{k+1} - y_k}\right) + \delta$$

We also have to take into account the magnetic compass accuracy of the glider by the addition of a white noise.

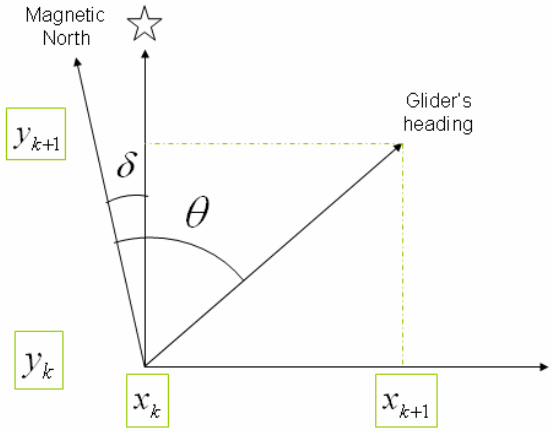

Figure A7-2: Heading determination in Ligurian Sea

In the Ligurian sea simulation the heading is only used in the dead reckoning process.

Arctic Ocean

We want in this section to add information in the positioning process thanks to the knowledge of the glider's heading. To perform this operation, we have first to simulate "virtual" glider's heading measurements thanks to a simple model.

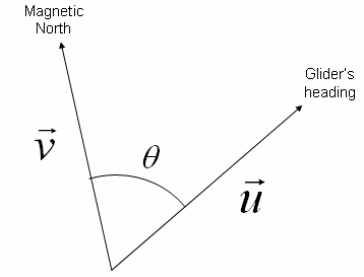

Figure A7-3: Heading determination in Arctic Ocean

We use here the scalar product between two vectors in order to determinate the glider's heading.

$$\cos\theta = \frac{\langle \vec{u}, \vec{v} \rangle}{\|\vec{u}\| \|\vec{v}\|}$$

We compute here the angle between the direction toward the magnetic north pole (dashed white line on the figure A7-4) and the direction of the real trajectory followed by the glider (the one constrained by currents represented by a black line on the figure A7-4). This heading angle is likely to be what the glider's magnetic compass is going to provide to the dead reckoning process. The heading angle is then used to estimate the glider's speed components (V_x, V_y).

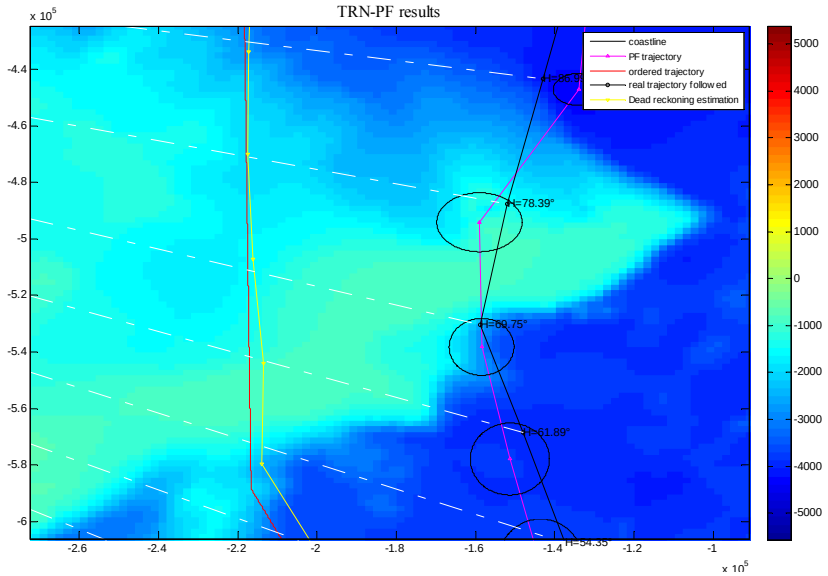

Figure A7-4: Heading information assimilation

- Particle filter trajectory: magenta line
- Particle filter position estimation uncertainty ellipse: black ellipse
- Dead reckoning trajectory: yellow line
- Desired trajectory: red line
- Direction toward the Magnetic North Pole: dashed white line

Evolution of glider's heading along the trajectory

We are involving here that the compass needle points toward the magnetic north pole, which is not exactly the case due to the complexity of the Earth's magnetic field. We just want here to see to what extent the knowledge of the glider's heading can help in the improvement of the positioning process. Figures illustrate the evolution of the glider's heading along the real trajectory followed (black line on the figure A7-5) if we consider that the compass needle is pointing toward the magnetic pole.

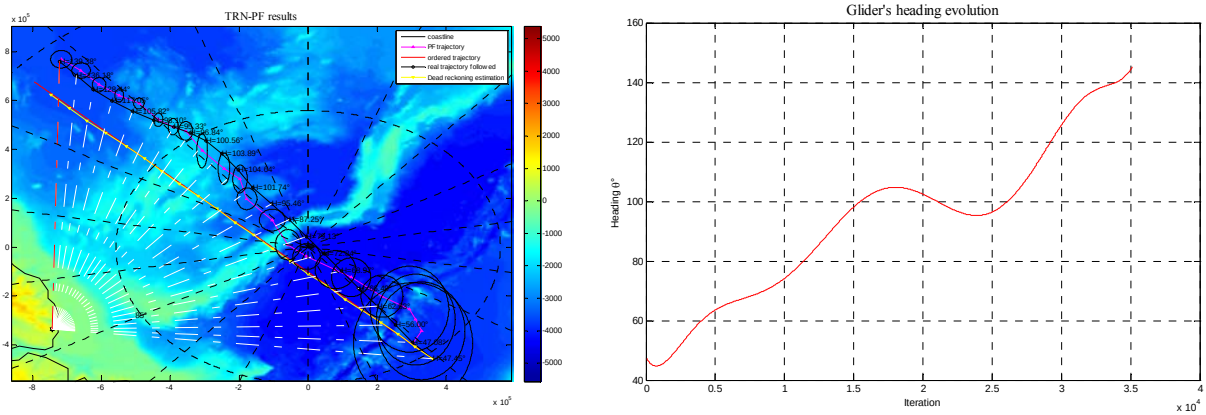

Figure A7-5: Glider's heading evolution along the trajectory

Heading assimilation idea

The idea is here to take the heading data into account and to assimilate it in the navigation estimation process. We would like to give more weight to particles that are at the "right location", or better said, inside the cone uncertainty, given the measured heading (see figure A7-6). This is in a way a low cost geophysical navigation process where we are willing to compare a data from a magnetometer with the *a priori* IGRF model.

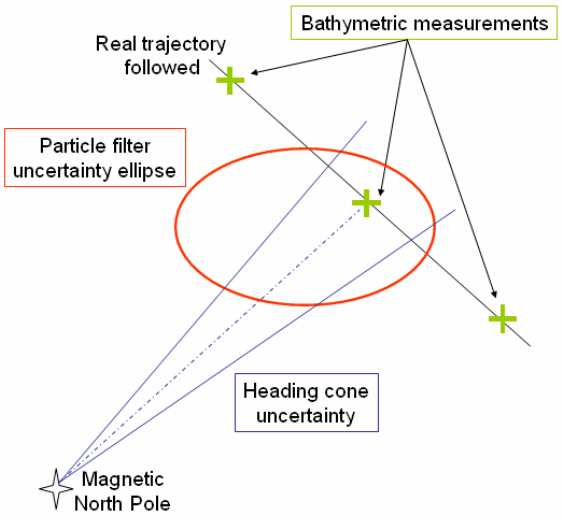

Figure A7-6: Heading assimilation idea

To perform this operation, we have to modify the likelihood function that intervenes in the update step of the particle filter process. Till now we have only taken the bathymetric data into account as the figure A7-7 outlines it. However, the likelihood function is able to take into account the heading information as illustrated on figure A7-8.

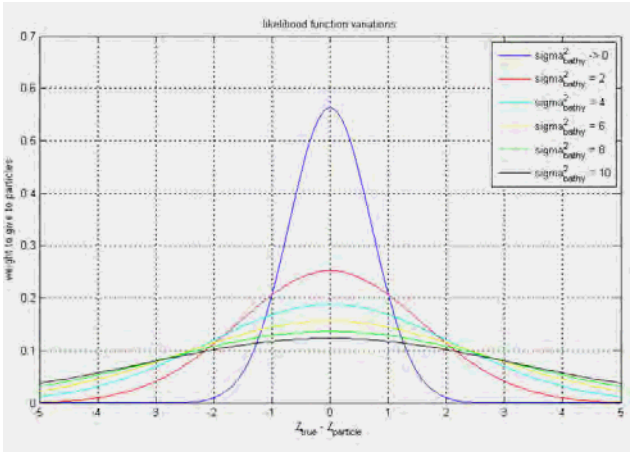

Figure A7-7: Terrain navigation likelihood function

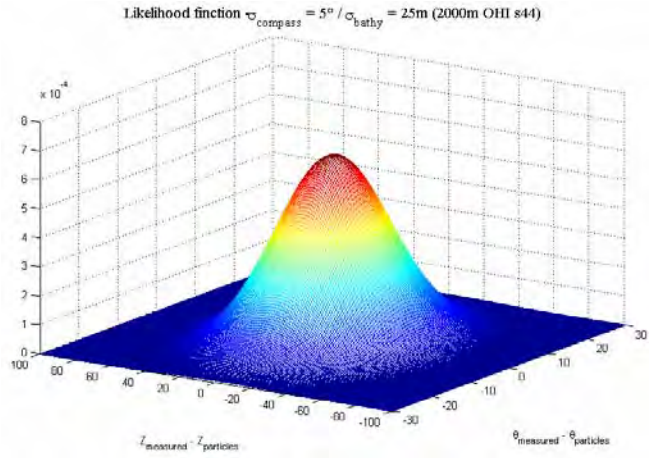

Figure A7-8: terrain navigation and heading coupling

$$like = \frac{1}{\sqrt{2\pi}.\sigma_{bathy}}.e^{\frac{-(Z-Zi)^2}{2.\sigma_{bathy}^2}}$$

$$like = \frac{1}{\sqrt{2\pi}.\sigma_{bathy}}.e^{\frac{-(Z-Zi)^2}{2.\sigma_{bathy}^2}} \frac{1}{\sqrt{2\pi}.\sigma_{compass}}.e^{\frac{-(\theta-\theta i)^2}{2.\sigma_{compass}^2}}$$

All the difficulty lies here in the determination of each particle's heading in order to compare with the measured heading, and so to distribute a coherent weight. However, each particle trajectory is too chaotic to retrieve any relevant particle's heading information (for example due to the re-sampling process). The figure A7-9, illustrates the trajectory of four different isolated particles.

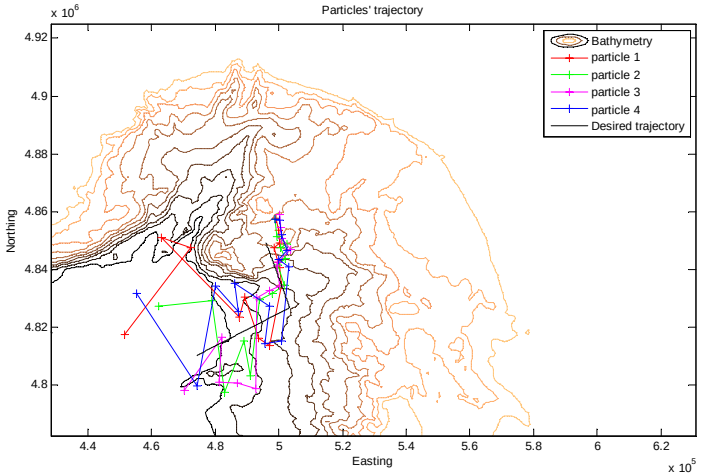

Figure A7-9: trajectory pattern of 4 different particles

In this context, instead of working with the measured value of heading, we would have to rely on the couple *measured/a priori* magnetic declination data. But this is the principle of the geophysical navigation. The main issue with this geophysical navigation is that IGRF model is not accurate enough close to magnetic poles compared to the accuracy we can reach using the terrain navigation alone. Thus, given all those considerations, the heading information seems difficult to assimilate in the loop of the particle filter process.